ARTIFICIAL NEURAL NETWORK BASED GEARBOX FAULT DIAGNOSIS

Ph.D. Thesis

By

AMANDEEP SINGH AHUJA

DISCIPLINE OF MECHANICAL ENGINEERING

INDIAN INSTITUTE OF TECHNOLOGY INDORE

April 2019

ARTIFICIAL NEURAL NETWORK BASED GEARBOX FAULT DIAGNOSIS

A THESIS

Submitted in partial fulfillment of the requirements for the award of the degree

of

DOCTOR OF PHILOSOPHY

by

AMANDEEP SINGH AHUJA

DISCIPLINE OF MECHANICAL ENGINEERING

INDIAN INSTITUTE OF TECHNOLOGY INDORE

April 2019

INDIAN INSTITUTE OF TECHNOLOGY INDORE

CANDIDATE'S DECLARATION

I hereby certify that the work which is being presented in the thesis entitled **ARTIFICIAL NEURAL NETWORK BASED GEARBOX FAULT DIAGNOSIS** in the partial fulfillment of the requirements for the award of the degree of **DOCTOR OF PHILOSOPHY** and submitted in the **DISCIPLINE OF MECHANICAL ENGINEERING, Indian Institute of Technology Indore**, is an authentic record of my own work carried out during the time period from Jan 2014 to April 2019 under the supervision of Prof. Anand Parey.

The matter presented in this thesis has not been submitted by me for the award of any other degree of this or any other institute.

(AMANDEEP SINGH AHUJA)

This is to certify that the above statement made by the candidate is correct to the best of my knowledge.

(PROF. ANAND PAREY)

AMANDEEP SINGH AHUJA has successfully given his/her Ph.D. Oral Examination held on

Signature of Chairperson (OEB)
Date:

Signature of External Examiner
Date:

Signature(s) of Thesis Supervisor(s)
Date:

Signature of PSPC Member #1
Date:

Signature of PSPC Member #2
Date:

Signature of Convener, DPGC
Date:

Signature of Head of Discipline
Date:

ACKNOWLEDGEMENTS

I would like to express my sincere gratitude to Prof. Anand Parey for providing me the opportunity and resources to work on this project. Without his relentless support and guidance, this project would not have come to fruition.

I also take this opportunity to thank Dr. Ram Bilas Pachori and Dr. Ritunesh Kumar for their valuable suggestions and guidance which helped me improve the quality of my work significantly.

My gratitude also goes to the staff at the Solid Mechanics Laboratory at IIT Indore for the assistance they rendered in acquisition of signatures from the experimental set-up.

SYNOPSIS

Gearboxes are employed in a wide range of applications such as in the automobile industry, marine propulsion systems, aviation industry etc. Breakdown of the gear train can not only result in significant financial losses but may also prove to be fatal. It is, therefore, necessary to identify a fault in a gearbox before catastrophic failure occurs.

The vibration and sound emission signatures (also referred to as *acoustic signatures* in the thesis) of a gearbox carry abundant information about its condition. Whenever a fault develops in a gearbox, its vibration and sound emission signatures exhibit a change. In order to ascertain the condition of the gearbox, meaningful parameters representing the gearbox health condition need to be extracted from the acquired gearbox signatures. This process is referred to as the feature extraction step. This step usually involves extraction of features in the time domain, frequency domain or the time-frequency domain. Not all features extracted during the feature extraction step have the same fault classification potential. Often feature reduction is required to retain only the parameters with superior fault discrimination capability. However, this feature reduction comes at the cost of additional computational burden.

An automated method of gearbox fault diagnosis is desirable wherein the condition of the gearbox can be assessed with minimal intervention of the operator. Artificial intelligence (AI) paves the path towards automated gearbox fault diagnosis (GFD). The present study is based on the application of artificial neural networks (ANNs), in particular, the back propagation neural network (BPNN) and the adaptive neuro-fuzzy inference system (ANFIS) in diagnosing gearbox faults. An ANFIS is a hybrid system of ANN and fuzzy inference system wherein the fuzzy sets and rules are automatically tuned as the network is trained. The features extracted from the acquired gearbox signals are utilized as inputs to train and test an intelligent classifier such as an ANN with the objective of diagnosing the condition of the gearbox. This step is referred to as the pattern recognition step.

The experimental set up from which vibration and sound emission signatures are acquired is a drive train diagnostic simulator (DDS) comprising of a single stage spur gearbox and a machinery fault simulator (MFS) comprising a bevel gearbox. Gearbox vibration signatures are acquired by mounting an accelerometer at appropriate locations on the gearbox casing while sound emission signatures are acquired under various gear health conditions by placing a microphone at a specific distance from the gearbox. The DDS allows both the speed profile as well as the load profile to be programmed. In Chapter 2, gearbox vibration signatures, acquired at a constant programmed speed of 15 Hz with sinusoidal load fluctuations at the output, are analyzed to diagnose three different pinion health conditions. In Chapter 3, gearbox vibration and sound emission signals, acquired at a constant programmed speed of 20 Hz, are analyzed to diagnose four different gearbox health conditions. Chapter 6 analyzes the acoustic signatures acquired under three different pinion health conditions at a constant programmed speed of 10 Hz and involves the application of ANFIS to identify the three gearbox health conditions.

Most of the research efforts based on GFD using AI do not take into account the non-stationary nature of gearbox signals. It has been found that gearbox signatures have a natural propensity to be non-stationary owing to fluctuating load-speed conditions and as a result of uncertainties associated with the drive and load mechanisms. The non-stationary nature of gearbox signals is evident from an unequal number of samples between tachometer pulses. Under non-stationary conditions, techniques such as time synchronous averaging (TSA) cannot be directly employed in order to improve the signal to noise ratio. Though a gearbox operates mostly under non-stationary conditions, research efforts directed towards GFD under such conditions are limited. The present study involves the application of ANNs to diagnose faults in a single stage spur and bevel gearbox under non-stationary conditions.

Another method of improving the signal to noise ratio is to carry out averaging of signals in the angular domain. As a novel approach, the independent angular re-sampling (IAR) technique is proposed in the present study to convert non-stationary signals in the time domain into quasi-stationary signals in the angular domain. This is accomplished experimentally by employing a multiple pulse tachometer arrangement such that the instants of time at three different shaft angular positions during a revolution are known. The IAR technique is based on the fact that the velocity profile of a single revolution can be represented by a small segment of the overall velocity profile and may be assumed to be linear. The IAR technique helps determine the time instants that correspond to constant angular increments. The amplitude of the signals at the re-sample time instants can be determined from interpolation theory. In the present study, piecewise cubic Hermite interpolation (PCHI) is employed to determine the amplitude of the vibration and sound emission signals at the re-sample time instants. The IAR technique, combined with interpolation theory, yields a number of angular domain signals, each representing one revolution of the gearbox drive shaft. These angular domain signals can be averaged in order to improve the signal to noise ratio. Alternatively, the resultant angular domain signals can be merged to generate the combined angular domain signal corresponding to the original time domain signal.

To extract meaningful parameters representing the gearbox health condition, the angular domain signals generated from the IAR technique are decomposed using continuous wavelet transform (CWT). This process of analyzing the angular domain signals in the time-frequency domain generates wavelet amplitude maps (WAMs) with as many continuous wavelet coefficients (CWCs) at each scale as the number of samples in the original angular domain signal. Inspired by recent research efforts in GFD, a range of optimal scales is identified based on the energy-Shannon's entropy ratio of CWCs. In Chapter 2, a range of optimal scales is identified based on the energy-Shannon's entropy ratio of CWCs from the WAM corresponding to the combined angular domain signal pertaining to the healthy pinion. In Chapter 4, on the other hand, a range of optimal scales is identified based on the energy-entropy ratio of CWCs pertaining to the healthy pinion angular domain averaged signal.

Once the angular domain signals generated from the IAR technique are decomposed using CWT, statistical parameters (SPs) representing each gear health condition can be computed from the CWCs at the various scales of the WAMs. In order to reduce the computational burden associated with extraction and selection of SPs, and inspired by recent research efforts in GFD, CWCs are employed directly as inputs to the BPNN in Chapters 2 and 3. In Chapter 4 and 5, CWCs from the optimal scales of the segmented WAMs are employed as inputs to train and test an ANFIS classifier. In Chapter 2, the classification accuracy of a BPNN is compared when CWCs from all scales and when CWCs from only the optimal scales are fed to the ANN. Superior gear fault diagnostic accuracy is attained when CWCs from only the optimal scales are employed as inputs to the ANN. In Chapter 3, CWCs derived from the vibration and sound emission signatures are fed directly to the ANN. The available data set is divided into two parts, 50% of which is used to train the neural network while the remaining 50% is utilized to test its classification accuracy. The number of neurons in the hidden layer of the ANN is determined by trial and error and the sigmoidal transfer function is employed as the activation function for the hidden and output neurons. Chapter 2 deals with a three class gear fault identification problem and hence the ANN has only three output neurons. In Chapter 3, on the other hand, there are four output neurons as the problem is a four class gear fault identification problem.

To the best of the author's knowledge, ANFIS has not yet been employed to diagnose gearbox faults taking into account the non-stationary conditions associated with gearbox operation. Chapters 4 and 5 of the present study are, therefore, based on the application of ANFIS in diagnosing gearbox faults under non-stationary conditions arising from uncertainties associated with the drive and load mechanisms. The IAR technique is combined with PCHI to generate angular domain averaged (ADA) signals representing each gear health condition. CWCs at the optimal scales of the segmented WAMs and employed as inputs to train and test an ANFIS. Approximately 50% of the data samples are randomly selected to train the ANFIS while the remaining data samples are reserved for testing. There is a choice of membership functions that can be adopted for the inputs and output to the ANFIS classifier. The Gaussian membership function is chosen for the inputs and the linear membership function for the output. The membership functions of each input are divided into three regions: small, medium and large. Reasonably good test accuracy is obtained when the selected parameters are utilized to diagnose the condition of the gearbox.

To summarize, the IAR technique is a simple yet powerful method of converting non-stationary signals in the time domain into quasi-stationary signals in the angular domain. Implementation of the technique demands only minor changes in hardware such as the introduction of an additional tachometer reflective strip. The angular domain signals resulting from the IAR technique can be averaged in order to improve the signal to noise ratio. The ADA signals can be decomposed using CWT and CWCs employed directly as inputs to the ANN resulting in superior gear fault diagnostic results. CWCs at the optimal scales of the segmented WAMs can also be employed as inputs to an ANFIS classifier resulting in reasonably good gear fault classification accuracy. The results demonstrate that the methods proposed in this study can be applied successfully to ascertain the condition of a gearbox under non-stationary conditions.

TABLE OF CONTENTS

LIST OF FIGURES

LIST OF TABLES

NOMENCLATURE

$\theta(t)$	Angular rotation as a function of time
b_0, b_1, b_2	Constants defining the angular rotation
k	Increments at which re-sample time instants are required. For example, *k* varies from 1 to 360 for the first revolution.
$\Delta\phi$	1° or $\pi/180$ rad
$P(x)$	Cubic polynomial in x
$c_3,\ c_2, c_1, c_0$	Constants defining the third degree polynomial, *P(x)*
x_k	Knot point at the beginning of the *k th* interval
x_{k+1}	Knot point at the end of the *k th* interval
y_k	The value of *P(x)* corresponding to x_k
$y_{k+!}$	The value of *P(x)* corresponding to x_{k+1}
g_k	The gradient of *P(x)* corresponding to x_k
g_{k+1}	The gradient of *P(x)* corresponding to x_{k+1}
u	Local variable
$h_1(u),..,h_4(u)$	Piecewise cubic Hermite basis functions
W_x	Wavelet transform of the time domain signal $x(t)$
s	Scale parameter
τ	Translation parameter
w_{ij}	Synaptic weight between the *i th* node in layer $l-1$ and the *j th* node in layer *l*

$x^{(n)}$	Input feature vector during the *n th* iteration
$d^{(n)}$	Desired output during the *n th* iteration
$y^{(n)}$	Actual output during the *n th* iteration
N	Number of training patterns
C	Number of classes
x, y	Inputs to the ANFIS classifier
A_i, B_i	Fuzzy sets
O_i^l	Output of the *i th* node in layer l
$\mu_A(x)$	Membership function of x in A
$\{a_i, b_i, c_i\}$	Premise parameters
π	Multiplier operator
$\{p_i, q_i, r_i\}$	Consequent parameters
N	Normalization operator
w_i	Firing strength of the *i th* node
$Energy(n)$	Energy of the continuous wavelet coefficients at the *n th* scale
$Entropy_{Sh}(n)$	Shannon's entropy at the *n th* scale
m	Number of continuous wavelet coefficients at the *n th* scale

ACRONYMS

GFD	Gearbox fault diagnosis
AI	Artificial intelligence
ANN	Artificial neural network
BPNN	Back propagation neural network
ANFIS	Adaptive neuro-fuzzy inference system
CWT	Continuous wavelet transform
CWCs	Continuous wavelet coefficients
PCHI	Piecewise cubic Hermite interpolation
SPs	Statistical parameters
IAR	Independent angular re-sampling
GA	Genetic algorithm
DWT	Discrete wavelet transform
WPT	Wavelet packet transform
TSA	Time synchronous averaging
WAM	Wavelet amplitude map
ADA	Angular domain averaged (signals)
DDS	Drive train diagnostic simulator
HP	Healthy pinion
CT	Cracked tooth
CHT	Chipped tooth
MT	Missing tooth
RBF	Radial basis function

Chapter 1

Review of Past Work and Problem Formulation

1.1. Background and Motivation

Gearboxes are employed in a wide range of applications to transmit power from one shaft to another and/ or to change the direction of motion. Breakdown of the gear train can not only result in shutdown of the machinery causing significant financial losses but may also prove to be fatal [1]. Gearbox failure in certain critical applications such as single engine aircraft and propulsion systems of warships is totally unacceptable. It is, therefore, necessary to identify a fault in a gearbox before catastrophic failure occurs.

An automated method of GFD is desirable wherein the condition of the gearbox can be ascertained automatically with minimal intervention of the operator. AI, in the form of ANNs, fuzzy inference systems and hybrid systems such as ANFIS, paves the path towards automated methods of GFD. This thesis, therefore, is based on the application of AI, in particular ANNs, in diagnosing gearbox faults.

A gearbox operates under fluctuating load-speed conditions for most of its useful life, sometimes at the demand of the operator. Where a gearbox has been designed to run at a rated constant speed of operation, it can be shown that there are still fluctuations in the speed of the gearbox drive shaft. This may be attributed to uncertainties associated with the drive and load mechanisms. Considering the widespread application of gearboxes and their significance in power transmission, considerable amount of research efforts have been devoted in the last two decades to devise new and effective methods of GFD. Even though gearbox signals are mostly non-stationary, research efforts directed towards GFD under non-stationary conditions at present are limited. This thesis, therefore, focuses on diagnosing faults in a single stage spur and in a bevel gearbox under non-stationary conditions.

1.2. Gearbox fault detection techniques

Condition monitoring and fault diagnosis of gearboxes has been attracting considerably increasing attention [2-4]. The characteristic frequencies, including the gear rotating frequency, the meshing frequency, etc., are critical to fault detection of gears. The identification of faults is related to the occurrence of the characteristic frequencies which is linked to the given fault [5]. Fig. 1.1 shows the transmission diagram of a fixed axis gearbox containing two meshing pairs.

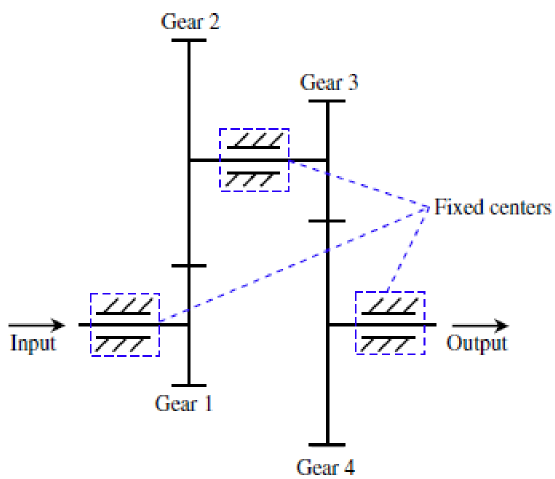

Fig. 1.1. *Transmission diagram of a fixed-axis gear system having two meshing pairs [5]*

Let us define the following notation:

N_j is the number of teeth of gear j, $j = (1,2,3,4)$.

f_j is the rotating frequency of gear j, $j = (1,2,3,4)$. The rotating frequency of gear 1 f_1 is the input frequency of the whole gear transmission and is generally known beforehand.

i_k is the transmission ratio of meshing pair k $(k = 1,2)$ and is defined as the ratio between the rotating frequency of the driving gear and that of the driven gear in a meshing pair. It also equals the ratio between the number of teeth of the driven gear and that of the driving gear, for example, $i_1 = \frac{N_2}{N_1}$ and $i_2 = \frac{N_4}{N_3}$ in Fig. 1.1.

f_{m_k} is the meshing frequency of meshing pair k $(k = 1,2)$.

Then the characteristic frequencies, i.e. the rotating frequencies of each gear and the meshing frequencies of each meshing pair, can be expressed as a function of the input frequency f_1 and the number of teeth of gears as follows:

$$f_2 = \frac{f_1}{i_1} = \frac{N_1}{N_2} f_1 \tag{1.1}$$

$$f_3 = f_2 = \frac{N_1}{N_2} f_1 \tag{1.2}$$

$$f_4 = \frac{f_3}{i_2} = \frac{N_1 N_3}{N_2 N_4} f_1 \tag{1.3}$$

$$f_{m_1} = N_1 f_1 \tag{1.4}$$

and

$$f_{m_2} = N_3 f_3 = \frac{N_1 N_3}{N_2} f_1 \tag{1.5}$$

The equations of the characteristic frequencies are also summarized in Table 1.

Table 1.1
Characteristic frequencies of fixed axis gearbox.

f_1	f_2	f_3	f_4	f_{m_1}	f_{m_2}
Known	$\frac{N_1}{N_2} f_1$	$\frac{N_1}{N_2} f_1$	$\frac{N_1 N_3}{N_2 N_4} f_1$	$N_1 f_1$	$\frac{N_1 N_3}{N_2} f_1$

There are mainly two types of approaches to gear fault diagnostics: data-driven based methods and physical model-based methods. Data-driven based methods rely on the analysis of historical data collected from gearboxes to diagnose and/or predict their health conditions. The measured data could be vibration signals, motor voltage and current signals, torque load signals, acoustic signals, metal scan data, gear weight loss data, gearbox strain signals, gear damage images and so on [6-16].The physical models of gearboxes can be divided into two subsets: modulation based models and dynamics based models. Modulation based models are developed via the understanding of amplitude modulation, frequency modulation and phase modulation characteristics of vibration signals. The studies on the development of modulation based models are available in Refs. [17-22]. Dynamics based models are developed based on a fundamental analysis of gear mesh mechanism and dynamics. Then, dynamic characteristics in various health conditions can be simulated and fault symptoms revealed.

1.3. Dynamic modeling of gearbox faults

Dynamic modeling can help understand gearbox dynamics, fault symptoms and fault generation mechanisms. In addition, the cost involved in dynamic simulation is negligible compared with that for conducting experiments. However, gearbox transmissions are very complicated and it is hard to model all details of a transmission. Researchers generally simplify a real system into a simplified discrete model while retaining all of the important and relevant features [23]. Lumped parameter modeling (LPM) and finite element modeling (FEM) are two commonly used techniques to model gear trains. A lumped parameter model is one in which the components are considered to be solid with the masses concentrated at a set of points [24]. A finite element model discretizes a physical model into disjoint components of simple geometry called finite elements and its system response is obtained by connecting or assembling the collection of all elements [24]. It is hard to simply tell which method is better. As stated in Ref. [25]: ‘‘Both methods are equally accurate if proper attention is paid to defining the boundary conditions and the degree of discretization, which may be different for the two methods. Solution costs will differ depending on the discretization characteristics of the LPM and various FEM derivations and, of course, on the efficiency of the programmer.”

Gear mesh stiffness is one of the main internal excitations of gear dynamics [26]. It is time varying caused by the change of tooth contact number and contact position [27]. Four methods are commonly applied to evaluate time-varying gear mesh stiffness for gear fault diagnosis: square waveform method, potential energy method, finite element method, and experimental method [28].

Dynamics-based fault diagnosis techniques on various types of gear faults such as gear tooth cracking, tooth pitting/ spalling, wear, tooth tip chipping, manufacturing errors, misalignment, eccentricity etc. have been reviewed in [28]. Some of the commonly occurring faults in gearboxes have been described in the succeeding paragraphs.

1.3.1. Gear tooth cracking

The crack effect can be simulated using the lumped parameter modeling or the finite element modeling [29]. In the lumped parameter modeling, gear crack fault is mostly reflected in the time-varying mesh stiffness. Tooth crack causes gear mesh stiffness reduction leading to abnormal vibration of gears. Gear mesh stiffness can be evaluated using the square waveform method, the potential energy method, the finite element method or the experimental method. Ma et al. [29] did a literature review on gear tooth crack modeling.

1.3.2. Gear tooth pitting/ spalling

Tooth pitting is a common failure mode of gears. When several pits join, a larger pit (or spall) is formed. According to American Society for Metals (ASM) handbook [30], the main causes of tooth pitting/ spalling are summarized as follows:

(a) Subsurface cracks caused by figure or inclusions in gear materials

(b) Metal-to-metal contact of asperities or defects due to low lubricant film thickness

(c) Foreign particle contamination of lubricant

1.3.3. Tooth wear

According to ASM handbook [30], ‘‘Gearsets are susceptible to wear caused by adhesion, abrasion, and polishing. Adhesive wear is classified as ‘‘mild” if it is confined to the oxide layers of the gear tooth surfaces. If, however, the oxide layers are disrupted and bare metal is exposed, the transition to severe adhesive wear usually occurs. Scuffing is defined as localized damage caused by solid-phase welding between sliding surfaces. Abrasive wear on gear teeth is usually caused by contamination of the lubricant by hard, sharp-edged particles. If the extreme-pressure anti-scuff additives in the lubricant are too chemically reactive, they may cause polishing of the gear tooth surfaces until they attain a bright mirror finish. Although the polished gear teeth may look good, polishing wear is undesirable because it generally reduces gear accuracy by wearing the tooth profiles away from their ideal form.”

1.3.4. Tooth tip chipping

Gear tooth tip chipping refers to a small piece of material breaking away from the tip of a tooth. According to [31], ‘‘Failures of this kind may be caused by deficiencies in the gear tooth, which results in a high stress concentration at a particular area. Sometimes flaws or minute grinding cracks will propagate under repeated stress cycling and a fracture will eventually develop. Foreign material passing through the gear mesh will also produce short-cycle failure of a small portion of a tooth. High residual stresses due to improper heat treatment can cause local fractures that do not originate in the tooth root section.”

1.3.5. Manufacturing errors

Gear manufacturing errors are generated in the production process of each individual gear, such as profile errors and tooth spacing errors [32]. Cooley and Parker [32] reviewed the investigations on manufacturing errors for planetary gears. Investigations on manufacturing errors for fixed-axis gears and some papers not covered in Ref. [32] for planetary gears have been reviewed in [28].

1.3.6. Research prospects

(a) It is common for gearboxes to work under varying operation condition. Some studies [33-42] have modeled gearbox transmission systems under varying operation condition but the systems do not have damages involved. Very limited work has been accomplished on gearbox damage dynamic modeling under varying operation condition. Only four papers [43-46] have modeled gearbox damage under varying operation condition. More studies are required to model gear faults under varying operation condition.

(b) Simulated vibration signals do not have noise interference. The noise could be from the environment or from some other components in a gear transmission system. The noise effect should be modeled and investigated in developing fault diagnosis techniques.

(c) Some dynamics based fault diagnosis techniques are tested to be effective on one set of data or one experimental test rig. Repeatability tests and tests on multiple machines are required for these techniques to be used in real applications.

1.4. Gearbox fault diagnosis under non-stationary conditions

A gearbox is likely to transit through a run-up or run-down period during start-up and shut-down of the machinery. Therefore, most of the research works on GFD under non-stationary conditions have involved an analysis of gearbox vibration signals under either the run-up or run-down condition of the drive mechanism. In such works, it has been assumed that the velocity of the gearbox drive shaft increases or decreases linearly from one speed to another and hence the angular acceleration remains constant over the considered rotational period. Li et al. [47] employed the angular domain averaging technique for diagnosing gear crack faults during the run-up of gear drive and converted non-stationary signals in the time domain into quasi-stationary signals in the angular domain. Meltzer and Ivanov [48, 49] proposed the time-frequency and the time-quefrency methods to recognize faults in a planetary gearbox during the start-up and run-down processes. Li et al. [50] combined computed order tracking, cepstrum analysis and radial basis function neural network for gear fault detection during the speed-up process. Bafroui and Ohadi [51] converted the non-stationary vibration signals collected under the speed-up process of a gear drive into quasi-stationary signals in the angular domain.

In practical applications, a gearbox is likely to be subjected to variable loads and speeds resulting in fluctuating speed conditions. Research efforts in diagnosing gearbox faults under fluctuating speed conditions, however, are limited. Jafarizadeh et al. [52] proposed a new noise cancelling technique based on time averaging method for asynchronous input and then implemented the complex Morlet wavelet for feature extraction and diagnosis of different kinds of local gear damages. Ahamed et al. [53] devised the multiple pulse independently re-sampled time synchronous averaging (MIR-TSA) technique to diagnose the crack propagation levels in the pinion tooth of a single stage spur gearbox under fluctuating speed conditions. Sharma and Parey [54] proposed the modified time synchronous averaging (MTSA) technique to improve the signal to noise ratio and compared various condition indicators to diagnose gearbox health conditions such as no crack, initial crack and advanced crack under fluctuating speed conditions.

1.4.1. Research prospects

Limited work in GFD has been accomplished under non-stationary conditions even though a gearbox mostly operates under such conditions. Even when the gearbox has been designed to operate at a constant rated speed of rotation, it can be shown that there are still fluctuations in the speed of the gears owing to uncertainties associated with the drive and load mechanisms. Considering this natural propensity of gearbox operation to be non-stationary, more attention is required to be paid to GFD under non-stationary conditions.

1.5. Features used for gearbox fault detection

The time-domain signal acquired from a gearbox usually changes when damage occurs in a gear. Both its amplitude and distribution may be different from those of the time-domain signal of a normal gear. To know the fault appearing phenomenon, condition indictors (CIs) are applied, i.e., statistical measurement of the vibration signal energy is conducted. Sharma and Parey [55] reviewed the various CIs for gearbox fault diagnosis. Some of the commonly employed CIs are listed below:

(a) **Mean value:** the average of the signal.

(b) **Range:** difference between peak to peak or maximum and minimum value of a signal.

(c) **Root mean square (RMS):**

It reflects the vibration amplitude and energy of a signal in the time domain. The RMS is defined as the square root of the average of the sum of squares of the signal samples and is given by [56]:

$$RMS = \sqrt{\frac{1}{n}[\sum_{i=1}^{n}(x_i)^2]} \tag{1.6}$$

where $x_i (i = 1,...,n)$ is i th sampling point of the signal x and n is the number of points in the signal.

(d) **Standard deviation (STD):**

It measures the amount of variation from the mean value and can be expressed as:

$$STD = \sqrt{\frac{1}{n-1}\sum_{i=1}^{n}(x_i - \overline{x})^2} \tag{1.7}$$

where $x_i (i = 1,...,n)$ is i th sampling point of the signal x; n is the number of points in the signal, and $\overline{x}$ is the average of the signal.

(e) **Kurtosis (KR):**

It is the fourth order normalized moment of a given signal x and provides a measure of the peakedness of the signal, i.e. the number of peaks present in the signal. It is given by [56]:

$$KR = \frac{n\sum_{i=1}^{n}(x_i - \overline{x})^4}{(\sum_{i=1}^{n}(x_i - \overline{x})^2)^2} \tag{1.8}$$

(f) **Crest factor (CF):**

It is defined as the ratio of maximum positive peak value of the signal x to RMS [56] and is given by:

$$CF = \frac{\max|x_i|}{\sqrt{\frac{1}{n}\sum_{i=1}^{n}(x_i)^2}} \tag{1.9}$$

It is devised to boost the presence of small number of high-amplitude peaks, such as those caused by some types of local tooth damage.

(g) **Shape factor (SF):**

It is used to represent the time series distribution of the signal in the time domain and is given by [57]:

$$SF = \frac{\sqrt{\frac{1}{n}\sum_{i=1}^{n}(x_i)^2}}{\frac{1}{n}\sum_{i=1}^{n}|x_i|} \tag{1.10}$$

Additional time domain features, which were specifically developed for gear damage detection and reported in several NASA technical reports, [58, 59] but seldom cited in the published literature [60], include FM0, FM4, NA4, NB4, Energy ratio (ER) and energy operator (EOP). The application results to helicopter gearbox systems reported in the NASA reports suggest that these features display different degrees of effectiveness in detecting gear damage. These features are defined as follows [58-61]:

(h) **Zero Order Figure of Merit (FM0):**

It was developed by Stewart in 1977 as a robust indicator of major faults in a gear mesh. Considerable changes in the meshing pattern were found out by comparing the maximum peak-to-peak amplitude of the signal to the sum of the amplitudes of the mesh frequencies and their harmonics. FM0 is given by:

$$FM0 = \frac{PP_x}{\sum_{h=0}^{H} P_h} \tag{1.11}$$

where PP_x is the maximum peak-to-peak value of signal x, P_h is the amplitude of the hth harmonic of the meshing frequency, and H is the total number of harmonics considered.

The shaft frequencies and their harmonics, the meshing frequencies and their harmonics, and all first-order sidebands are defined to be the regular meshing components. By removing the regular meshing components from signal x, the so called difference signal is generated.

(i) **Fourth Order Figure of Merit (FM4):**

It is designed to complement FM0 by detecting damage isolated to only a limited number of teeth and is supposed to work well for detection of initial faults.

$$FM4 = \frac{n\sum_{i=1}^{n}(d_i - \bar{d})^4}{(\sum_{i=1}^{n}(d_i - \bar{d})^2)^2} \tag{1.12}$$

where d_i is the ith measurement of the difference signal of the signal x and $\bar{d}$ is the average of the difference signal. FM4 is actually the kurtosis of the difference signal.

(j) **NA4:**

It was drawn in 1993 by Zakrajsek, Townsend and Decker as a general fault indicator which reacts to damage and continuing growth of the fault as well [62]. Initially, the residual signal r is constructed. The residual signal is generated by removing the regular meshing elements which include the shaft frequencies and their harmonics, and the meshing frequencies and their harmonics. NA4 is given by:

$$NA4 = \frac{\frac{1}{n}\sum_{i=1}^{n}(r_i - \bar{r})^4}{(\frac{1}{N}\sum_{j=1}^{N}(\frac{1}{n}\sum_{k=1}^{n}r_{jk} - \bar{r}_j)^2)^2} \tag{1.13}$$

where r_i is the ith measurement of the residual signal of time record x_i and $\bar{r}$ is the average of r_i, r_{jk} is the kth measurement in the jth time record residual signal r_j, $\bar{r}_j$ is the average of r_j, and N is the number of time records in a run ensemble. The complete data series collected is called a run ensemble. It is further divided into N time records each including n data points. NA4 is created to overcome the shortcoming of FM4 that becomes less sensitive to the progression of fault in both number and severity. For this reason, it is supposed to be able to not only detect the onset of fault, as FM4 does, but also continue to react to the damage as it spreads and increases in magnitude.

(k) **NB4:**

It was developed in 1994 by Zakrajsek, Handschuh and Decker [63] to indicate localized gear tooth fault. Similar to NA4, NB4 also uses the quasi-normalized kurtosis. However, alternative to difference signal, NB4 employs the envelope of the signal bandpass filtered about the mesh frequency. NB4 is given by:

$$NB4 = \frac{\frac{1}{n}\sum_{i=1}^{n}(s_i - \bar{s})^4}{\left(\frac{1}{N}\sum_{j=1}^{N}\left(\frac{1}{n}\sum_{k=1}^{n} s_{jk} - \bar{s}_j\right)^2\right)^2} \tag{1.14}$$

where $s(t)$ is the envelope expressed by $s(t) = \left|b(t) + i\{H[b(t)]\}\right|$, $b(t)$ is the signal bandpass filtered about the meshing frequency, $H[b(t)]$ is the Hilbert transform of $b(t)$, s_{jk} is the k th measurement in the j th time record envelope s_j; $\bar{s}_j$ is the average of s_j, and N is the number of time records in a run ensemble. The theory behind NB4 is that the damage on gear teeth will cause transient load fluctuation that is different from that caused by normal teeth, and that this can be seen in the envelope of the signal.

(l) **Energy ratio (ER):**

ER is defined as the ratio of the root mean squares between the difference signal and the signal containing only regular meshing components. ER is given by:

$$ER = \sqrt{\frac{\frac{1}{n}\sum_{i=1}^{n}(d_i)^2}{\frac{1}{n}\sum_{i=1}^{n}(d_i')^2}} \tag{1.15}$$

where d_i is the i th measurement of the difference signal, and $d_i^{'}$ is the i th measurement of the regular meshing components, which include the shaft frequencies and their harmonics, the meshing frequencies and their harmonics, and all first-order sidebands. ER is designed to increase in the presence of heavy uniform wear.

(m) **Energy operator (EOP):**

An impulse in time averaged vibration signal initiated by damaged gear tooth is supported by the energy operator, thus allowing the impulse to be more easily detected [64].

$$EOP = \frac{n\sum_{i=1}^{n}(re_i - \overline{re})^4}{(\sum_{i=1}^{n}(re_i - \overline{re})^2)^2} \tag{1.16}$$

where re_i equals $x_i^2 - x_{i-1}x_{i+1}$ and is the i th measurement of the resulting signal re, and $\overline{re}$ is the average of the resulting signal. EOP is developed by first calculating the value $x_i^2 - x_{i-1}x_{i+1}$ for every point $x_i (i = 1, 2, ..., n)$ of the signal. The energy operator is then computed by taking the kurtosis of the resulting signal.

(n) **M6A:**

It was proposed by Martin in 1989 as a surface damage indicator for machinery components [59]. The fundamental idea is the same as that of FM4, only the moment is normalized by the cube of the variance. It is expected that M6A will be more sensitive to peaks in the difference signal because of using the sixth moment. M6A is given by:

$$M6A = \frac{N^2\sum_{i=1}^{N}(d_i - \overline{d})^6}{(\sum_{i=1}^{N}(d_i - \overline{d})^2)^3} \tag{1.17}$$

(o) **M8A:**

It was developed for being more sensitive than M6A to peaks in the difference signal [59]. It applies the eighth moment normalized by the variance to the fourth power and is given by:

$$M8A = \frac{N^2 \sum_{i=1}^{N} (d_i - \bar{d})^8}{(\sum_{i=1}^{N} (d_i - \bar{d})^2)^4} \tag{1.18}$$

(p) **Sideband level factor (SLF):**

The sideband level factor [65] is defined as the ratio of sum of the first order sideband about the fundamental gear mesh frequency to the standard deviation of the time signal average.

$$SLF = \frac{\sum_{i=1}^{n} si_{gearmesh \pm i}}{s_{std}} \tag{1.19}$$

Where, si is the amplitude of the i th sideband around the fundamental gear meshing frequency, s_{std} is the standard deviation of the time signal average. For a gearbox in healthy condition, this factor is near zero.

(q) **Sideband index (SI):**

The sideband index [66] is defined as the mean amplitude of the sidebands of the fundamental gear mesh frequency and is given by:

$$SI = \frac{1}{k} \sum_{i=1}^{k} s_{\max_i} \tag{1.20}$$

where k is the number of sidebands and $s_{\max_i}$ is the i th maximum linear amplitude of the sideband. It is a way to measure sidebands in the spectrum for pinion quality for commissioning of gears.

(r) **Impulse indicator (II):**

$$II = \frac{\max(|x_i|)}{\frac{1}{N} \sum_{i=1}^{N} |x_i|} \tag{1.21}$$

(s) **Clearance factor (CF):**

$$CF = \frac{\max(|x_i|)}{(\frac{1}{N}\sum_{i=1}^{N}\sqrt{|x_i|})^2} \tag{1.22}$$

(t) **Mean frequency (MF):**

It is a frequency domain parameter, extracted from the frequency spectrum of the gear vibration signal [67].

$$MF = \frac{1}{K}\sum_{k=1}^{K} X_k \tag{1.23}$$

where X_k is the k th measurement of the frequency spectrum of signal x and K is the total number of spectrum lines. MF indicates the vibration energy in the frequency domain.

(u) **Frequency center (FC)** [67]**:**

$$FC = \frac{\sum_{k=1}^{K} f_k X_k}{\sum_{k=1}^{K} X_k} \tag{1.24}$$

where f_k is the frequency value of the k th spectrum line and X_k is the k th measurement of the frequency spectrum.

(v) **Root mean square frequency ($RMSF$)** [67]**:**

$$RMSF = \sqrt{\frac{\sum_{k=1}^{K} f_k^{\,2} X_k}{\sum_{k=1}^{K} X_k}} \tag{1.25}$$

FC and $RMSF$ show the position changes of the main frequencies.

(w) **Standard deviation frequency (STDF)** [67]**:**

$$STDF = \sqrt{\frac{\sum_{k=1}^{K} (f_k - FC)^2 X_k}{\sum_{k=1}^{K} X_k}} \tag{1.26}$$

STDF describes the convergence degree of the spectrum power.

(x) **Shannon entropy:**

It is a statistical indicator used in the time-frequency domain analysis to describe the distribution of energy of wavelet coefficients of the gear vibration signal. The uncertainty of signal wavelet coefficients is measured by Shannon entropy [52] which is defined by:

$$H_e = -\sum_{j=1}^{J} p_j \log p_j \tag{1.27}$$

where $p_j = E_j / E$ is the percentage of energy of the j th frequency band signal of WPT, where $E = \sum_{j=1}^{J} E_j$.

(y) **Delta RMS:**

This parameter is the difference between two consecutive RMS values [68]. This parameter focuses on the pattern of vibration and is sensitive to vibration signal changes.

Table 1.2

Condition monitoring indicators of time domain and respective fault [55].

Condition indicator	**Fault**
RMS, Delta RMS	General fault progression

Kurtosis	Breakage, wear
Crest factor	Impulsive vibration due to tooth breakage
Energy ratio	Heavy wear (more than one tooth on the gear)
Energy operator	Scuffing, severe pitting
FM0, FM4	Wear/ scuffing/ pitting and tooth bending due to root crack
NA4	Progressive damage (localized to distributed transformation)
SLF	Misalignment
SI	Pinion quality indicator
M6A, M8A	Surface damage indicators
NB4	Localized fault

1.5.1. Research prospects

(a) Many of the established CIs for gearbox fault diagnosis were devised for stationary speed operations. However, for variations in speeds and loads, there may be a change in the performance of a CI, which needs to be taken into account.

(b) Most of the researchers have treated the elements of a gearbox such as bearings, gears and shafts separately. It must be borne in mind that a gearbox is a combination of gears, shafts, bearings and case; hence the whole combination from gears to shafts and shafts to bearings will tend to degrade. Condition indicators that can predict the degradation of the gearbox as a whole entity need to be devised.

(c) Many researchers have illustrated the usefulness of their techniques utilizing their own typical readings for machinery such as helicopters and rolling mills. There is no certainty whether the proposed CIs will still work well for other equipment. Thus, there is a need to perform more investigations with different and mixed fault modes and severities to test the efficacy of the diagnosis indicators.

(d) In certain cases, statistical parameters derived from raw vibration signals may not be efficient in diagnosing the condition of the gearbox. Moreover, parameters found to yield satisfactory results for a particular application may not be suitable for another application. Superior gear fault diagnostic results have been reported with wavelet coefficients being employed directly as inputs to an intelligent classifier [131]. The process of feeding wavelet coefficients directly to an intelligent classifier also eliminates the need to identify statistical parameters with superior gear fault discrimination capability, thereby saving on computational burden.

1.6. Application of AI to gearbox fault diagnosis

An automated method of GFD is desirable such that the condition of the gearbox can be ascertained with minimal intervention of the operator. Before an intelligent classifier such as an ANN can be employed for diagnosing the condition of the gearbox, meaningful parameters representing the gearbox health condition need to be extracted from the gearbox signatures. This feature extraction step usually involves the application of signal processing techniques. This section describes the application of AI in GFD based on the intelligent classifier employed for fault diagnosis. A separate section on signal processing techniques for GFD has been excluded to avoid duplicity.

1.6.1. Back propagation neural network (BPNN)

Various methods of GFD involving BPNNs have been proposed. Rafiee et al. [69] employed a two-layer BPNN to diagnose faults in a 4-speed motorcycle gearbox. The raw vibration signals acquired from the gearbox (motor-driven at a constant rotational speed) under 4 different gear health conditions (normal gear, slightly worn tooth, medium worn tooth and broken tooth) were synchronized using PCHI. The synchronized vibration signals were then decomposed with WPT and the standard deviation values of wavelet packet coefficients at each of the resulting frequency sub-bands utilized as input vectors to the ANN as shown in Fig. 1.2.

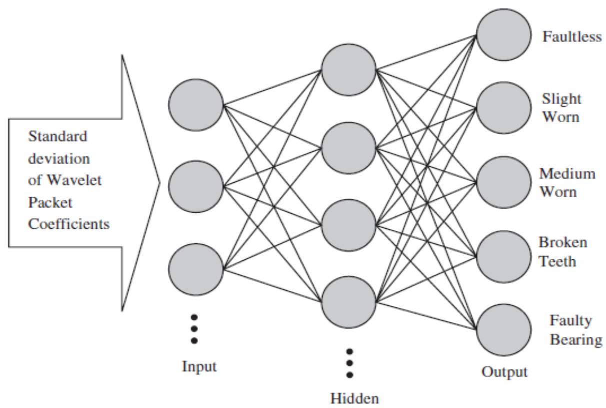

Fig. 1.2. *A two layer MLP neural network for diagnosing gear and bearing faults in a gearbox [69]*

Saravanan and Ramachandran [70] proposed a BPNN for fault diagnosis of a bevel gearbox under various loading and lubrication conditions, utilizing as input feature vectors, the statistical features derived from discrete wavelet transform (DWT) coefficients and identified for their high classification potential using the ID3 decision tree algorithm. Paya et al. [71] applied wavelet transforms to pre-process the vibration signals acquired from a five-speed vehicle gearbox using the ten most dominant features of the faulty signals as input features to a BPNN consisting of 6 output nodes, each node corresponding to a particular gear-bearing condition. Sanz et al. [72] used statistical parameters, sensitive to torsional stiffness decrease and derived from DWT coefficients, as input features to a BPNN to quantify gear damage, considering the mesh stiffness reduction associated with local failures. Bafroui and Ohadi [51] employed a BPNN to diagnose tooth chip and wear in a helical gear pinion during the run-up of a gearbox from idle speed to a steady speed of 2100 rpm. The time domain vibration signals collected under four different pinion health conditions were re-sampled to obtain angular domain signals which were then decomposed into wavelet coefficients using CWT employing the Morlet as the mother wavelet. Statistical parameters derived from wavelet coefficients at each scale were used to train and test the neural network. Superior gear fault classification efficiency was achieved when a reduction in feature set was accomplished by identifying the optimal scales based on energy-Shannon's entropy ratio criterion and when the energy and entropy of the optimal scales were utilized as additional inputs to the neural network. Fig. 1.3 [51] shows the energy-Shannon's entropy ratio for 64 continuous wavelet scales in case of the healthy gear. Scales between 17 and 40 were selected as optimal considering their higher energy-Shannon's entropy ratio compared to the other scales.

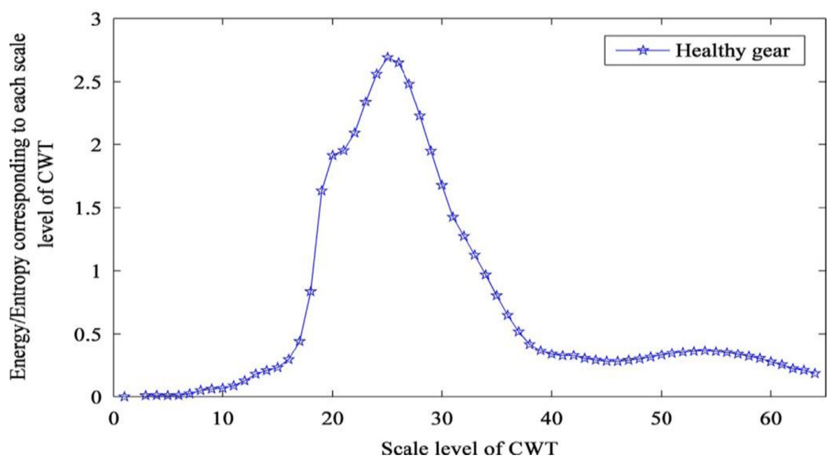

Fig. 1.3 *Distribution of energy to Shannon entropy ratio versus scale level of continuous wavelet transform for healthy gear [51]*

Wu and Fang [73] proposed a fault diagnosis system for a mechanical reducer gear-set using Wigner-Ville distribution for feature extraction and compared the fault recognition capability of the general regression neural network and the conventional BPNN. Tang et al. [74] compared the

Levenberg-Marquardt neural network with the conventional BPNN and found the former to have reduced training epochs and superior gear fault diagnostic accuracy. Yang et al. [75] adopted wavelet denoising for the vibration signals acquired from a wind turbine gearbox, using a classical BPNN to identify four typical gearbox faults. Sanchez et al. [76] devised a gearbox failure classifier based on a BPNN to identify four different failure conditions viz., gear tooth breakage, gear misalignment, pinion with face wear and pinion pitting, under different load and speed conditions, using time and frequency domain statistical parameters as input to the neural network. Xiang et al. [77] adopted the wavelet BPNN utilizing the energy of each sub-band, obtained from wavelet analysis of the vibration signal, as the input feature vector to a BPNN with the objective of identifying different gear conditions such as normal, wear and broken tooth. Shang et al. [78] proposed an improved genetic search strategy to select fault features so as to reduce the dimension of feature vector set obtained from order spectrum analysis of vibratory signal. The selected feature vector sets were input into the BPNN for fault identification and classification of a newly assembled automobile transmission.

1.6.2. Radial basis function (RBF) neural network

Another form of ANN that has been successfully employed for diagnosing faults in gearboxes is the RBF neural network. The construction of an RBF network, in its most basic form, involves three layers with entirely different roles. The input layer is made up of source nodes (sensory units) that connect the network to its environment. The second layer, the only hidden layer in the network, applies a non-linear transformation from the input space to the hidden space. According to Cover [79], a complex pattern-classification problem cast in a high-dimensional space nonlinearly is more likely to be linearly separable than in a low-dimensional space. Thus, in most applications the hidden space is of high dimensionality. The output layer is linear, supplying the response of the network to the activation pattern (signal) applied to the input layer.

Wuxing et al. [80] employed an RBF neural network for fault diagnosis of a helical gear train using third order cumulants of the temporal vibration signals as the input feature vectors. Li et al. [81] applied order cepstrum to the vibration signals acquired under speed-up condition of a gearbox to diagnose normal, wear and crack fault conditions as outputs of an RBF network. In [82], bi-spectrum analysis was applied to the vibration signals of a marine gearbox to extract feature vectors which were classified using BPNN and RBF network. Li et al. [50] combined computed order tracking, cepstrum analysis and RBF neural network for gear fault detection during the speed-up process.

1.6.3. Self organizing maps (SOM)

Several researchers have utilized SOM neural networks to diagnose faults in gear systems. The SOM has the desirable property of topology preservation. In a topology-preserving mapping, nearby input patterns should activate nearby output units on the map. The basic network architecture of Kohonen's [83] SOM consists of a two dimensional array of units, each connected to all n input nodes. Each neuron computes the Euclidean distance between the input vector and the stored weight vector. The SOM is a special type of competitive learning network that defines a spatial neighborhood for each output unit. Initial neighborhood size is often set to one half to two thirds of the network size and shrinks over time according to a schedule (for example, an exponentially decreasing function). During competitive learning, all the weight vectors associated with the winner and its neighboring units are updated. The design parameters include the dimensionality of the neuron array, the number of neurons in each dimension, the shape of the neighborhood, the shrinking schedule of the neighborhood, and the learning rate.

Cheng et al. [84] employed an SOM neural network for GFD using features extracted from Hilbert transform of the IMFs. Yu et al. [85] presented a method of gear multi-fault diagnosis based on autoregressive model and SOM neural networks for diagnosing nine different gear working conditions such as normal, single crack, single wear, compound fault of wear, spalling etc. and found the proposed method to be feasible for early and combined gear faults classification. Yu et al. [86] adopted an SOM-BP composite neural network with the preliminary pattern recognition classification for training samples achieved by the SOM network and details of fault classification accomplished by the BP network.

1.6.4. Support vector machines (SVMs)

Support vector machines (SVMs) have recently been successfully employed for GFD and superior results than ANNs have been reported by several researchers. SVMs have their foundation in the statistical learning theory [87]. The basic SVM deals with the two-class problem where the data are separated by a hyperplane defined by a number of support vectors. The SVM can be considered to create a line or hyperplane between two sets of data for classification. In case of two-dimensional situation, the action of the SVM can be explained easily without any loss of generality. The SVM attempts to place a linear boundary between the two different classes and orient it in such a way that the margin is maximized. The SVM tries to orient the boundary such that the distance between the boundary and the nearest data point in each class is maximal. The boundary is then placed in the middle of this margin between the two points. The nearest data points are used to define the margins and are known as support vectors (SVs). Once the SVs are selected, the rest of the feature set can be discarded since the SVs contain all the necessary information for the classifier.

Bansal et al. [88] applied SVM to multiclass GFD using the gear vibration signals and based on frequency domain data. Bordoloi and Tiwari [89] applied SVM to multi-fault classification of gears with statistical features extracted from wavelet transforms and SVM parameters optimized by the grid-search method, GA and artificial bee colony algorithm. SVM was employed by Bordoloi and Tiwari [90] for multi-fault classification of gears using frequency domain data of the vibration signals, the SVM parameters being optimized using the same evolutionary algorithms. Wu et al. [91] employed the SVM to classify the vibration patterns of a gear transmission system, using as the input features, the energy distribution at the normalized dimensionless frequencies calculated based on the rotational speed of shaft and the instantaneous frequencies of IMFs decomposed by the EMD process. Shen et al. [92] proposed a fault diagnosis model based on EMD and multi-class transductive SVM to diagnose faults in a gear reducer with insufficient number of labeled samples. Zamanian and Ohadi [93] applied linear SVM to GFD using a method of feature extraction based on maximization of local Gaussian correlation function of wavelet coefficients and the signal. Saravanan et al. [94] compared the ANN and proximal SVM in fault classification of a bevel gear box using the J48 algorithm to select predominant statistical features derived from Morlet wavelet coefficients. Implementing a similar method for feature extraction and selection, Saravanan et al. [95] compared the relative efficiency of SVM and proximal SVM in gear fault classification while Saravanan & Ramachandran [96] considered a fast single-shot multiclass proximal SVM for fault diagnosis of a gear box consisting of twenty four classes. Tang et al. [97] employed Shannon wavelet SVM for fault identification of a wind turbine gearbox using a manifold learning algorithm called orthogonal neighborhood preserving embedding (ONPE) to compress the high-dimensional feature set into low-dimensional eigenvectors which were input to the SVM. Wenyi et al. [98] proposed a wind turbine gearbox fault diagnosis method based on diagonal spectrum and clustering binary tree SVM. Jiang et al. [99] constructed a multi-fault SVM classifier based on binary classifiers for GFD and found the classifier to have good classification ability and high efficiency, suitable for online diagnosis of mechanical systems. Yang et al. [100] compared the efficiencies of ANN and SVM in diagnosing faults in a power generation industry gearbox using time domain statistical parameters extracted from WPT of the acquired vibration signal, implementing the compensation distance evaluation technique to select optimal features via sensitivities ranking. Gao et al. [101] decomposed the fault signals with WPT and implemented SVM for gear pitting identification using changes in the energy percentage of the frequency bands as the fault index. Ma et al. [102] applied SVM to identify three individual fault modes, viz., no fault gear mode, crack of dedendum mode and tooth surface abrasion mode in a gear system at two different rotational speeds. Li et al. [103] developed a complete system including signal processing, feature extraction, feature selection and gear fault classification using the wavelet transform, the entropy, the mutual information and the least-square SVM. Zhang et al. [104] implemented a GFD scheme based on EMD of the acceleration vibration signals using the entropy of singular values as the fault characteristic input vectors to an SVM. Kang et al. [105] presented an intelligent method for GFD utilizing the standard deviations of wavelet packet coefficients of the vibration signals, normalized and dimension-deducted using principal component analysis, as the feature vector for training the SVM with the parameters of SVM optimized using particle swarm optimization (PSO). Samanta [106] compared the performance of ANNs and SVMs in GFD without and with GA-based selection of features and classifier parameters. The number of nodes in the hidden layer, in case of ANNs, and the RBF kernel parameter, in case of SVMs, along with the selection of input features were optimized using GAs. Chen et al. [107] developed immune GA to determine the optimal parameters for a wavelet SVM with feature vectors for fault diagnosis obtained from vibration signal preprocessed by EMD.

1.6.5. Fuzzy inference system (FIS)

A fuzzy inference system uses fuzzy set theory to map inputs (features in case of fuzzy classification) to outputs (classes in the case of fuzzy classification). An FIS employing fuzzy if-then rules can model the qualitative aspects of human knowledge and reasoning processes without employing precise quantitative analysis. An FIS consists of five functional blocks: a rule base containing a number of fuzzy if-then rules, a database which defines the membership functions of the fuzzy sets used in the fuzzy rules, a decision-making unit which performs the inference operations on the rules, a fuzzification interface which transforms the crisp inputs into degrees of match with linguistic values and a defuzzification interface which transforms the fuzzy results of the inference into a crisp output. Usually, the rule base and the database are jointly referred to as the knowledge base. The functional blocks of an FIS are depicted in Fig. 1.4.

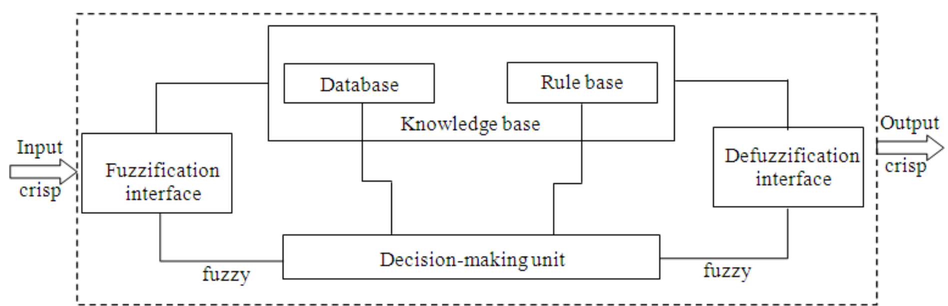

Fig. 1.4. *Fuzzy inference system*

Fuzzy reasoning (inference operations upon fuzzy if-then rules) consists of fuzzification (comparing the input variables with the membership function on the premise part to obtain the membership values of each linguistic label), combining (through a specific T norm operator such as multiplication or min) the membership values on the premise part to get the firing strength (weight) of each rule and finally generating the qualified consequent (either fuzzy or crisp) of each rule depending on the firing strength.

Wu and Hsu [108] proposed an FIS for fault identification of a gear-set experimental platform after applying DWT to the vibration signals for feature extraction. Saravanan et al. [109] proposed a fuzzy classifier to identify defects in a bevel gear box under various loading and lubrication conditions utilizing the decision tree algorithm to extract features and to generate a rule set automatically from the extracted feature set.

1.6.6. Genetic algorithm (GA)

Genetic algorithm (GA) provides a learning method motivated by an analogy to biological evolution. GA has been successfully employed in intelligent GFD to select the input features with high classification potential from a high dimensional feature vector thereby eliminating redundant features. The numbers of hidden neurons in ANNs as well as SVM classifier parameters have been optimized with GA. The algorithm involves initializing a current population P consisting of p hypotheses generated at random [110]. Hypotheses in GAs are often represented by bit strings, so that they can be easily manipulated by genetic operators. Each hypothesis h in P is evaluated for its fitness by computing a fitness function $Fitness(h)$. The process forms a generate-and-test beam-search of hypotheses, in which the best current hypotheses are most likely to be considered for the new population. A new population P_s is then generated by probabilistically selecting the fittest individuals from the current population. Some of these selected individuals are carried forward into the next generation population intact. Others are used as the basis for creating new offspring individuals by applying genetic operations such as crossover and mutation. Crossover takes two parent hypotheses from the current generation and creates two offspring hypotheses by recombining portions of both parents. A fraction of the population r is to be replaced by crossover at each step. As long as the best fitness value amongst all hs in P is lesser than a threshold value, a new generation P_s is created by probabilistically selecting $(1-r)p$ members of P and adding them to P_s. The probability of selecting hypothesis h_i from P is given by

$$\Pr(h_i) = \frac{Fitness(h_i)}{\sum_{i=1}^{p} Fitness(h_j)} \tag{1.28}$$

Crossover operator is applied to $\frac{r.p}{2}$ pairs of hypotheses from P. The crossover operator produces two new offspring from two parent strings, by copying selected bits from each parent. The bit at position i in each offspring is copied from the bit at position i in one of the two parents. All offspring thus generated are added to P_s. A certain percentage of members of P_s with uniform probability are mutated by inverting one randomly selected bit in their representations. The current population P is thus updated by the new population P_s. Again, each h in P, is evaluated for $Fitness(h)$ and the hypotheses from P that has the highest fitness function is returned. Thus, GAs generate successor hypotheses by repeatedly mutating and recombining parts of the best currently known hypotheses.

Yang et al. [111] applied GAs to select the significant input features to the BPNN for GFD using time domain statistical parameters extracted from WPT of the vibration signal. Tang et al. [112] applied an ANN for gear fault diagnosis using the Niche technique based on crowding mechanism in GA and adopted a punishing function to adjust the individual fitness so as to promote global search capability. Hajnayeb et al. [113] designed a system for GFD based on ANNs optimizing the system by eliminating unimportant features using a feature selection method called the UTA method and verified it to be as accurate as GA despite its simple algorithm. Lei et al. [2] proposed a multidimensional hybrid intelligent diagnosis method combining multiple classifiers based on several classification algorithms and input features with GA to identify different categories and levels of gear damage automatically. Hilbert transform, WPT and EMD were performed on gear vibration signals to extract additional fault characteristic information. Then, multidimensional feature sets including time-domain, frequency-domain and time–frequency-domain features were generated to reveal gear health conditions.

1.6.7. Adaptive neuro-fuzzy inference system (ANFIS)

Considering that no standard method exists for transforming human knowledge or experience into the rule base of an FIS and the need for effective methods for tuning the membership functions, an architecture called ANFIS was proposed to serve as a basis for constructing a set of fuzzy if-then rules [114, 115]. The ANFIS is a fuzzy Sugeno model put in the framework of adaptive systems to facilitate learning and adaptation. Such framework makes the ANFIS modeling more systematic and less reliant on expert knowledge.

ANFIS has been successfully employed in the field of gearbox fault diagnosis. Wu et al. [116] employed discrete wavelet transform and ANFIS to identify gear fault positions and to classify various gear fault conditions. Attoui et al. [117] applied discrete wavelet packet transform and principal component analysis for feature extraction along with ANFIS for fault classification of a gearbox. Zhang et al. [118] employed a neuro-fuzzy ensemble to diagnose faults such as normal, slight worn, medium worn and broken tooth in a motorcycle gearbox. Ali Soleimani [119] compared the gear fault identification capability of ANN and ANFIS utilizing the standard deviation values of wavelet packet coefficients as inputs to the classifiers. Amongst numerous applications, ANFIS has been successfully employed in the field of biomedical engineering [120, 121], transmission line fault detection [122] and fault diagnosis of rotating machinery [123-127].

1.6.8. Research prospects

(a) Considering the influence of fast varying load and rotational speed on vibration signals, there is a need to develop methods which can solve the problem of condition monitoring and fault diagnosis under varying load-speed operations.

(b) Vibration signals have been widely utilized in monitoring and diagnosing gearboxes, thanks to their ease of measurement and the rich information they contain. The application of artificial intelligence in diagnosing gearbox faults through an analysis of sound emission signatures needs to be explored.

(c) Many researchers have demonstrated the effectiveness of their methods using their own typical data in detecting faults in gearboxes. However, there is no certainty that these methods will work well for other data. Conducting more experiments with different fault modes and severities is necessary to test the robustness of new diagnosis methods. Moreover, there is a need to devise gear fault diagnosis methods that can be implemented on different types of gearboxes.

1.7. Gearbox fault diagnosis based on an analysis of sound emission signatures

Most of the research efforts directed towards GFD are based on an analysis of vibration signals acquired from the gearbox. The sound emission signals may serve as an alternative to vibration signals when diagnosing the condition of the gearbox. Limited work has been accomplished on GFD based on an analysis of sound emission signatures, though promising results have been reported by some researchers. Baydar and Ball [128] carried out a comparative study of sound emission and vibration signals in detection of gear failures using Wigner-Ville distribution. Sound emission signals were found to be very effective for early detection of gear faults. In [129], Baydar and Ball examined whether sound emission signals can be used effectively along with vibration signals to detect various local faults such as tooth crack and tooth breakage in gearboxes using wavelet transform. The results suggested that sound emission signals were very effective for early detection of faults and to indicate various types of progressing faults in gearboxes. Wu and Chan [130] compared the gear fault diagnostic accuracy of a BPNN and probabilistic neural network utilizing sound emission signatures acquired from a gear-set platform. A CWT technique combined with a feature selection of energy spectrum was proposed for analyzing fault signals in the gear-set platform. The experimental results pointed out that sound emission signals can be used to monitor the condition of the gearbox.

1.8. Summary

Considering their widespread application and significance in power transmission, numerous research efforts have been devoted with the objective of devising new and effective methods of GFD. Section 1.2 introduces the various techniques employed for GFD along with the characteristic frequencies of a fixed axis gearbox. Dynamic modeling of gearbox faults such as tooth crack, tooth pitting/ spalling, tooth wear, tooth tip chipping and manufacturing errors is the subject of Section 1.3. Section 1.4 summarizes some of the research efforts in GFD under non-stationary conditions. Even though a gearbox mostly operates under non-stationary conditions, research in GFD under non-stationary conditions still merits attention. Various condition indicators employed for ascertaining the condition of the gearbox have been summarized in Section 1.5. These parameters, extracted from the time domain, frequency domain or the time-frequency domain, represent the condition of the gearbox with varying degrees of effectiveness. The application of AI to GFD has been summarized in Section 1.6. AI paves the path towards automated GFD. However, meaningful parameters representing the gearbox health condition need to be extracted from the acquired gearbox signatures before an intelligent classifier can be employed to diagnose the condition of the gearbox. This usually involves the application of signal processing techniques. Promising results have been obtained when parameters from the time-frequency domain are employed as inputs to an intelligent classifier. Further, limited work, as highlighted in Section 1.7, has been accomplished on an analysis of sound emission signatures to diagnose the condition of a gearbox, though promising results have been reported by some researchers. Further potential lies in the analysis of sound emission signatures to diagnose gearbox faults and needs to be explored.

1.9. Objectives of the present study

Since a gearbox mostly operates under non-stationary conditions, there is a need to devise a simple yet effective method of GFD under non-stationary conditions. At times, a gearbox designed to operate at a constant speed of operation may be subjected to varying loads which may cause speed fluctuations. Under such non-stationary conditions, techniques such as conventional time synchronous averaging cannot be directly applied. Thus, another method of improving the signal to noise ratio needs to be devised.

A considerable amount of research effort has been devoted towards identifying statistical parameters with superior fault discrimination capability. The statistical parameters found to have superior gear fault identification potential in case of a particular gearbox may not work well for another gearbox. Promising results in GFD have been reported when coefficients obtained in the time-frequency domain are employed directly as inputs to an intelligent classifier. It is to be ascertained whether the method of feeding wavelet coefficients directly to an intelligent classifier, such as an ANN, yields superior gear fault diagnostic results.

Most of the literature on GFD is based chiefly on an analysis of vibration signals acquired from the gearbox under healthy and faulty conditions. Considering the limited work accomplished in GFD through an analysis of the acquired sound emission signatures, there is a need to explore the possibility of diagnosing the condition of a gearbox through an analysis of the sound emission signatures and to compare the results with those obtained through an analysis of the vibration signals acquired from the gearbox.

Limited work has been accomplished on the application of hybrid intelligent classifiers such as ANFIS to GFD. There is a need to explore the possibility of employing such hybrid classifiers to diagnose the condition of a gearbox. Very often the GFD methods that work for a particular gearbox do not work well for another gearbox. Therefore, there is a need to devise a method that is effective at diagnosing faults in different types of gearboxes.

Based on the research gaps identified above, the objectives of the present research are as follows:

(a) To study the application of an ANN in diagnosing gearbox faults under fluctuating load conditions.

(b) To study the application of an ANN in diagnosing gearbox faults under non-stationary conditions arising from uncertainties associated with the drive and load mechanisms.

(c) To study the gear fault diagnostic accuracy of an ANN through an analysis of gearbox vibration and acoustic signatures.

(d) To study the application of an ANFIS classifier in diagnosing gearbox faults through an analysis of the non-stationary gearbox acoustic signatures.

(e) To study the application of an ANFIS classifier in diagnosing gearbox faults through an analysis of the non-stationary vibration signatures and to verify the efficacy of the proposed method by applying the technique to another gearbox.

1.10. Organization of the thesis

Chapter 2 is based on GFD under fluctuating load conditions applying the independent angular re-sampling (IAR) technique, continuous wavelet transform and ANN. Chapter 3 of the thesis focuses on GFD under non-stationary conditions with IAR technique applied to vibration and sound emission signals. Gearbox fault diagnosis using acoustic signals, continuous wavelet transform and adaptive neuro-fuzzy inference system is the subject of Chapter 4. Chapter 5 focuses on fault diagnosis of a bevel and spur gearbox based on vibration signals using continuous wavelet transform and adaptive neuro-fuzzy inference system. The thesis ends with a conclusion and scope for further research.

Chapter 2

Gearbox Fault Diagnosis under Fluctuating Load Conditions with IAR technique, CWT and MLP Neural Network

2.1. Introduction

The gearbox forms an integral part a vast majority of machines and great attention has been directed towards fault diagnosis of gearboxes to prevent unexpected breakdown and possible loss of life. Gearbox failure in certain critical applications such as single engine aircraft and propulsion systems of warships is totally unacceptable.

A gearbox is likely to transit through a run-up or run-down period during start-up and shut-down of the machinery. Therefore, most of the research works on gearbox fault diagnosis under non-stationary conditions have involved an analysis of gearbox vibration signals under either the run-up or run-down condition of the drive mechanism. In such works, it has been assumed that the velocity of the gearbox drive shaft increases or decreases linearly from one speed to another and hence the angular acceleration remains constant over the considered rotational period. Li et al. [47] employed the angular domain averaging technique for diagnosing gear crack faults during the run-up of gear drive and converted non-stationary signals in the time domain into stationary signals in the angular domain. Meltzer and Ivanov [48, 49] proposed the time-frequency and the time-quefrency methods to recognize faults in a planetary gearbox during the start-up and run-down processes. Li et al. [50] combined computed order tracking, cepstrum analysis and radial basis function neural network for gear fault detection during the speed-up process. Bafroui and Ohadi [51] converted the non-stationary vibration signal collected under the speed-up process of a gear drive into quasi-stationary signals in the angular domain. Further, a range of optimal scales was identified based on the energy-Shannon's entropy ratio of the wavelet coefficients.

In practical applications, a gearbox is likely to be subjected to variable loads and speeds resulting in fluctuating speed conditions. Research efforts in diagnosing gearbox faults under fluctuating speed conditions, however, are limited. Jafarizadeh et al. [52] proposed a new noise cancelling technique based on time averaging method for asynchronous input and then implemented the complex Morlet wavelet for feature extraction and diagnosis of different kinds of local gear damages. Ahamed et al. [53] devised the multiple pulse independently re-sampled time synchronous averaging (MIR-TSA) technique to diagnose the crack propagation levels in the pinion tooth of a single stage spur gearbox under fluctuating speed conditions. Sharma and Parey [54] proposed the modified time synchronous averaging (MTSA) technique to improve the signal to noise ratio and compared various condition indicators to diagnose gearbox health conditions such as no crack, initial crack and advanced crack under fluctuating speed conditions.

Recently, promising results in gearbox fault diagnosis have been reported with wavelet coefficients being utilized directly as input feature vectors to an intelligent classifier rather than utilizing statistical parameters derived from raw vibration signals. Jedlinski and Jonak [131] compared the gear fault diagnosis accuracy of support vector machines and multilayer perceptron neural networks feeding continuous wavelet coefficients directly into the two classifiers. Optimal scales were selected as those over which significant changes in frequency were identified in the wavelet amplitude maps. A superior gear fault diagnostic accuracy was obtained when continuous wavelet coefficients, rather than statistical parameters derived from the raw vibration signals, were fed into the classifiers.

A gearbox is expected to operate under non-stationary conditions for most of its useful life owing to fluctuations in load-speed conditions and as a result of uncertainties associated with the drive and load mechanisms. A gearbox is capable of transmitting torque even when eccentricity is introduced between one of the shafts and the gear. This Chapter attempts to diagnose faults in an eccentric single stage spur gearbox under fluctuating load conditions and employs the independent angular re-sampling (IAR) technique to synchronize such signals from the revolution point of view. In the present work, segments of the vibration signals corresponding to 30 complete revolutions are selected and synchronized. The synchronized vibration signals are then decomposed with continuous wavelet transform and the classification accuracy of a multilayer perceptron neural network compared for two different feature sets viz., continuous wavelet coefficients (CWCs) from all scales are fed to the ANN and CWCs from only the optimal scales (based on energy-Shannon's entropy ratio) are fed to the ANN for fault classification. Fig. 2.1 shows the flowchart for the proposed gear fault diagnostic procedure.

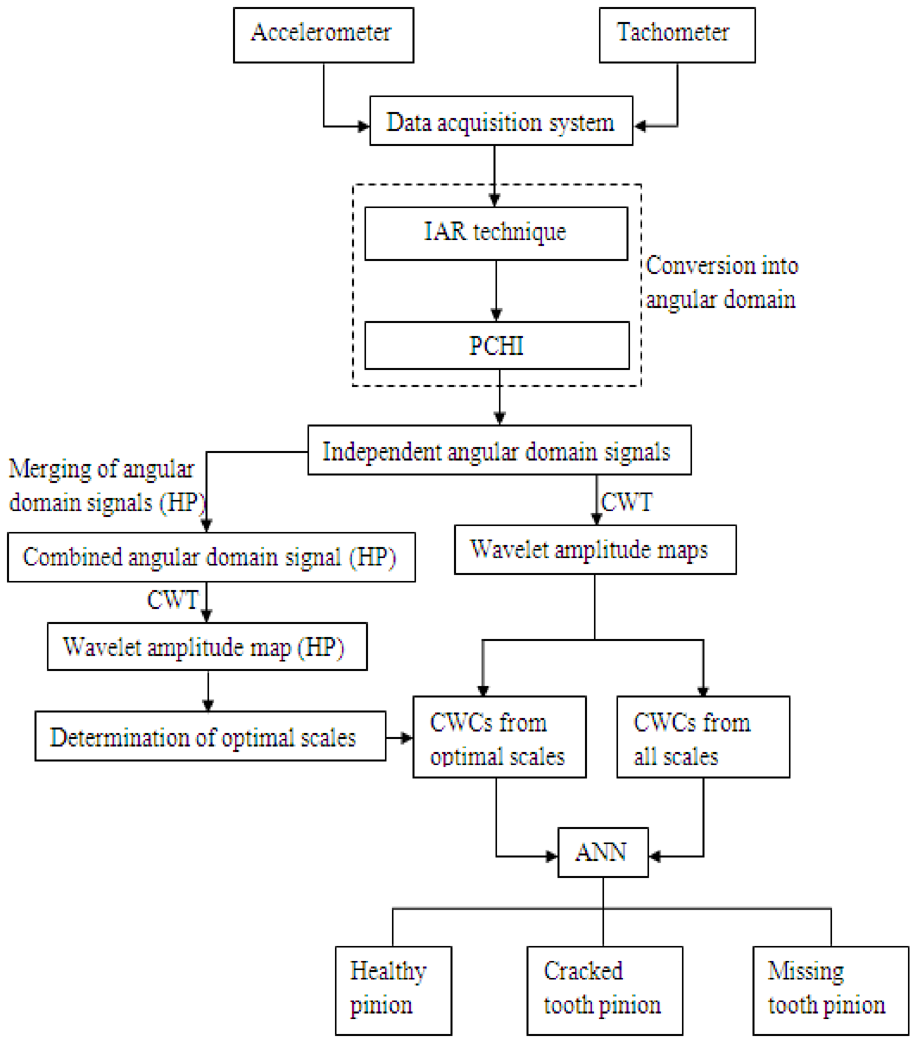

Fig. 2.1. *Flowchart of the proposed gear fault diagnostic procedure*

The remainder of this Chapter is organized as follows: The experimental set-up and data acquisition system are described in Section 2.2. Section 2.3 explains the independent angular re-sampling technique which is employed in the present work to convert non-stationary signals in the time domain into quasi-stationary signals in the angular domain. A brief introduction to continuous wavelet transform is given in Section 2.4. Determination of optimal scales based on energy-Shannon's entropy ratio of continuous wavelet coefficients is the subject of Section 2.5. Section 2.6 gives a brief introduction to the back propagation neural network. The experimental results are discussed in Section 2.7 and concluding remarks drawn in Section 2.8.

2.2. Experimental set-up and data acquisition

The experimental set-up consists of a single stage spur gearbox that forms an integral part of the drive train diagnostic simulator (DDS) shown in Fig. 2.2 (a). The DDS gearbox consists of a 32-tooth pinion in mesh with an 80-tooth gear mounted on the output shaft. The pinion is mounted on a shaft driven by a 3Φ, 3HP, 0-5000 rpm synchronous motor while the output torque produced the magnetic particle brake ranges from 4-220 lb-in (0% to 100%). The DDS allows both the speed profile as well as the load profile to be programmed. In the present work, the speed of the gearbox drive shaft is maintained constant at 15 Hz while the load at the output is programmed to fluctuate in a sinusoidal manner between 0% and 40%, i.e., between 4 and 88 lb-in. The load fluctuations at the output coupled with eccentricity between the output shaft and the gear result in speed fluctuations. The objective of the present work is to diagnose gear faults such as a cracked and missing tooth under fluctuating speed conditions.

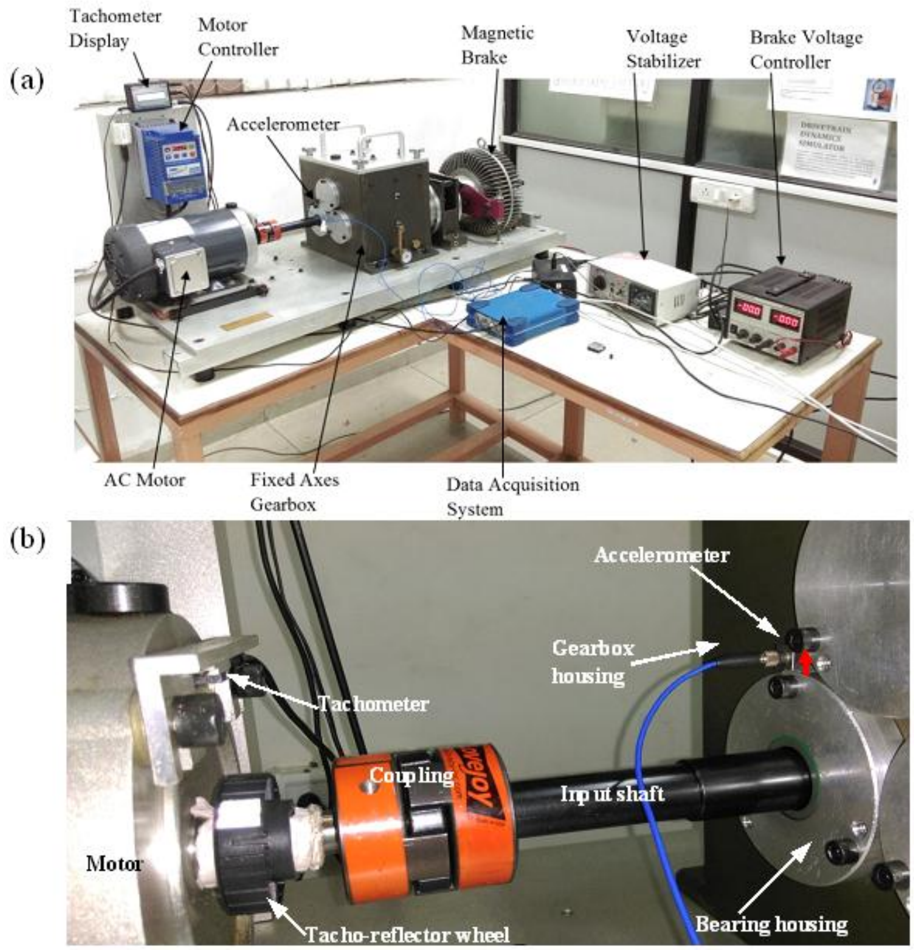

Fig. 2.2. *(a) Drive train diagnostic simulator (DDS) and (b) sensor arrangement*

The most common gear diagnosis method is to analyze the vibration signals obtained from the machinery, specifically the shafts containing the gears [53]. The uni-axial accelerometer for acquiring the vibration signal is mounted on the bearing housing of the gearbox input shaft to measure vibration signals along the vertical axis (z-axis) as shown in Fig. 2.2 (b). The multiple pulse tachometer arrangement is facilitated by mounting a multiple strip tacho-reflector wheel on the motor output shaft. The accelerometer and tachometer are interfaced to a PC via a data acquisition system.

Vibration signatures are acquired under sinusoidal load fluctuations (0% to 40%) under three different gearbox health conditions, viz., healthy pinion (HP), pinion with a cracked tooth (CT) and pinion with a broken/ missing tooth (MT). Eccentricity between the output shaft and the gear remains undisturbed in each case. The various pinion wheels employed for the experiment are shown in Fig. 2.3.

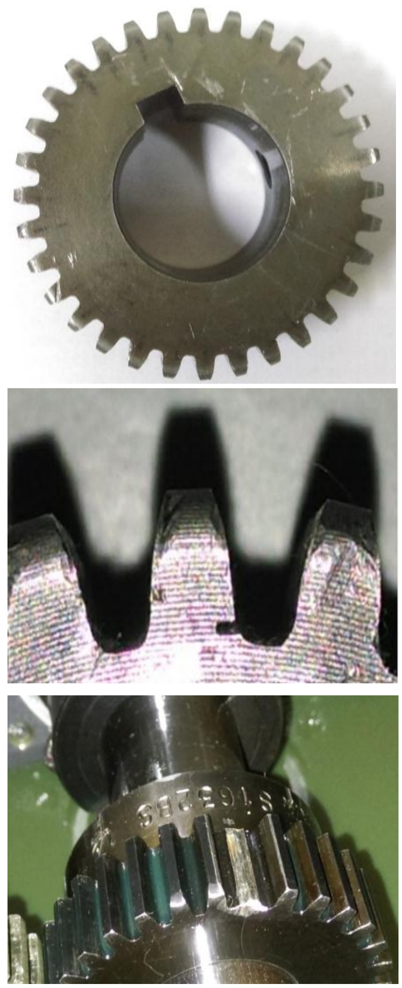

Fig. 2.3. *(a) Healthy pinion (HP), (b) cracked tooth (CT) pinion and (c) missing tooth (MT) pinion*

For simplicity, as well as to keep the computational burden under control, only segments of vibration signals during which the gearbox drive shaft undergoes 30 complete revolutions have been considered for analysis. Fig. 2.4 (a) shows the vibration signal collected from a healthy gearbox over 30 randomly selected consecutive revolutions when the load at the output shaft is made to fluctuate in a sinusoidal manner between 0% and 40%. Eccentricity between the output shaft and the gear results in an impulsive nature of the gearbox vibration signal. Diagnosing gearbox faults embedded in signals masked by impulses arising from eccentricity poses a challenge and is the subject of the present work. Fig. 2.4 (b) shows the time taken for each of the 30 revolutions of the gearbox drive shaft. Variation in speed as a result of load fluctuations is evident from Fig. 2.4 (b) as the time elapsed is not the same for each revolution.

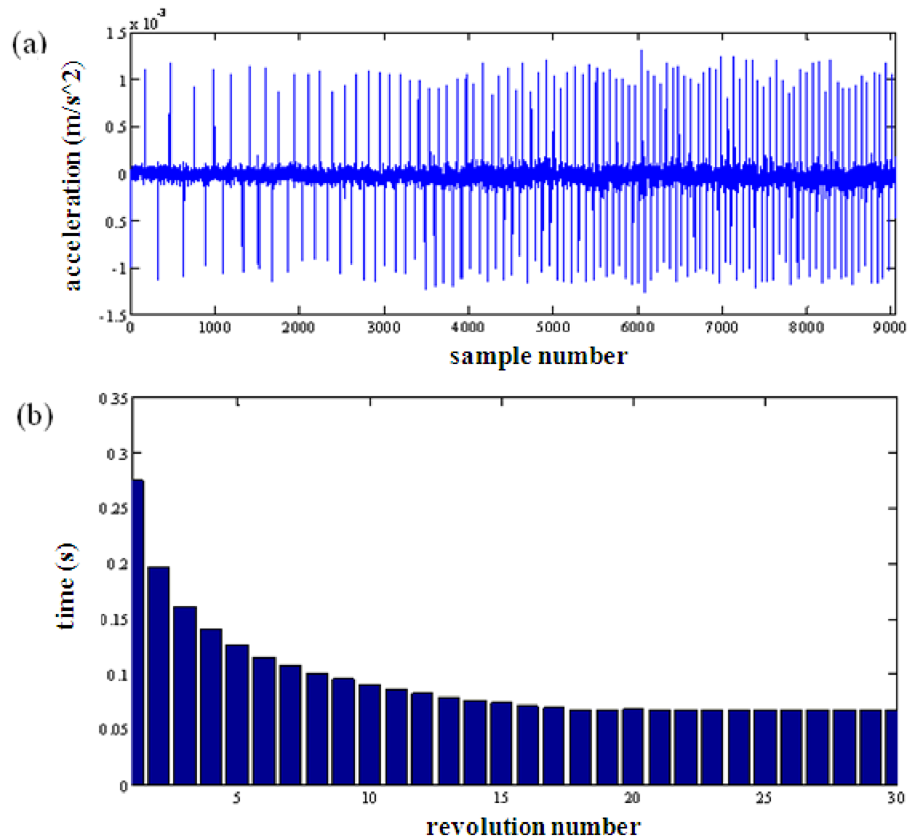

Fig. 2.4. *(a) Vibration signal acquired over 30 complete revolutions of the healthy pinion and (b) time taken for each revolution*

The time domain vibration signals acquired from the gearbox can be converted into the angular domain employing the independent angular re-sampling technique as explained in Section 2.3.

2.3. Independent angular re-sampling (IAR) technique

A standard electrical tachometer generates a pulse once per revolution by receiving light reflected from a single reflective strip mounted on the shaft. The output, generated in terms of pulse versus time, indicates the speed of rotation in revolutions per minute (rpm) of the shaft. The occurrence of a fault in a geared system is usually identified by comparing the vibration or sound emission signals collected under the fault and no-fault conditions. The vibration or sound emission signal acquired using the accelerometer or microphone is sampled at a pre-defined sampling frequency. A constant speed of rotation is characterized by an equal number of samples between tachometer pulses (though an equal number of samples between tachometer pulses does not necessarily imply a constant speed of rotation). Variation in the number of the samples between successive tachometer pulses indicates fluctuations in speed.

Sinusoidal load fluctuations at the output along with uncertainties associated with the drive and load mechanisms inevitably produce speed fluctuations. If, however, a very small segment of the overall speed profile, representing only a single revolution of the gearbox drive shaft, is taken into consideration, it may be assumed linear. This is the basis of the IAR technique.

Most of the research efforts in GFD under the speed-up process assume constant angular acceleration over the complete speed-up period, the angular rotation being defined by Eq. (2.1) [47].

$$\theta(t) = b_0 + b_1 t + b_2 t^2 \tag{2.1}$$

where b_0, b_1 and b_2 are constants to be determined based on the angular positions at three different time instants. As a novel method, in this work it has been assumed that the angular acceleration remains constant during each independent revolution of the gearbox drive shaft. This implies that the shaft angular velocity may increase or decrease linearly or remain constant during a given revolution. The underlying assumption of a linear variation in velocity during each revolution is based on the fact that the velocity profile of each revolution can be represented by a very small segment of the overall velocity profile and may be represented by a straight line. Accordingly, the value of angular acceleration may vary from one revolution to another. For example, a constant angular velocity during a revolution would be characterized by a value of zero angular acceleration for that revolution.

The objective of employing the IAR technique is to convert non-stationary signals in the time domain into a number of quasi-stationary signals in the angular domain. The original time domain signal is split into a number of segments, each representing one revolution of the gearbox drive shaft. In order to convert into the angular domain, the IAR technique demands that the constants b_0, b_1 and b_2 in Eq. (2.1) be determined independently for each revolution. This requires that the instants of time at three different shaft angular positions be known. This is accomplished experimentally by mounting an additional reflective strip on the tacho-reflector wheel at $110°$ from the reference strip. The resultant multiple pulse tachometer arrangement, therefore, enables determination of time instants at three different shaft angular positions during a revolution. The next revolution is assumed to commence immediately after the pulse marking the end of a revolution is generated as demonstrated in Fig. 2.5.

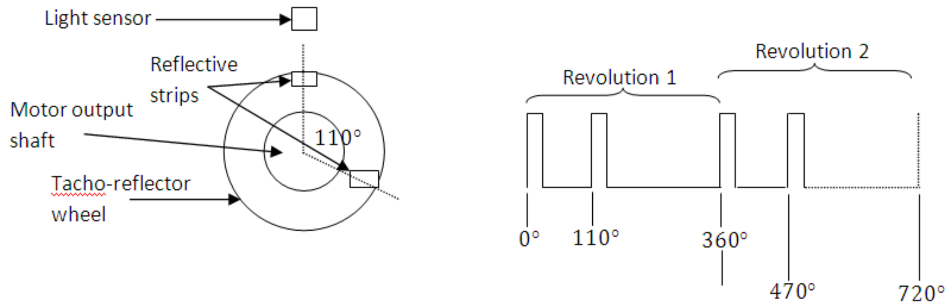

Fig. 2.5. *Multiple pulse tachometer arrangement*

Once the constants b_0, b_1 and b_2 have been determined for each of the 30 revolutions, the re-sample time instants corresponding to constant angular increments of $\Delta\varphi = 1°$ are obtained independently for each revolution from Eq. (2.2) [47].

$$t = \frac{1}{2b_2}[\sqrt{4b_2(k\Delta\varphi - b_0) + b_1^2} - b_1] \tag{2.2}$$

Piecewise cubic Hermite interpolation (PCHI) [69, 132] is applied to determine the amplitude of vibration signals at the re-sample time instants.

2.3.1 Piecewise cubic Hermite interpolation (PCHI)

The IAR technique helps determine the time instants that correspond to constant angular increments during a revolution. In the present work, PCHI is applied to determine the amplitude of signals at the re-sample time instants. Among interpolation techniques, PCHI has the most efficiency as it tackles with high fluctuations and less smoothness of vibration signals [69].

Piecewise cubic interpolation involves fitting a cubic polynomial to each interval. PCHI is based on making the fit by specifying the values and first derivatives at the end point of each interval.

For the polynomial,

$$P(x) = c_3x^3 + c_2x^2 + c_1x + c_0 \tag{2.3}$$

We seek c_3, c_2, c_1, c_0 such that

$$P(x_k) = y_k, \quad P(x_{k+1}) = y_{k+1}$$

$$P'(x_k) = g_k, \quad P'(x_{k+1}) = g_{k+1} \tag{2.4}$$

We can do this by setting up 4 simultaneous equations and solving for c_3, c_2, c_1, c_0

$$c_3 x_k^3 + c_2 x_k^2 + c_1 x_k + c_0 = y_k$$

$$3c_3 x_k^2 + 2c_2 x_k + c_1 = g_k$$

$$c_3 x_{k+1}^3 + c_2 x_{k+1}^2 + c_1 x_{k+1} + c_0 = y_{k+1}$$

$$3c_3 x_{k+1}^2 + 2c_2 x_{k+1} + c_1 = g_{k+1} \tag{2.5}$$

The above equations can be written in matrix form and solved for c_3, c_2, c_1, c_0

$$\begin{bmatrix} x_k^3 & x_k^2 & x_k & 1 \\ 3x_k^2 & 2x_k & 1 & 0 \\ x_{k+1}^3 & x_{k+1}^2 & x_{k+1} & 1 \\ 3x_{k+1}^2 & 2x_{k+1} & 1 & 0 \end{bmatrix} \begin{Bmatrix} c_3 \\ c_2 \\ c_1 \\ c_0 \end{Bmatrix} = \begin{Bmatrix} y_k \\ g_k \\ y_{k+1} \\ g_{k+1} \end{Bmatrix} \tag{2.6}$$

There is a neater form for the cubic Hermite polynomial over each interval. In the linear interpolation function, the interpolated estimate for y is given by:

$$y = y_k + \frac{x - x_k}{x_{k+1} - x_k}(y_{k+1} - y_k) \tag{2.7}$$

Eq. (2.7) can be re-written as

$$f_k(u) = (1-u)y_k + uy_{k+1} \tag{2.8}$$

where the local variable u is defined as

$$u = \frac{x - x_k}{x_{k+1} - x_k} \tag{2.9}$$

For the interval, $[x_k, x_{k+1}]$, u varies from 0 to 1.

For each interval in our data, $[x_k, x_{k+1}]$, $k = 1,....,N$, and given the values and the gradients, $y_k, y_{k+1}, g_k, g_{k+1}$, we write the interpolating function as

$$f_k(u) = y_k h_1(u) + y_{k+1}h_2(u) + g_k h_3(u) + g_{k+1}h_4(u) \tag{2.10}$$

where the weights are the cubic Hermite basis functions defined as

$$h_1(u) = 2u^3 - 3u^2 + 1$$

$$h_2(u) = -2u^3 + 3u^2$$

$$h_3(u) = u^3 - 2u^2 + u$$

$$h_4(u) = u^3 - u^2 \tag{2.11}$$

To make PCHI able to reproduce data, the slopes at the end points of each interval are required to be defined. The amplitude of the signals at the re-sample time instants having been determined from PCHI, the signals in the time domain are converted into a number of quasi-stationary signals in the angular domain.

The IAR technique thus generates a number of angular domain signals from the original time domain vibration signal. These signals may be merged to produce the angular domain signal for the complete rotational period. shows the combined angular domain signal corresponding to the vibration signal of Fig. 2.4 (a).

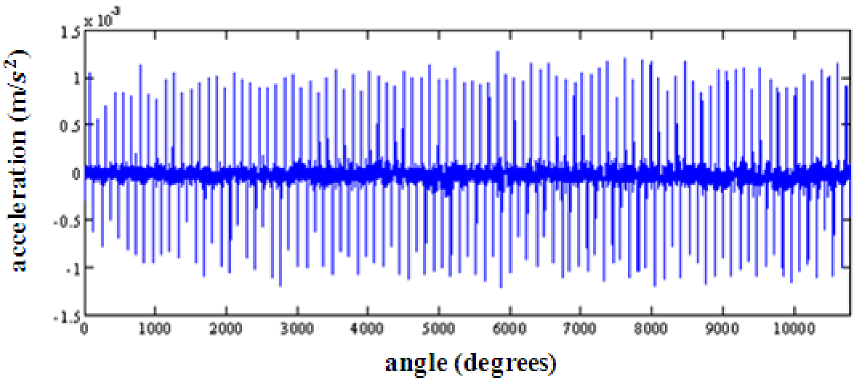

Fig. 2.6. *IAR technique-generated angular domain signal for the healthy pinion*

In order to determine the optimal scales based on energy-Shannon's entropy ratio of wavelet coefficients, the angular domain signal of Fig 2.6 is decomposed with continuous wavelet transform.

2.4. Continuous wavelet transform

Once the vibration signals have been synchronized from the revolution point of view, each angular domain signal representing one revolution of the gearbox drive shaft is decomposed with continuous wavelet transform. The continuous wavelet transform of a signal $x(t)$ is defined as a convolution integral of $x(t)$ with scaled and dilated versions of a mother wavelet function $\Psi_{s,\tau}(t)$ and is given by Eq. (2.12) [137].

$$W_x(s,\tau) = \frac{1}{\sqrt{s}} \int_{-\infty}^{+\infty} x(t).\Psi^*(\frac{t-\tau}{s})dt \tag{2.12}$$

where $\Psi^*(t)$ is the complex conjugate of $\Psi(t)$, s is the scale parameter for changing the oscillating frequency and τ is the translation parameter. There are a number of different real and complex valued functions that can be utilized as analyzing wavelets. In the present work, the Morlet wavelet is employed as the mother wavelet owing to its similarity to an impulse component that is characteristic of a fault in a geared system. Fig 2.7

shows the wavelet amplitude map corresponding to the angular domain signal of Fig 2.6. There are as many wavelet coefficients at each of the 64 scales as the number of samples in the angular domain signal.

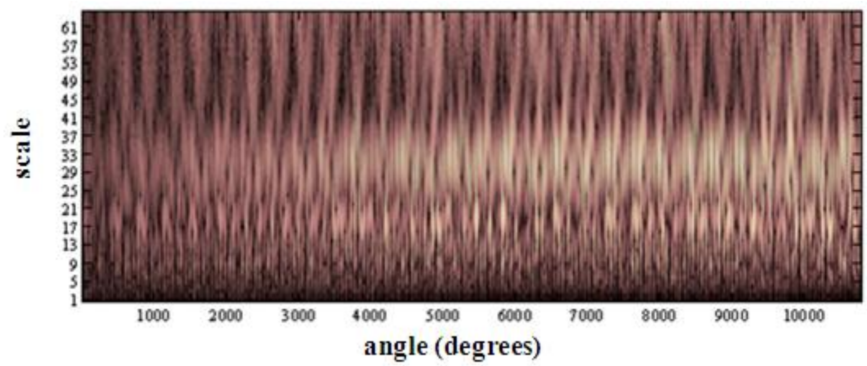

Fig. 2.7. *Wavelet amplitude map corresponding to the angular domain signal of Fig. 2.6*

Identification of optimal scales based on energy-Shannon's entropy ratio of continuous wavelet coefficients is explained in Section 2.5.

2.5. Energy-Shannon's entropy ratio

In [51], a range of optimal scales was identified based on the energy-Shannon's entropy ratio of the wavelet coefficients for the healthy gear. One of the objectives of the present work is to ascertain whether there is an optimal range of scales when the IAR technique is employed for converting the time domain signals into the angular domain and if there is an optimal range of scales, whether or not it serves to be optimal when continuous wavelet coefficients are employed directly for fault identification. The energy and Shannon's entropy of wavelet coefficients at scale n is defined by Eq. (2.13) and Eq. (2.14) respectively.

$$Energy\ (n) = \sum_{i=1}^{m} \left|C_i(n)\right|^2 \tag{2.13}$$

$$Entropy_{Sh}(n) = -\sum_{i=1}^{m} P_i \ \log P_i \tag{2.14}$$

where P_i is the distribution of the energy probability for each wavelet coefficient with $\sum_{i=1}^{m} P_i = 1$, given by:

$$P_i = \frac{|C_i(n)|^2}{Energy\ (n)} \tag{2.15}$$

Fig. 2.8 shows the energy-Shannon's entropy ratio of wavelet coefficients at various scales of the wavelet amplitude map of Fig 2.7. The 13 scales ranging from 25 to 37 have a higher value of energy-Shannon's entropy ratio than the other scales and are referred to in this work as the 'optimal scales'.

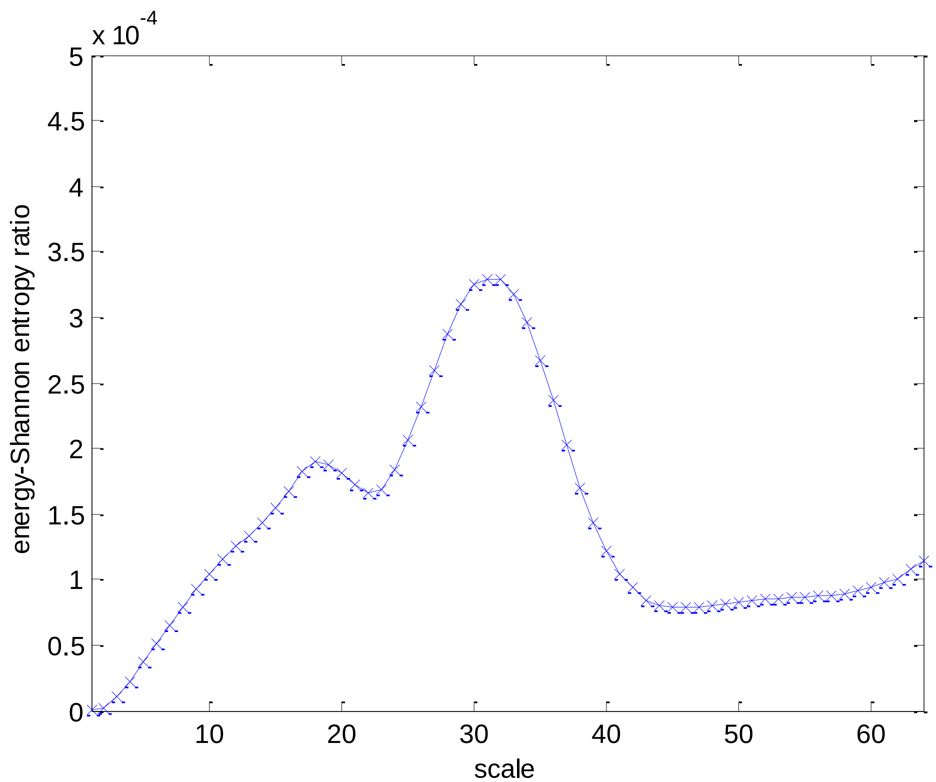

Fig. 2.8. *Energy-Shannon's entropy ratio of wavelet coefficients for the healthy pinion*

The present work attempts to compare the classification accuracy of a back propagation neural network for two different features sets. In Case A, continuous wavelet coefficients (CWCs) from all scales are fed to the neural network while in Case B, CWCs from only the optimal scales (25 to 37) are utilized for fault classification. An introduction to the back propagation neural network is given in Section 2.6.

2.6. Back propagation neural network

One of the most commonly employed forms of artificial neural networks (ANNs) for fault diagnosis is the multilayer perceptron (MLP) neural network trained with the back propagation algorithm. Such a neural network is also referred to as the back propagation neural network. The back propagation neural network was proposed by McClelland and Rumelhart [133]. In its simplest form, a back-propagation neural network consists of an input layer, one or more hidden layers and an output layer. The neurons in the different layers are connected to each other with connecting links called synapses and each such link is associated with a synaptic weight.

The number of neurons in the input layer depends upon the dimensionality of the input feature vectors and the number of output neurons depends on the number of classes into which the dataset is to be classified. Back propagation neural networks have been applied successfully to gearbox fault diagnosis by training them in a supervised manner with a highly popular algorithm known as the error back-propagation algorithm. This algorithm is based on the error-correction leaning rule. Basically, error back propagation learning rule consists of two passes through the different layers of the network: a forward pass and a backward pass. In the forward pass, an input pattern (vector) is applied to the sensory nodes of the network, and its effect propagates through the network layer by layer. Finally, a set of outputs is produced as the actual response of the network. During the forward pass, the synaptic weights of the network are all fixed. During the backward pass, on the other hand, the synaptic weights are all adjusted in accordance with an error-correction rule. Specifically, the actual response of the network is subtracted from a desired (target) response to produce an error signal. The error signal is then propagated backwards through the network against the direction of synaptic connections. The synaptic weights are adjusted to make the actual response of the network move closer to the desired response.

The error signal at the output of neuron j at the iteration n (i.e., presentation of the n th training example) is defined by

$$e_j(n) = d_j(n) - y_j(n) \tag{2.16}$$

where neuron j is an output node. The instantaneous value of the error energy for neuron j can be defined as $\frac{1}{2}e_j^2(n)$. Correspondingly, the instantaneous value $\xi(n)$ of the total energy is obtained by summing $\frac{1}{2}e_j^2(n)$ over all the neurons in the output layer. Thus,

$$\xi(n) = \frac{1}{2}\sum_{j=C} e_j^2(n) \tag{2.17}$$

where the set C includes all the neurons in the output layer of the network.

The correction $\Delta w_{ji}(n)$ applied to $w_{ji}(n)$ is defined by the *delta rule*:

$$\Delta w_{ji}(n) = -\eta \frac{\partial \xi(n)}{\partial w_{ji}(n)} \tag{2.18}$$

where η is the learning parameter of the back-propagation algorithm. The use of the minus sign in Eq. (2.18) accounts for *gradient descent* in weight space (i.e., seeking a direction for weight change that reduces the value of $\xi(n)$). It can be shown that

$$\Delta w_{ji}(n) = \eta \delta_j(n) y_i(n) \tag{2.19}$$

In other words, the correction $\Delta w_{ji}(n)$ applied to the synaptic weight connecting neuron i to j is defined by the delta rule:

$$\begin{pmatrix} Weight \\ correction \\ \Delta w_{ji}(n) \end{pmatrix} = \begin{pmatrix} learning- \\ rate\ parameter \\ \eta \end{pmatrix} . \begin{pmatrix} local \\ gradient \\ \delta_j(n) \end{pmatrix} . \begin{pmatrix} input\ signal \\ of\ \ neuron\ j \\ y_i(n) \end{pmatrix} \qquad (2.20)$$

In Eq. (2.20), the local gradient $\delta_j(n)$ depends on whether neuron j is an output node or a hidden node.

(a) If the neuron j is an output node, $\delta_j(n)$ equals the product of the derivative $\phi_j^{'}(v_j(n))$ and the error signal $e_j(n)$, both of which are associated with the neuron j, i.e.,

$$\delta_j(n) = e_j(n)\varphi_j^{'}(v_j(n)) \qquad (2.21)$$

(b) If the neuron j is a hidden neuron, $\delta_j(n)$ equals the product of the associated derivative $\varphi_j^{'}(v_j(n))$ and the weighted sum of the δs computed for the neurons in the next hidden or output layer that are connected to neuron j, i.e.,

$$\delta_j(n) = \varphi_j^{'}(v_j(n))\sum_k \delta_k(n) w_{kj}(n) \qquad (2.22)$$

A comprehensive derivation of the algorithm can be found in [134].

The present work deals with a three-class gear fault identification problem and hence there are only three output neurons. The dimensionality of the input feature vectors is 360. 50% of the feature set in each case is used to train the neural network while the remaining 50% is utilized to test its classification accuracy. There is only one hidden layer and the sigmoidal transfer function is employed as the activation function for the hidden and output neurons.

2.7. Experimental results and discussions

In Case A, 2880 input feature vectors are used to train the neural network while the remaining 2880 feature vectors are reserved for testing its classification accuracy. In Case B, 585 feature vectors are used to train the ANN while the remaining 585 feature vectors are used to test its classification accuracy. Fig. 2.9 shows the test accuracy of the ANN for hidden neurons ranging from 1 to 13 when CWCs from all scales and when CWCs from only the optimal scales are employed as input feature vectors. Clearly, the test accuracy of the ANN is superior when CWCs from only the optimal scales are employed as feature vectors. While the test success in Case A is acceptable, the time taken for fault classification is large owing to a large size of the input feature set. In Case B, however, the size of the feature set is reduced by almost 80% and not only is the test accuracy superior to Case A but also the time taken for fault classification is considerably lesser. For hidden neurons greater than 3, the test accuracy ranges between 84.4% and 95.9% in Case A and between 92.8% and 98.8% in Case B. The improved fault classification accuracy is consistent with the results reported in [51]. With the IAR technique, too, the scales based on energy-Shannon's entropy ratio of wavelet coefficients are optimal when CWCs are employed for fault classification.

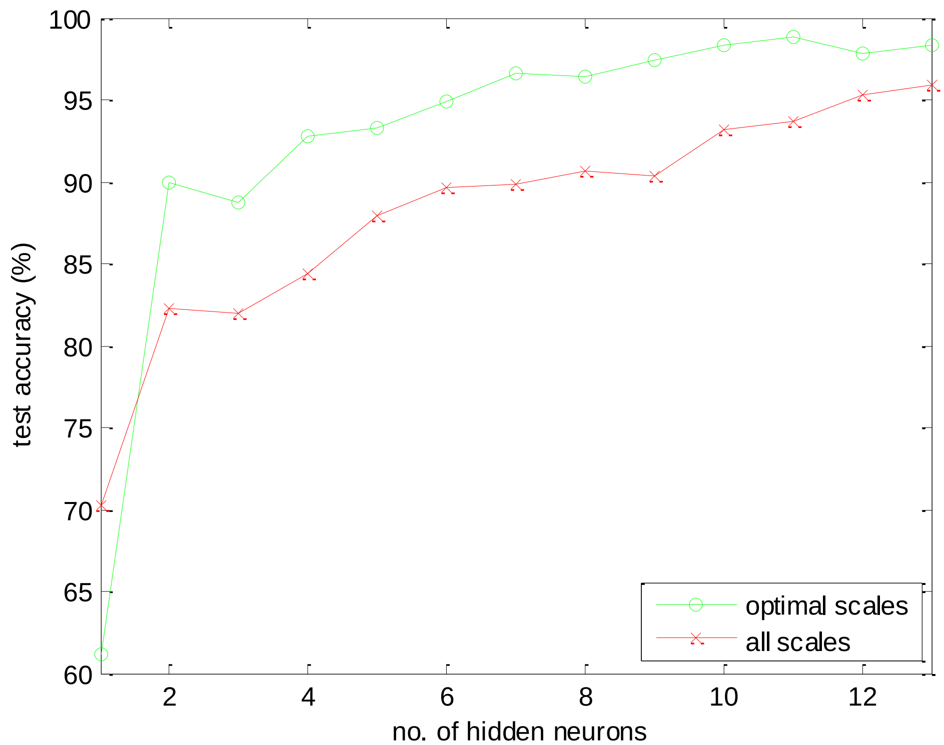

Fig. 2.9. *Test accuracy when CWCs from all scales and optimal scales are employed as feature vectors*

2.8. Conclusion

Uncertainties associated with the drive and load mechanisms, load fluctuations at the output and eccentricity between the shaft and gear inevitably result in non-stationary conditions even when the drive mechanism has been programmed to be driven at a constant speed. The non-stationary vibration signals collected from a single stage spur gearbox are synchronized from the revolution point of view utilizing the independent angular re-sampling technique. The IAR technique is a simple method and demands only minor changes in hardware such as the introduction of an additional tachometer reflective strip. The classification accuracy of a back propagation neural network is compared for different features sets derived from continuous wavelet coefficients. The scales determined to be optimal based on energy-Shannon's entropy ratio of wavelet coefficients result in superior gear fault diagnostic accuracy when wavelet coefficients are directly fed to the neural network.

Chapter 3

Gearbox Fault Diagnosis under Non-stationary Conditions with Independent Angular Re-sampling Technique Applied to Vibration and Sound Emission Signals

3.1. Introduction

An analysis of gearbox vibration signals is almost always the default choice when diagnosing the condition of a gearbox because of the rich information contained in the vibration signals and their ease of measurement. In other words, most of the conventional techniques used for condition monitoring and fault diagnosis of gearboxes are based chiefly on an analysis of vibration signals acquired from the gearbox under healthy and faulty conditions. The sound emission signal may serve as a promising alternative to vibration signals when diagnosing the condition of a gearbox. Research efforts in diagnosing gearbox faults through an analysis of sound emission signals, however, are limited.

It can be shown that even when acquired under a designed constant speed of rotation, gearbox vibration and sound emission signals are mostly non-stationary owing to uncertainties associated with the drive and load mechanisms. The signals acquired from the gearbox are then required to be converted into stationary signals for further analysis. In this Chapter, the IAR technique is employed to convert non-stationary vibration signals (acquired in two mutually perpendicular directions) and sound emission signals into quasi-stationary signals in the angular domain. The vibration and sound emission signals generated from the IAR technique are averaged in order to improve the signal to noise ratio. The resulting angular domain averaged (ADA) signals for each gear health condition are then decomposed with CWT and CWCs fed directly to a BPNN with the objective of diagnosing the condition of the gearbox. Promising results are obtained when sound emission signals are analyzed to diagnose the condition of the gearbox. Fig. 3.1 shows the flowchart for the proposed gear fault diagnostic procedure.

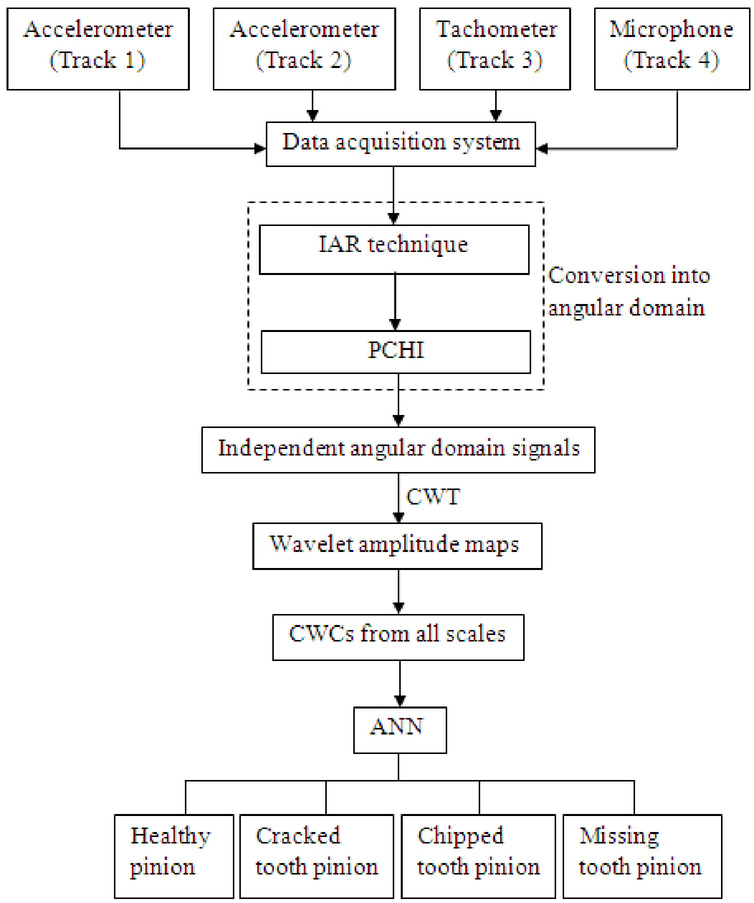

Fig. 3.1. *Flowchart of the proposed gear fault diagnostic procedure*

One of the objectives of the present work is to verify the efficacy of the IAR technique in synchronizing sound emission signals acquired from the gearbox. A comparison of the gear fault diagnostic accuracy is drawn when features extracted from the sound emission signals and when features extracted from the vibration signals are fed to a back propagation neural network.

3.2. Data acquisition

Since the present work involves fault diagnosis of a single stage spur gearbox, vibration signals are measured along the z-axis (Track 1) and x-axis (Track 2) as shown in Fig. 3.2 (a). One of the objectives of the present research is to determine whether there is any advantage gained in analyzing gearbox vibration signatures in two mutually perpendicular directions. As demonstrated in Fig. 3.2 (b), a microphone is placed at a distance of 20 cm from the gearbox to acquire sound emission signals under various pinion health conditions.

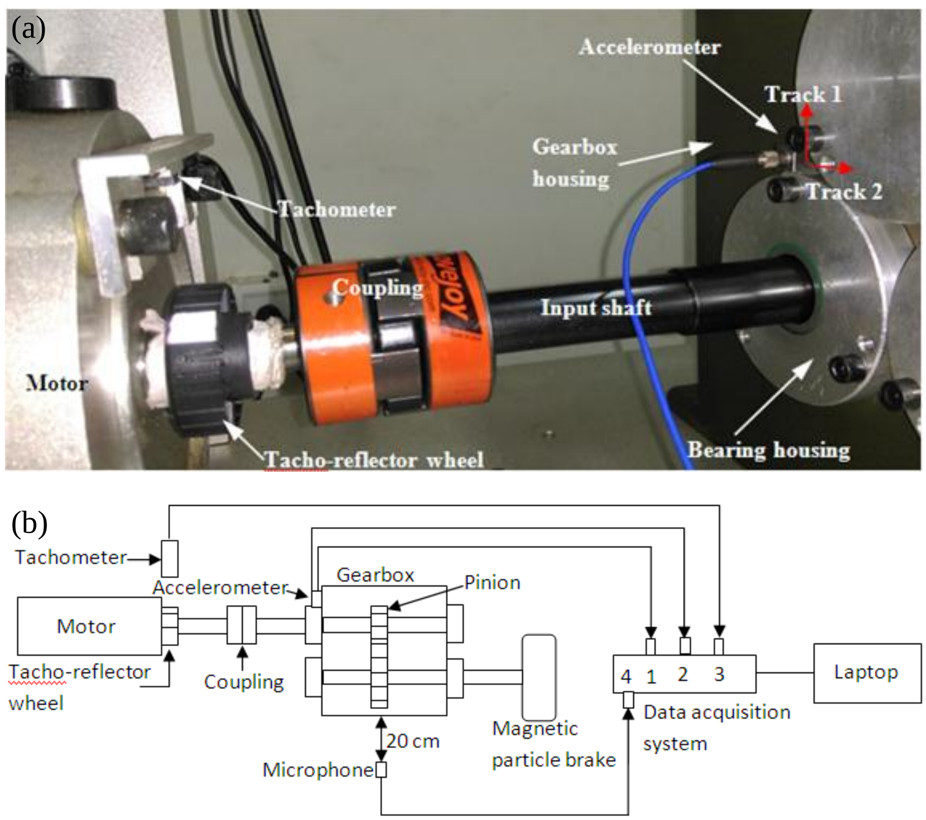

Fig. 3.2. *(a) Sensor arrangement and (b) schematic diagram of the DDS*

Unlike the previous Chapter where gearbox vibration signatures were acquired under three pinion health conditions, in this Chapter vibration and sound emission signatures are acquired under four different gearbox health conditions, viz., healthy pinion, pinion with a cracked tooth, pinion with a chipped tooth and pinion with a missing tooth.

Gearbox signatures are acquired at a constant programmed speed of 20 Hz under 0% load. The sampling frequency is selected as 8192 Hz and the gear wheel remains the same in each of the experiments. For simplicity, as well as to keep the computational burden under control, segments of sound and vibration signals during which the gearbox drive shaft undergoes only 20 complete revolutions have been considered for analysis. It is important to note that even though the vibration and sound emission signatures have been acquired at a constant programmed speed of 20 Hz under 0% (4 lb-in) load, the gearbox signals are not necessarily stationary. This is evident from Fig. 3.3 which shows the time taken for twenty (Track 1) consecutive revolutions of the gearbox drive shaft with the healthy pinion.

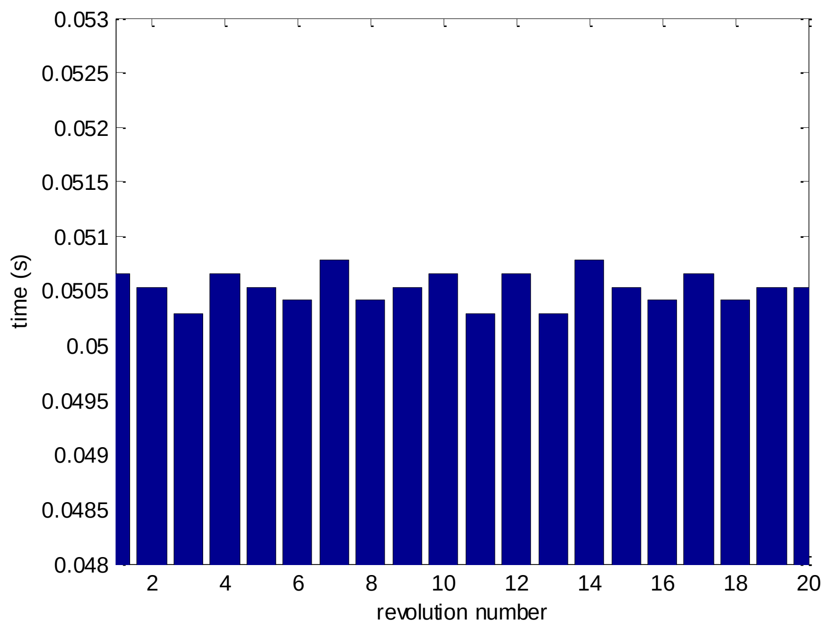

Fig. 3.3. *Time taken for 20 in number Track 1 consecutive revolutions in case of the healthy pinion*

Since the sound and vibration signatures are non-stationary, techniques such as time synchronous averaging cannot be directly employed to improve the signal to noise ratio and there is a need to first synchronize the acquired signals from the revolution point of view. In the present work, the IAR technique, combined with interpolation theory, is employed to convert the non-stationary signals in the time domain into quasi-stationary signals in the angular domain.

3.3. Angular domain averaged (ADA) signals and wavelet amplitude maps (WAMs)

The angular domain signals produced by the IAR technique, each representing one revolution of the gearbox drive shaft, are averaged to produce ADA signals for each gear health condition. Fig 3.4 (a), 3.5 (a) and 3.6 (a) show respectively the sound emission, Track 1 and Track 2 vibration signals acquired from the healthy gearbox over 20 complete revolutions of the gearbox drive shaft. Fig 3.4 (b), 3.5 (b) and 3.6 (b) show the ADA signals for the sound emission, Track 1 and Track 2 vibration signals acquired from the healthy gearbox. The ADA signals are decomposed using CWT employing the Morlet wavelet as the mother wavelet. Fig. 3.4 (c), 3.5 (c) and 3.6 (c) show the WAMs corresponding to the ADA signal of Fig 3.4 (b), 3.5 (b) and 3.6 (b) respectively. Similarly, Fig. 3.7 to Fig. 3.15 show the sound emission and vibration signatures acquired from the gearbox with cracked tooth, chipped tooth and missing tooth pinion along with the corresponding ADA signals and WAMs. There are as many wavelet coefficients at each of the 64 scales in the WAMs as the number of samples in the ADA signals.

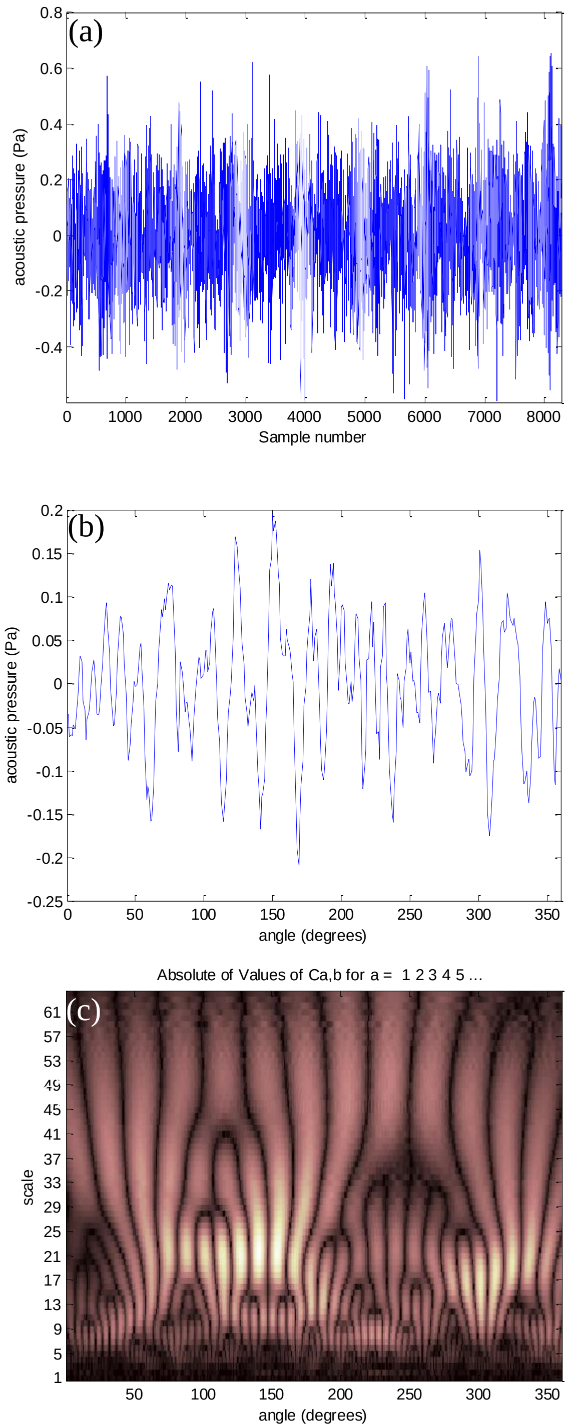

Fig. 3.4. *Healthy gearbox (a) sound emission signal (b) ADA signal and (c) wavelet amplitude map*

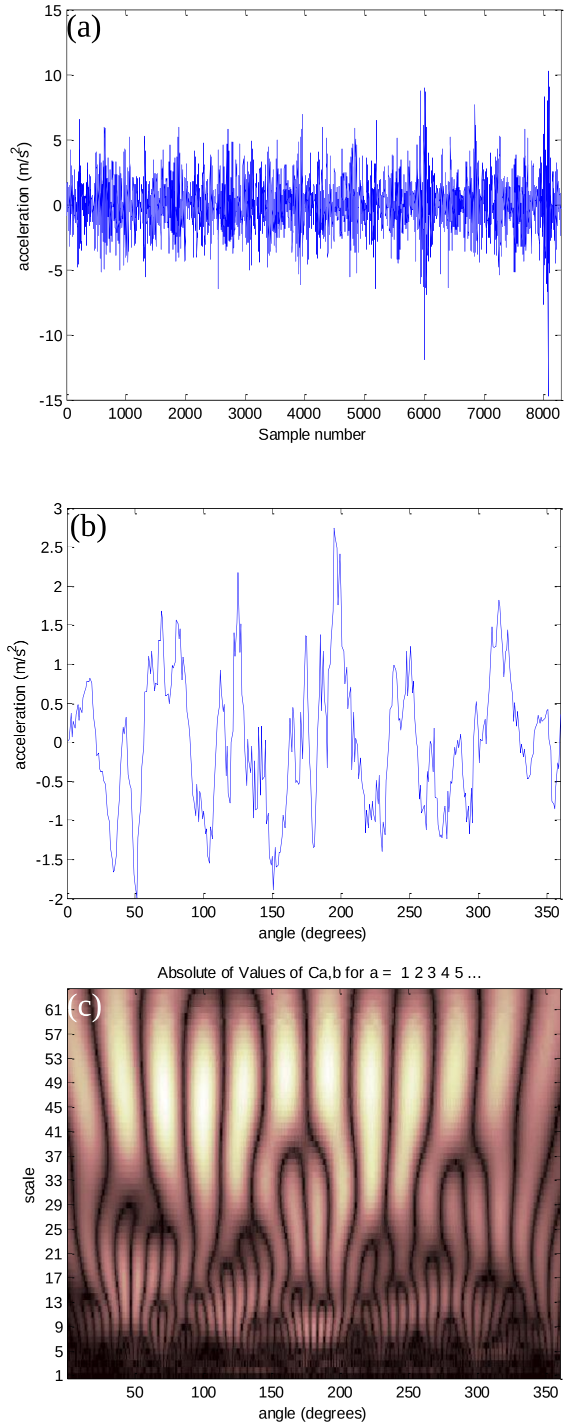

Fig. 3.5. *Healthy gearbox (a) Track 1 vibration signal (b) ADA signal and (c) wavelet amplitude map*

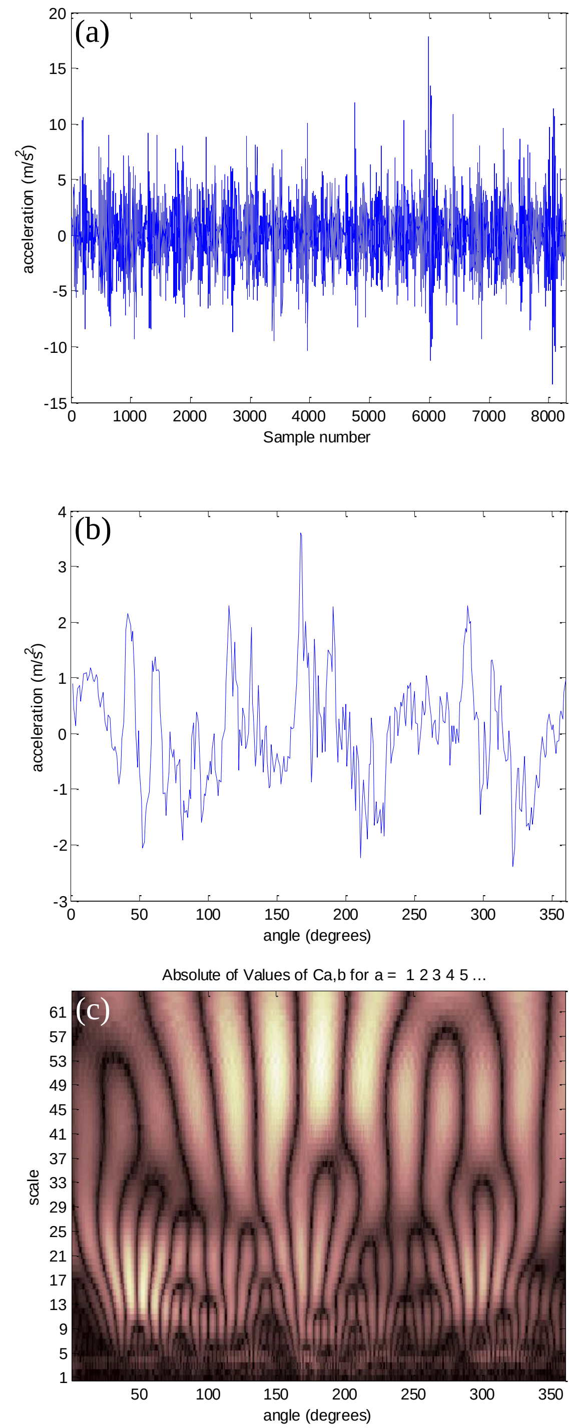

Fig. 3.6. *Healthy gearbox (a) Track 2 vibration signal (b) ADA signal and (c) wavelet amplitude map*

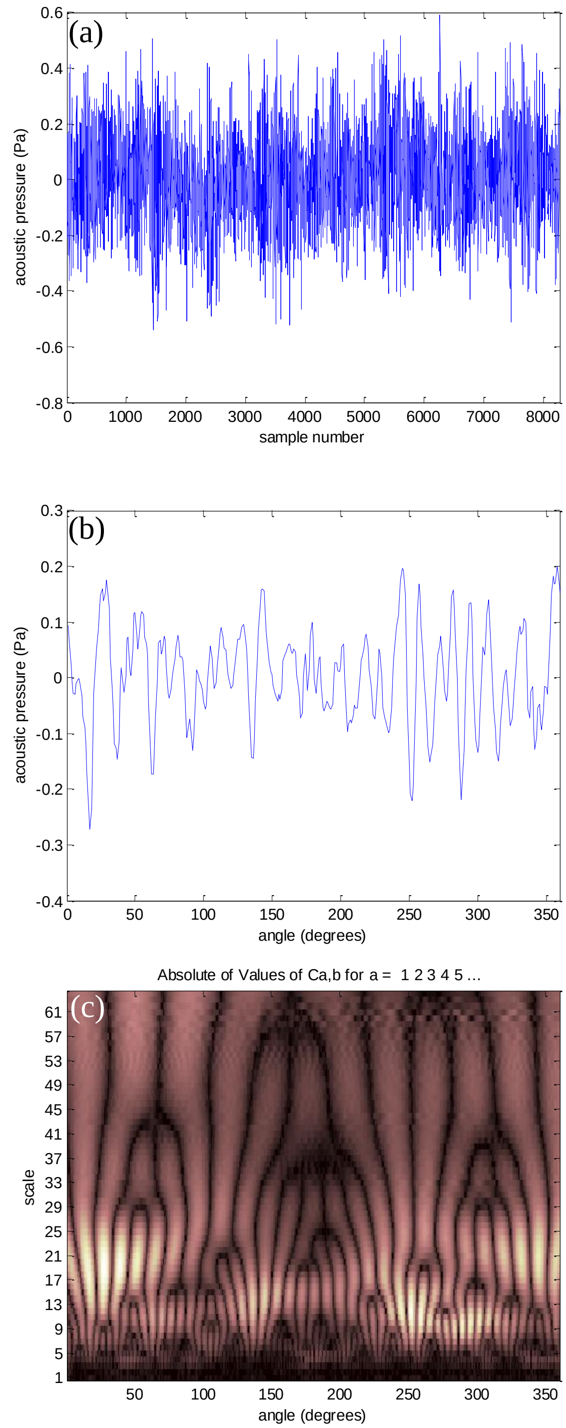

Fig. 3.7. *Cracked tooth pinion (a) sound emission signal (b) ADA signal and (c) wavelet amplitude map*

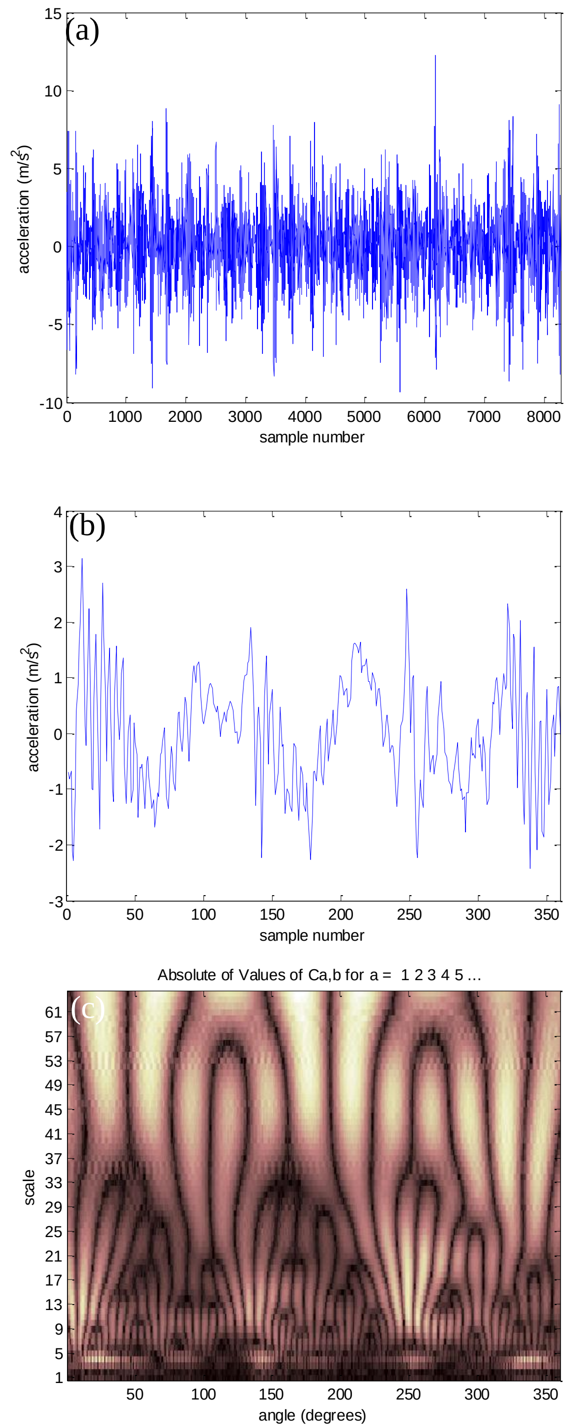

Fig. 3.8. *Cracked tooth pinion (a) Track 1 vibration signal (b) ADA signal and (c) wavelet amplitude map*

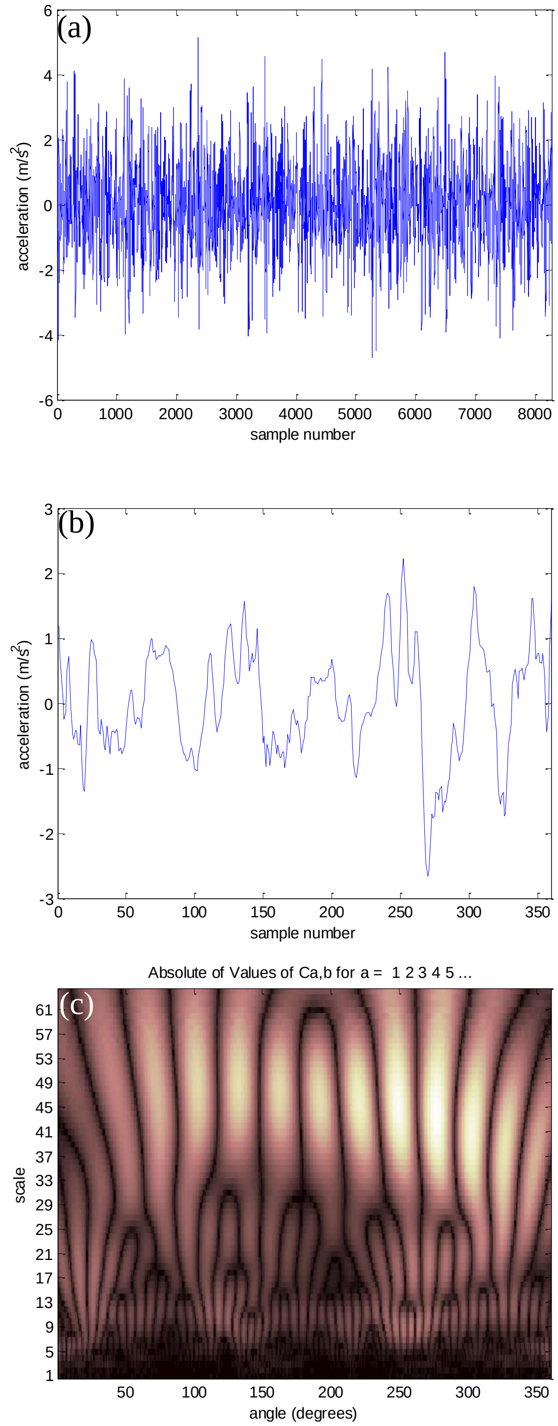

Fig. 3.9. *Cracked tooth pinion (a) Track 2 vibration signal (b) ADA signal and (c) wavelet amplitude map*

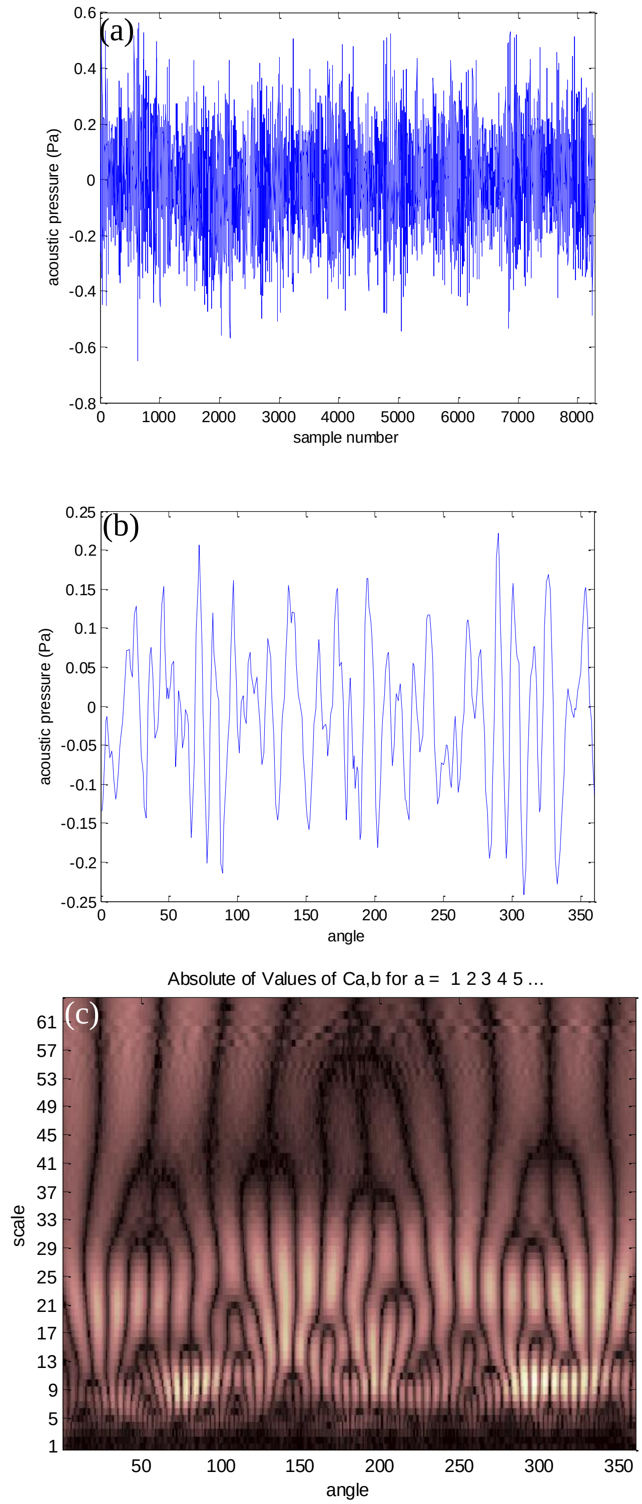

Fig. 3.10. *Chipped tooth pinion (a) sound emission signal (b) ADA signal and (c) wavelet amplitude map*

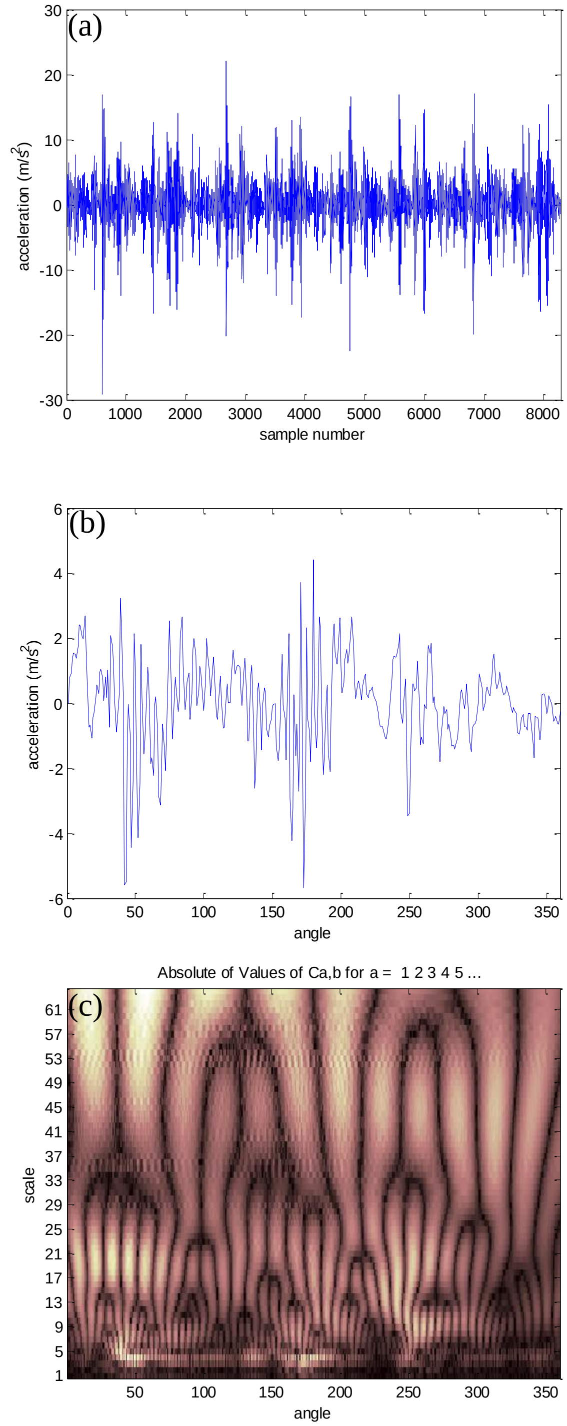

Fig. 3.11. *Chipped tooth pinion (a) Track 1 vibration signal (b) ADA signal and (c) wavelet amplitude map*

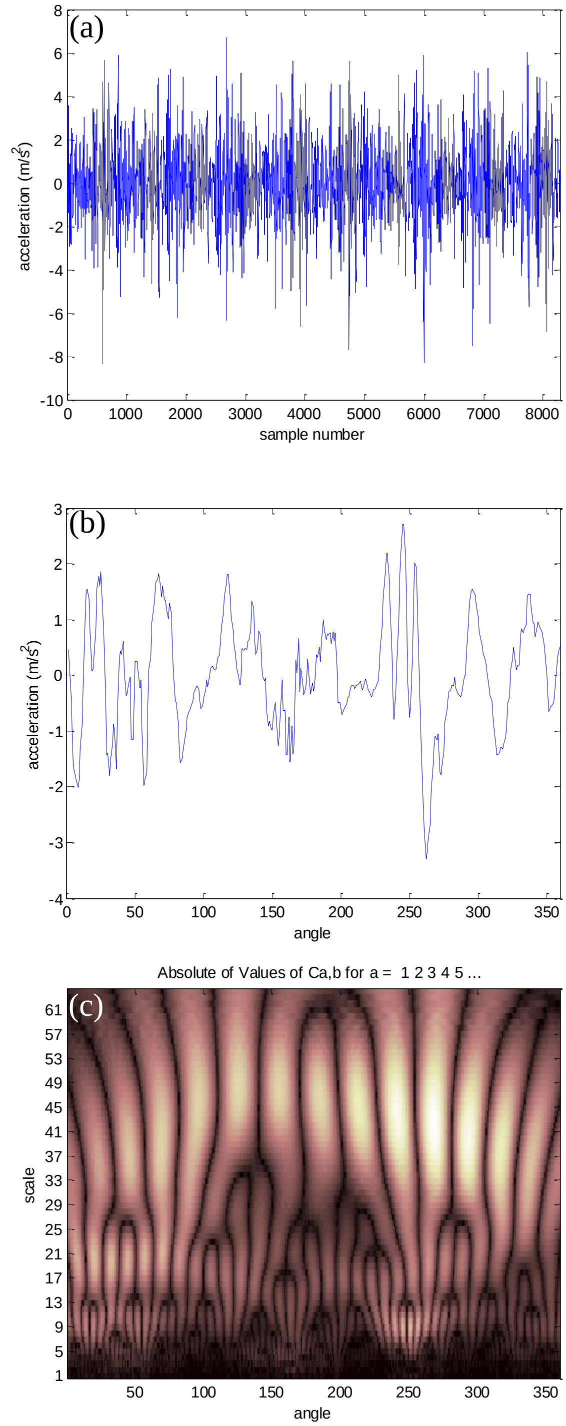

Fig. 3.12. *Chipped tooth pinion (a) Track 2 vibration signal (b) ADA signal and (c) wavelet amplitude map*

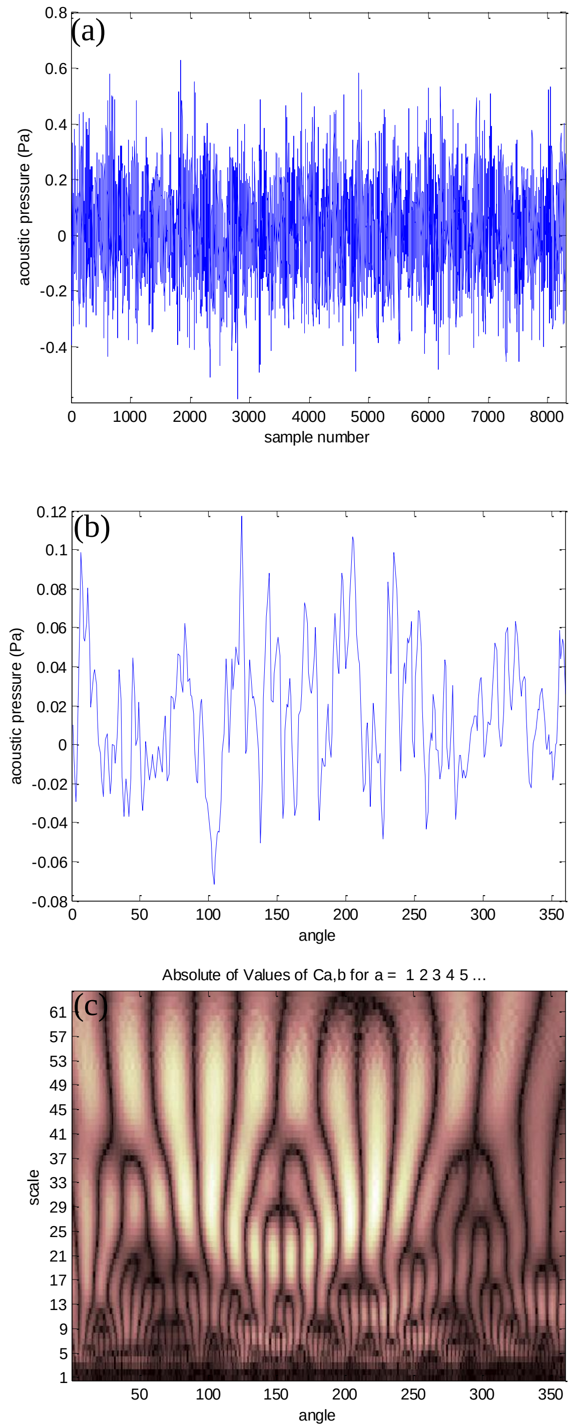

Fig. 3.13. *Missing tooth pinion (a) sound emission signal (b) ADA signal and (c) wavelet amplitude map*

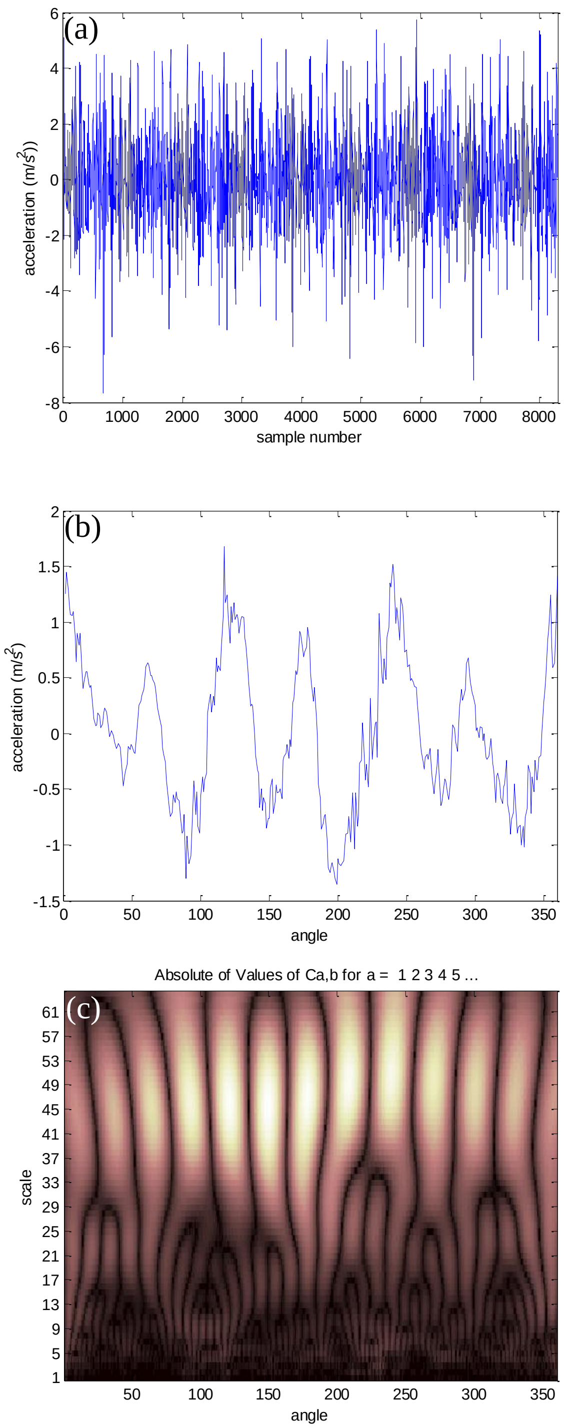

Fig. 3.14. *Missing tooth pinion (a) Track 1 vibration signal (b) ADA signal and (c) wavelet amplitude map*

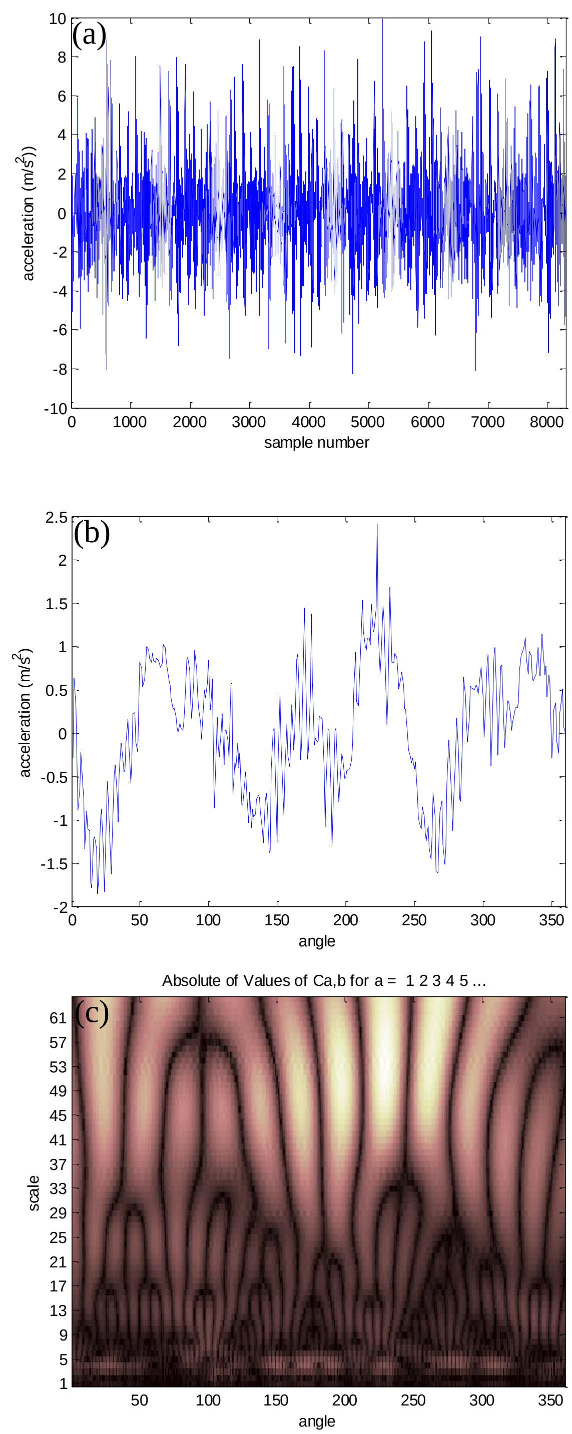

Fig. 3.15. *Missing tooth pinion (a) Track 2 vibration signal (b) ADA signal and (c) wavelet amplitude map*

3.4. Experimental results

The condition of the gearbox cannot be ascertained from only a visual inspection of the time domain sound emission/ vibration signals, the ADA signals or the resulting wavelet amplitude maps. For this reason, an intelligent classifier such as an ANN is employed to discriminate between the various gear health conditions. In the present work, a BPNN fed with CWCs in the form of input feature vectors, is employed for diagnosing the condition of the gearbox.

Table 3.1 illustrates the ANN architecture employed for GFD in the present work. In each case, the features set consists of 256 input feature vectors, 50% of which are used to train the neural network and the remaining 50% utilized to test its classification accuracy.

Table 3.1

Architecture of the ANN.

Network type	Back propagation neural network
No. of neurons in the input layer	360
No. of neurons in the hidden layer	09
No. of neurons in the output layer	04
Transfer function	Sigmoidal transfer function for hidden and output neurons

Three hundred and sixty dimensional input feature vectors comprising of CWCs are fed directly to the neural network with the objective of diagnosing the condition of the gearbox. The gear fault diagnostic accuracy of a 360:9:4 BPNN is compared under the following conditions:

(a) CWCs derived from WAMs of ADA sound emission signals are fed in the form of input feature vectors to the neural network,

(b) CWCs derived from WAMs of Track 1 ADA vibration signals are fed in the form of input feature vectors to the neural network, and

(c) CWCs derived from WAMs of Track 2 ADA vibration signals are fed in the form of input feature vectors to the neural network

Table 3.2 shows the classification accuracy of the BPNN for the above three cases.

Table 3.2

Classification performance of the BPNN.

	Healthy	Cracked	Chipped	Broken
Case A :Sound emission signal (Track 4)				
Training accuracy	100%	100%	97.7%	100%
Test accuracy	96.6%	100%	100%	97.4%
Case B: Track 1 vibration signal				
Training accuracy	100%	100%	97.1%	100%
Test accuracy	93.1%	100%	100%	97.4%
Case C: Track 2 vibration signal				
Training accuracy	100%	100%	100%	100%
Test accuracy	96.6%	96.9%	100%	97.4%

The test accuracy of the BPNN varies between 93.1% and 100% when Track 1 vibration signals are analyzed for diagnosing the gearbox health condition. The test accuracy, when Track 2 vibration signals are analyzed, varies between 96.6% and 100%. From these results, it may be concluded that the difference between the test accuracy of the BPNN is marginal when Track 1 and Track 2 vibration signals are analyzed for GFD. When sound emission signals are analyzed for diagnosing the gearbox health condition, the test accuracy of the BPNN varies between

96.6% and 100%. Though the results obtained from an analysis of gearbox vibration signals are satisfactory, the results achieved from the analysis of sound emission signals are marginally superior. It may thus be concluded that sound emission signals may serve as an alternative to vibration signals when diagnosing the condition of the gearbox.

However, there is a possibility that the sound emission signature may be corrupted by background noise and due attention is to be paid to the ambient conditions under which the sound emission signatures are acquired. If the sound emission signal is likely to be corrupted by background noise, it is advisable to carry out an analysis of the gearbox vibration signal.

3.5. Summary

Gearbox sound and vibration signatures are mostly non-stationary owing to uncertainties associated with the drive and load mechanisms. Reasonably good gear fault diagnostic results are obtained when CWCs derived from sound and vibration signatures are fed directly to the BPNN. No clear advantage is gained when vibration signatures acquired in two mutually perpendicular directions are analyzed to ascertain the condition of the gearbox. Marginally superior results are obtained when the sound emission signatures are analyzed by the proposed method to diagnose the gearbox health condition. It may, therefore, be concluded that an analysis of the gearbox sound emission signatures serves as a promising method to diagnose the condition of the gearbox.

Chapter 4

Gearbox Fault Diagnosis using Acoustic Signals, Continuous Wavelet Transform and Adaptive Neuro-Fuzzy Inference System

4.1. Introduction

Most of the research efforts directed towards gearbox fault diagnosis are based on an analysis of vibration signals acquired from the gearbox [3, 4]. At times, however, the acoustic (sound emission) signal may serve as an alternative to vibration signal when diagnosing the condition of a gearbox. As brought out in Chapter 1, limited work in GFD has been accomplished based on an analysis of acoustic signatures, though promising results have been reported by some researchers [128-130]. Further, in Chapter 3, the gear fault diagnostic accuracy of a back propagation neural network feeding continuous wavelet coefficients from the wavelet amplitude maps of vibration and acoustic signals directly to the neural network was compared. Marginally superior results were obtained when acoustic signals were analyzed to diagnose the condition of the gearbox.

Artificial neural networks (ANNs) have been extensively employed for fault diagnosis of gearboxes based on an analysis of the vibration signals. Further, fuzzy inference systems have attracted growing attention in GFD [108, 109]. A specific approach in neuro-fuzzy development is the adaptive neuro-fuzzy inference system (ANFIS) which has shown significant results in modeling nonlinear functions. ANFIS has been successfully employed in the field of GFD [116-119]. However, these research efforts are based on an analysis of gearbox vibration signatures acquired under various fault conditions. To the best of the authors' knowledge, the implementation of ANFIS to diagnose gearbox faults through an analysis of acoustic signatures has not been attempted.

This Chapter attempts to diagnose the condition of a single stage spur gearbox based on an analysis of acoustic signatures acquired under three different pinion health conditions, viz., healthy pinion (HP), cracked tooth (CT) pinion and chipped tooth (CHT) pinion. The acquired acoustic signals are converted into a number of angular domain signals, each representing one revolution of the gearbox drive shaft. The resultant angular domain signals are then averaged in order to improve the signal to noise ratio. Each angular domain averaged signal is decomposed using continuous wavelet transform and a range of optimal scales identified based on the energy-Shannon's entropy ratio of continuous wavelet coefficients. The wavelet amplitude maps for the three pinion health conditions are split into segments and continuous wavelet coefficients fed directly as inputs to an ANFIS in the form of data samples. Fig. 4.1 is a flowchart of the proposed gear fault diagnostic procedure.

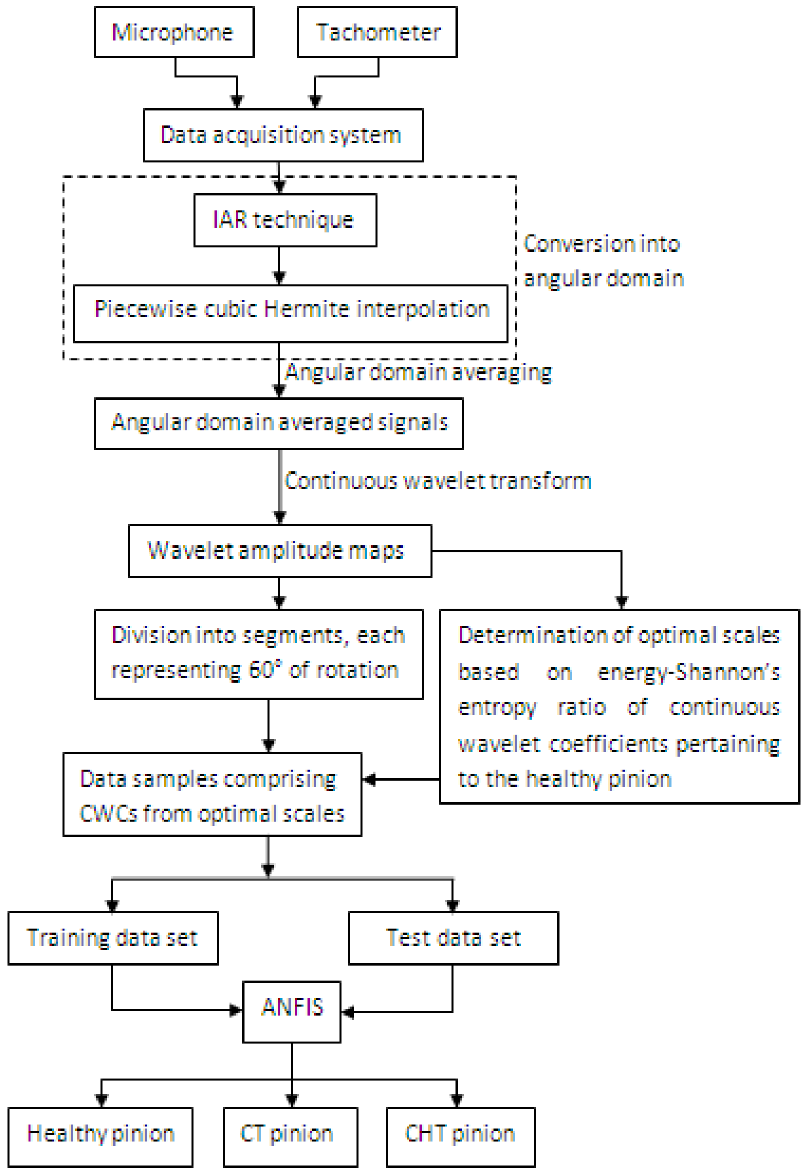

Fig. 4. 1. *Flowchart of the proposed gear fault diagnosis procedure*

4.2. Experimental set-up and data acquisition

The drive train diagnostic simulator (DDS) located at IIT Indore consists of a single stage spur gearbox as shown in Fig. 2.2. In order to acquire acoustic signals under various gear health conditions, a microphone is placed at a distance of 20 cm from the gearbox. The type of microphone used in the experiment is the Type 46 AE pre-polarized free field microphone. All signals are recorded during silent hours so as to minimize external noise. The tachometer and microphone are interfaced to a PC via a data acquisition system. Fig. 4.2 is a schematic diagram of the DDS.

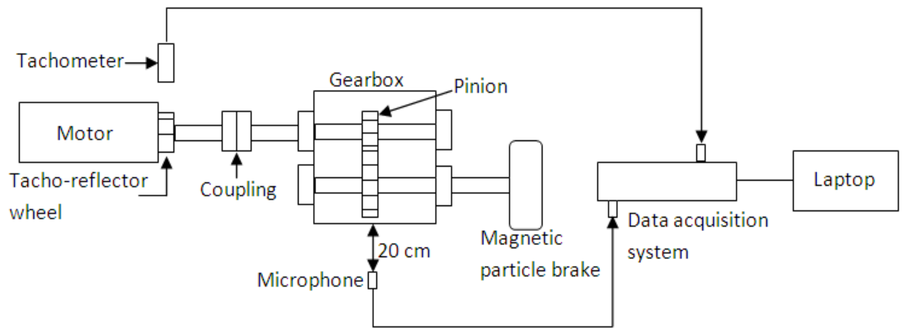

Fig. 4.2. *Schematic diagram of the DDS*

A tacho-reflector wheel with two reflective strips is mounted on the motor output shaft as shown in Fig. 2.2 (b) and Fig. 2.5. This is because the independent angular re-sampling (IAR) technique requires that the instants of time at three different shaft angular positions during each revolution be known.

Acoustic signatures are acquired under three different pinion health conditions at a constant programmed speed of 10 Hz at 0% load. Fig. 4.3 shows the healthy, cracked tooth and chipped tooth pinions used in the experiments. The sampling frequency is selected as 8192 Hz and the gear wheel remains the same in each of the experiments.

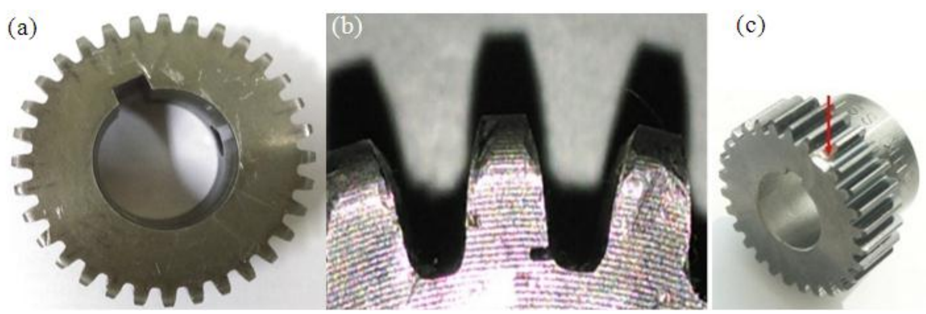

Fig. 4.3. *(a) Healthy pinion, (b) cracked tooth pinion and (c) chipped tooth pinion*

Fig. 4.4 shows the acoustic signals acquired under the various pinion health conditions over 20 complete revolutions of the gearbox drive shaft. Alongside the time domain acoustic signals are the corresponding angular domain averaged signals obtained using the IAR technique and PCHI.

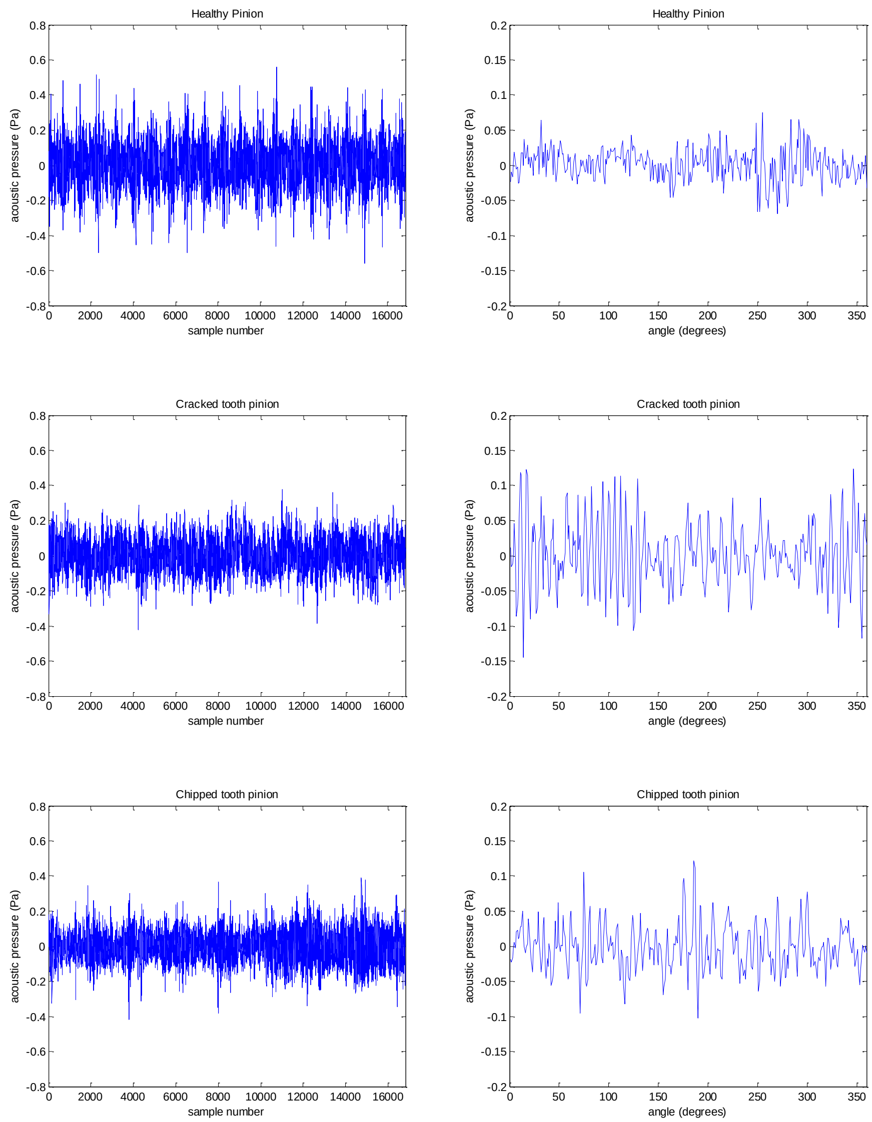

Fig. 4.4. *Time domain acoustic signals (left) and the corresponding angular domain averaged signals (right)*

Though the time domain acoustic signal for the healthy pinion has greater amplitude than the other two cases and exhibits impulses, the corresponding angular domain averaged signal has lower amplitude. This is because the procedure of averaging the angular domain signals obtained from the IAR technique reduces the external noise improving the signal to noise ratio. Further, it is difficult to distinguish between the cracked and chipped tooth pinions from only a visual inspection of the time domain or angular domain averaged signals. An automated method of gearbox fault diagnosis is desirable and is in the present work accomplished using an ANFIS. The ANFIS, however, needs to be fed with meaningful features representing the gearbox health condition. In the present work, the angular domain averaged acoustic signals are decomposed using continuous wavelet transform and continuous wavelet coefficients from optimal scales fed to the ANFIS in the form of data samples to ascertain the condition of the gearbox. The procedure of determining the optimal scales from the angular domain averaged wavelet amplitude map pertaining to the healthy pinion is explained in Section 4.3.

4.3. Continuous wavelet transform and determination of optimal scales

The continuous wavelet transform of a signal $x(t)$ is defined as a convolution integral of $x(t)$ with scaled and dilated versions of a mother wavelet function $\Psi_{s,\tau}(t)$ and is given by Eq. (2.12). In the present work, the Morlet wavelet is employed as the mother wavelet. Fig. 4.5 shows the wavelet amplitude map corresponding to the angular domain averaged acoustic signal for the healthy pinion.

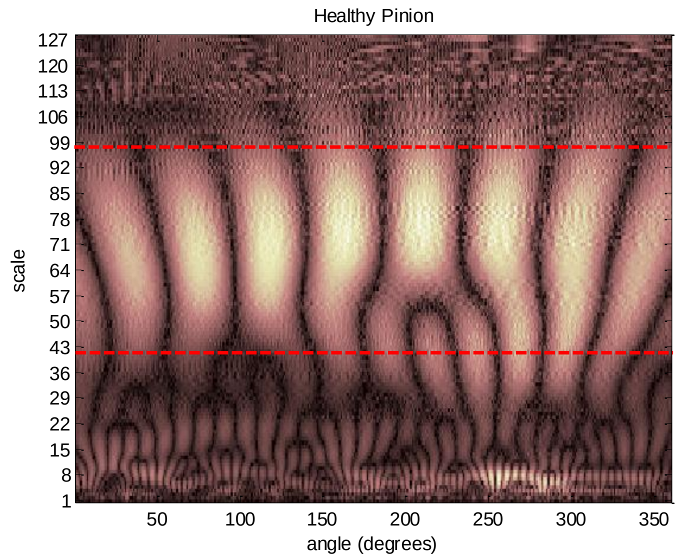

Fig. 4.5. *Wavelet amplitude map corresponding to the healthy pinion angular domain averaged acoustic signal*

In [51], a range of optimal scales was identified based on the energy-Shannon's entropy ratio of continuous wavelet coefficients from the wavelet amplitude map pertaining to the healthy pinion. An improvement in the classification accuracy of the ANN was reported when statistical parameters from only the optimal scales were employed as input feature vectors. Fig. 4.6 shows a plot of the energy-Shannon's entropy ratio of continuous wavelet coefficients from the wavelet amplitude map of Fig. 4.5.

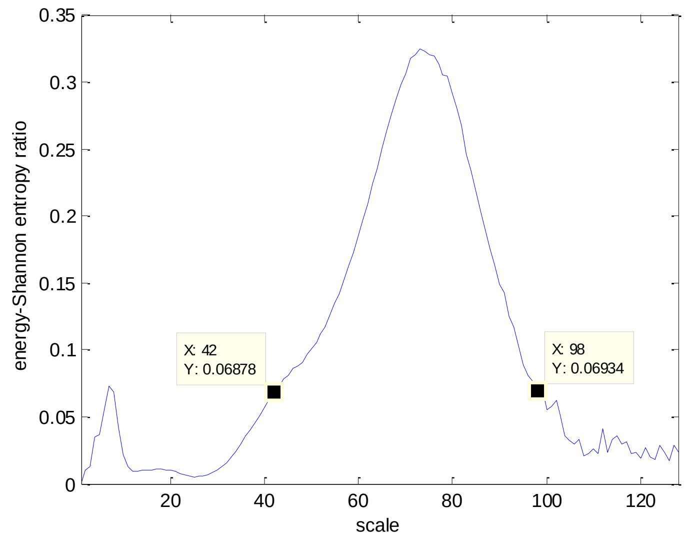

Fig. 4.6. *Energy-Shannon's entropy ratio of continuous wavelet coefficients from the wavelet amplitude map of the healthy pinion*

It can be observed from Fig. 4.6 that scales ranging from 42 to 98 have superior energy-entropy ratio compared to the other scales. Clear changes in signal frequencies can also be observed for this range of scales in the wavelet amplitude map of Fig. 4.5 and is indicated by dashed lines. Wavelet amplitude maps for the three pinion health conditions are later segmented and CWCs from optimal scales fed directly in the form of data samples to an ANFIS with the objective of identifying the condition of the gearbox. Section 4.4 explains the adaptive neuro-fuzzy inference system (ANFIS).

4.4. Adaptive neuro-fuzzy inference system (ANFIS)

The ANFIS is a fuzzy Sugeno model put in the frame work of adaptive systems to facilitate learning and adaptation. Such framework makes the ANFIS modeling more systematic and less reliant on expert knowledge. To present the ANFIS architecture, two fuzzy if-then rules based on a first order Sugeno model are considered [114, 115]:

Rule 1: If $(x \text{ is } \mathrm{A}_1)$ and $(y \text{ is } \mathrm{B}_1)$ then $(f_1 = p_1 x + q_1 y + r_1)$

Rule 2: If $(x \text{ is } \mathrm{A}_2)$ and $(y \text{ is } \mathrm{B}_2)$ then $(f_2 = p_2 x + q_2 y + r_2)$

where x and y are the inputs, A_i and B_i are the fuzzy sets, f_i are the outputs within the fuzzy region specified by the fuzzy rule; p_i, q_i and r_i are the design parameters that are determined during the training process. The ANFIS architecture to implement these two rules is shown in Fig. 8 in which a circle indicates a fixed node whereas a square indicates an adaptive node.

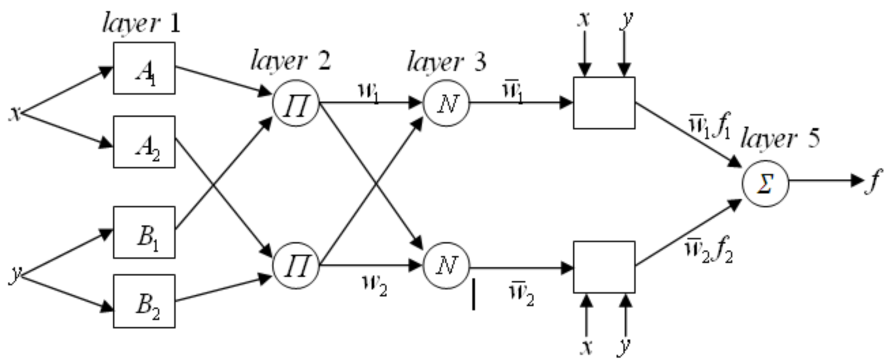

Fig. 4.7. *ANFIS architecture [114, 115]*

In the first layer, all the nodes are adaptive nodes. The outputs of layer 1 are the fuzzy membership grade of the inputs, which are given by [114, 115]:

$$O_i^1 = \mu_{A_i}(x) \quad i = 1,2 \tag{4.1}$$

and

$$O_i^1 = \mu_{B_{i-2}}(y) \quad i = 3,4 \tag{4.2}$$

where $\mu_{A_i}(x)$, $\mu_{B_i-2}(y)$ can adopt any fuzzy membership function. For example, if the bell shaped membership function is employed, $\mu_{A_i}(x)$ is given by [114, 115]:

$$\mu_{A_i}(x) = \frac{1}{1 + \left\{ \left(\frac{x - c_i}{\alpha_i} \right)^2 \right\}^{b_i}} \tag{4.3}$$

where a_i , b_i and c_i are the parameters of the membership function governing the bell shaped functions accordingly. In the second layer, the nodes are fixed nodes. They are labeled with Π indicating that they perform as a simple multiplier. The outputs of this layer can be represented as [114, 115]

$$O_i^2 = w_i = \mu_{A_i}(x)\mu_{B_i}(y) \quad i = 1, 2 \tag{4.4}$$

which are called firing strengths of the rules.

In the third layer, the nodes are also fixed nodes. They are labeled with N , indicating that they play a normalization role to the firing strengths from the previous layer. The outputs of this layer can be represented as [114, 115]:

$$O_i^3 = \overline{w}_i = \frac{w_i}{w_1 + w_2} \quad i = 1, 2 \tag{4.5}$$

which called normalized firing strengths.

In the fourth layer, the nodes are adaptive nodes. The output of each node in this layer is simply the product of the normalized firing strength and a first order polynomial. Thus, the outputs of this layer are given by [114, 115]:

$$O_i^4 = \overline{w}_i f_i = \overline{w}_i (p_i x + q_i y + r_i) \quad i = 1, 2 \tag{4.6}$$

In the fifth layer, there is only one single fixed node labeled with Σ . This node performs the summation of all incoming signals. Hence, the overall output of the model is given by [114, 115]:

$$O_i^5 = \sum_{i=1}^{2} \overline{w}_i f_i = \frac{\sum_{i=1}^{2} w_i f_i}{w_1 + w_2} \tag{4.7}$$

It can be observed that there are two adaptive layers in this ANFIS architecture, namely the first layer and the fourth layer. In the first layer, there are three modifiable parameters $\{a_i, b_i, c_i\}$, which are related to the input membership functions. These parameters are the called *premise* parameters. In the fourth layer, there are also three modifiable parameters $\{p_i, q_i, r_i\}$, pertaining to the first order polynomial. These parameters are called *consequent* parameters.

The task of the learning algorithm for this architecture is to tune all the modifiable parameters, namely $\{a_i, b_i, c_i\}$ and $\{p_i, q_i, r_i\}$ to make the ANFIS output match the training data. When the premise parameters a_i, b_i and c_i of the membership function are fixed, the output of the ANFIS model can be written as [114, 115]:

$$f = \overline{w_1}(p_1 x + q_1 y + r_1) + \overline{w_2}(p_2 x + q_2 y + r_2) \tag{4.8}$$

After rearranging terms in Eq. (9), the output can be expressed as [114, 115]:

$$f = (\overline{w_1 x}) p_1 + (\overline{w_1 y}) q_1 + \overline{w_1} r_1 + (\overline{w_2 x}) p_2 + (\overline{w_2 y}) q_2 + \overline{w_2} r_2 \tag{4.9}$$

which is a linear combination of the modifiable consequent parameters p_1, q_1, r_1, p_2, q_2 and r_2. The least squares method can be used to identify the optimal values of these parameters easily.

When the premise parameters are not fixed, the search space becomes larger and the convergence of the training becomes slower. A hybrid algorithm combining the least squares method and the gradient descent method is adopted to solve this problem. The hybrid algorithm is composed of a forward pass and a backward pass. The least squares method (forward pass) is used to optimize the consequent parameters with the premise parameters fixed. Once the optimal consequent parameters are found, the backward pass starts immediately. The gradient descent method (backward pass) is used to adjust optimally the premise parameters corresponding to the fuzzy sets in the input domain. The output of the ANFIS is calculated by employing the consequent parameters found in the forward pass. The output error is used to adapt the premise parameters by means of a standard back propagation algorithm. It has been proven that this hybrid algorithm is highly efficient in training the ANFIS [114, 115].

4.5. Results and discussions

Neuro-fuzzy systems are fuzzy systems which use ANNs theory in order to determine their properties (fuzzy sets and fuzzy rules) by processing data samples. The number of fuzzy rules in turn depends on the number of inputs and membership functions. A large number of inputs to the ANFIS or the number of membership functions for each input will increase the computational burden of the subsequent classifier. It has been shown that the process of feeding continuous wavelet coefficients directly to a neural network results in superior gear fault diagnostic results [131]. However, the number of inputs when feeding CWCs directly to an ANFIS classifier has to be restricted. This is accomplished in the present work by segmenting the wavelet amplitude maps pertaining to the three pinion health conditions into 6 regions, each representing 60° of rotation. Fig. 4.8 shows the segmented wavelet amplitude maps.

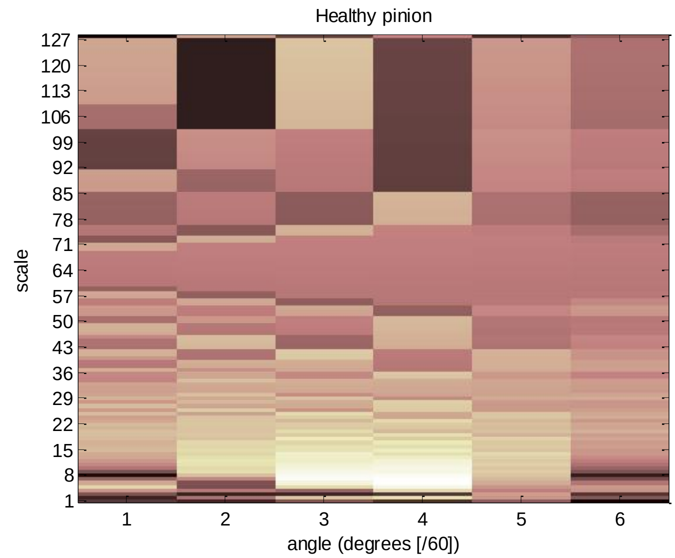
Healthy pinion
scale
127
120
113
106
99
92
85
78
71
64
57
50
43
36
29
22
15
8
1
1
2
3
4
5
6
angle (degrees [/60])

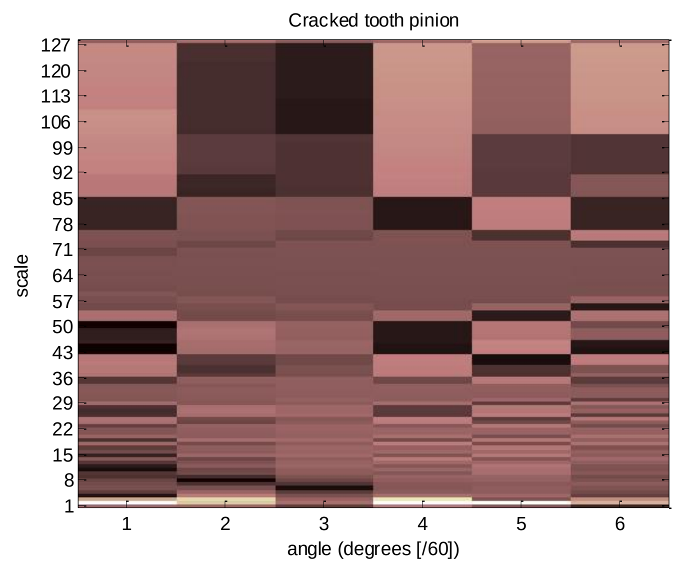
Cracked tooth pinion
scale
127
120
113
106
99
92
85
78
71
64
57
50
43
36
29
22
15
8
1
1
2
3
4
5
6
angle (degrees [/60])

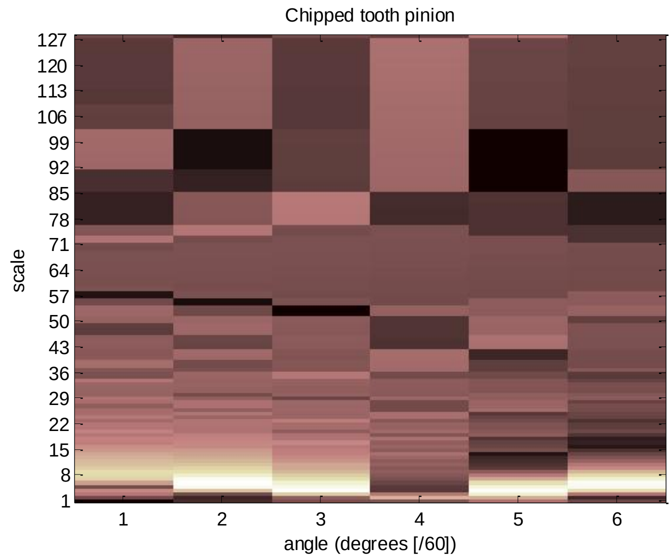

Fig. 4.8. *Segmented wavelet amplitude maps for the three pinion health conditions*

Continuous wavelet coefficients from the six segments and belonging to the optimal scales (42 to 98) are fed in the form of data samples to an ANFIS classifier. Table 4.1 shows the division of data samples used to train and test the ANFIS.

Table 4.1

Division of data samples.

Pinion health condition	No. of training data samples	No. of test data samples	Class label
Healthy pinion	29	28	1
Cracked tooth pinion	29	28	2
Chipped tooth pinion	29	28	3

As shown in Table 4.1, a total of 87 data samples are used to train the ANFIS while 84 data samples are utilized for testing. Each of the 6 inputs to the ANFIS is divided into two Gaussian membership functions, viz., small and large. The linear membership function is selected for the output. Fig. 4.9 illustrates the ANFIS architecture employed for GFD in the present work.

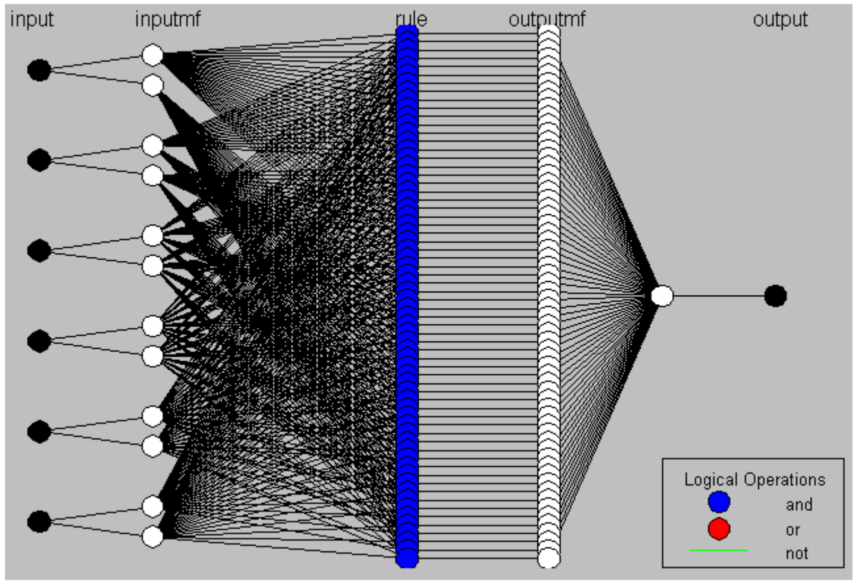

Fig. 4.9. *ANFIS architecture for the gearbox fault diagnosis problem*

As seen in Fig. 4.9, there are *six* inputs to the ANFIS as continuous wavelet coefficients from the *six s*egments of wavelet amplitude maps are fed in the form of data samples to the classifier. Each of the six inputs is divided into two membership functions which are represented by two nodes against each input in the second layer of the ANFIS. The number of rules in a fuzzy inference system is dependent on the number of inputs to the classifier and the number of membership functions against each input. The ANFIS classifier has only one output node which may assume class labels from 1 to 3 as specified in Table 4.1.

Fig. 4.10 shows the classification accuracy of the trained ANFIS when fed with training and test data samples. A part of the available data set is used to train the ANFIS while the remaining data set is utilized to test the classification accuracy of the ANFIS. The division of the available data set into training and test data samples has been elaborated in Table 4.1. The blue circles in Fig. 4.10 represent the training data samples which in the present case are 29 in number belonging to each class and assume class labels from 1 to 3. The blue circles represent the test data samples which number 28 for each gear health condition. The red asterisk symbols represent the ANFIS output. Once the ANFIS has been trained, when a data sample is presented to the ANFIS, it must ideally generate an output (in the form of a class label) that correctly identifies with the existing condition of the gearbox. It can be observed from the figure that in a majority of cases, the test instances to the ANFIS are correctly classified.

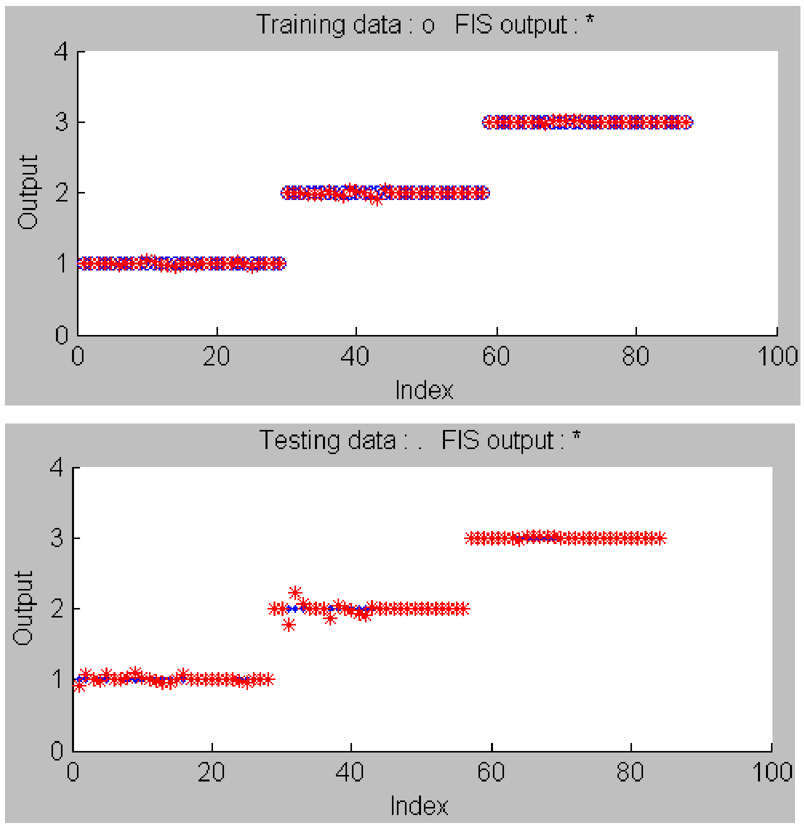

Fig. 4.10. *Classification accuracy of the trained ANFIS when fed with training and test data samples*

4.6. Conclusion

This Chapter attempted to diagnose the condition of a single stage spur gearbox through an analysis of acoustic signals acquired from the gearbox under various fault conditions. The IAR technique is a simple yet powerful method of converting the time domain acoustic signals into the angular domain and requires only minor changes in hardware such as the introduction of an additional tachometer reflective strip. An optimal range of scales based on energy-Shannon's entropy ratio of continuous wavelet coefficients is identified from the wavelet amplitude map pertaining to the healthy pinion. The wavelet amplitude maps pertaining to the three pinion health conditions are segmented into 6 regions from which continuous wavelet coefficients belonging to the optimal scales are fed directly to the ANFIS. It may be concluded that through a combination of IAR technique, continuous wavelet transform and ANFIS, acoustic signals can effectively be utilized for diagnosing the condition of a gearbox. As part of further research, the proposed method of gearbox fault diagnosis may be applied to the vibration signals acquired from a gearbox.

Chapter 5

Fault Diagnosis of a Bevel and Spur Gearbox based on Vibration Signals using Continuous Wavelet Transform and Adaptive Neuro-Fuzzy Inference System

5.1. Introduction

Bevel gears are used to transmit power between shafts whose axes intersect. They are most often mounted on shafts that are 90 degrees apart, but can also be designed to work at other angles as well [135]. Bevel gears have many diverse applications such as locomotives, marine applications, automobiles, printing presses, cooling towers, power plants, steel plants, railway track inspection machines, etc. Considerable amount of research effort has been devoted towards fault diagnosis of spur and planetary gearboxes. Research in fault diagnosis of bevel gearboxes still merits attention considering their widespread application and limited means available for fault diagnosis. Some of the research efforts in fault diagnosis of bevel gearboxes are enumerated in the succeeding paragraph.

Saravanan et al. [109] proposed vibration-based fault diagnosis of a spur bevel gearbox using fuzzy technique.Vibration signals were captured under the following conditions: good bevel gear, bevel gear with tooth breakage, bevel gear with crack at the root of the tooth and bevel gear with face wear of the teeth. Saravanan et al. [94] studied the effectiveness of wavelet-based features for fault diagnosis of a bevel gearbox using ANN and proximal support vector machines (PSVM). Statistical feature vectors from Morlet wavelet coefficients were classified using J48 algorithm and predominant features fed as input for training and testing the ANN and PSVM and their relative efficiency in classifying the faults in the bevel gearbox was compared. Saravanan & Ramachandran

[70] investigated the use of discrete wavelets for feature extraction and ANN for classification. Saravanan et al. [95] studied the effectiveness of wavelet-based features for fault diagnosis using support vector machines (SVM) and proximal support vector machines (PSVM). Statistical feature vectors from Morlet wavelet coefficients were classified using J48 algorithm and the predominant features fed as input for training and testing SVM and PSVM and their relative efficiency in classifying the faults in the bevel gearbox was compared. Saravanan & Ramachandran [96] proposed the application of a fast single-shot multiclass proximal support vector machine for fault diagnosis of a gearbox consisting of twenty four classes. The statistical feature vectors from Morlet wavelet coefficients were classified using J48 algorithm and the predominant features fed as input for training and testing the multiclass proximal support vector machine. The efficiency and time consumption in classifying the twenty four classes all-at-once was reported. In [136], they proposed fault diagnosis of a spur bevel gearbox using discrete wavelet features and decision tree classification.

A considerable amount of the above literature on bevel gearbox fault diagnosis focused on identification of statistical parameters with superior fault discrimination capability. Moreover, the experimental set-up consisted of a belt-driven bevel gearbox. Fluctuations in gear speeds as a result of uncertainties associated with the drive and load mechanisms and because of possible slippage between the belts and pulleys was neglected. A limited number of studies have focused on gearbox fault diagnosis under non-stationary conditions arising from fluctuating load-speed conditions [52-54]. Many of the research works on gearbox fault diagnosis under fluctuating speed conditions have involved an analysis of gearbox vibration signals under the run up condition [47-51]. In such works, since the angular velocity of the gearbox drive shaft was made to increase linearly from one speed to another, the angular acceleration was assumed to remain constant.

Artificial neural networks (ANNs) have been extensively employed for fault diagnosis of gearboxes. Further, fuzzy inference systems have attracted growing attention in gearbox fault diagnosis [108, 109]. Neuro-fuzzy systems are fuzzy systems which use ANNs theory in order to determine their properties (fuzzy sets and fuzzy rules) by processing data samples. Neuro-fuzzy systems harness the power of the two paradigms: fuzzy logic and ANNs by utilizing the mathematical properties of ANNs in tuning rule-based fuzzy systems that approximate the way humans process information. A specific approach in neuro-fuzzy development is the adaptive neuro-fuzzy inference system (ANFIS) which has shown significant results in modeling nonlinear functions. In ANFIS, the membership function parameters are extracted from a data set that describes the system behavior. The ANFIS learns features in the data set and adjusts the system parameters according to a given error criterion [114, 115]. ANFIS has been successfully employed in the field of gearbox fault diagnosis [116-119].

The present study aims at fault diagnosis of a belt-driven bevel gearbox under non-stationary conditions arising from uncertainties associated with the drive and load mechanisms and possible slippage between the belts and pulleys. No attempt is made to identify statistical parameters with superior fault discrimination capability, though a reduction in the size of the feature set based on energy-Shannon’s entropy ratio results in superior gear fault diagnostic accuracy. The independent angular re-sampling (IAR) technique is employed to convert non-stationary vibration signals in the time domain into quasi-stationary signals in the angular domain. The angular domain signals pertaining to 30 complete pinion revolutions are merged to generate the angular domain signal corresponding to the original time domain signal. This combined angular domain signal is then decomposed using CWT and a range of optimal scales identified based on the energy-entropy ratio of CWCs. Each independent angular domain signal representing one pinion revolution is segmented into six parts, each indicating 60° of pinion rotation. Thirty such independent angular domain signals are averaged to arrive at the angular domain averaged (ADA) signal for each gear health condition. Each such ADA signal is decomposed using CWT resulting in a WAM with only 6 data points. CWCs from the 6 columns are then employed directly as input to an ANFIS for fault diagnosis. Two cases are considered in the present work: in one case, CWCs from all scales are fed to the ANFIS for fault diagnosis and in the second case CWCs from only the optimal scales are fed to the ANFIS. In order to test the efficacy of the proposed method, the procedure is repeated for vibration signals acquired from a single stage spur gearbox.

The remainder of this Chapter is organized as follows: Section 5.2 describes the experimental set-up used to acquire the bevel gearbox vibration signatures. Section 5.3 gives a brief introduction to the independent angular re-sampling technique from the perspective of the present work while Section 5.4 gives an overview of the continuous wavelet transform and its application in the present study. Section 5.5 discusses the results obtained by applying the proposed method to fault diagnosis of the bevel gearbox. Section 5.6 applies the proposed methodology to fault diagnosis of a single stage spur gearbox. Concluding remarks are given in Section 5.7.

5.2. Experimental set-up and data acquisition

The experimental set-up, also called the machinery fault simulator (MFS), consists of a belt-driven bevel gearbox whose output shaft is interfaced with a magnetic load which can produce a torque up to 5 N-m. The prime mover is a variable speed electrical motor and drives a shaft supported on two bearings. On the other end of the shaft is mounted a small pulley which drives a larger pulley through a belt drive. A speed reduction of the ratio 2.5:1 is achieved owing to a smaller pulley driving a larger one. For example, if the motor speed is set to 30 Hz, the pinion must ideally rotate at 12 Hz. In reality, however, owing to factors such as uncertainties associated with the drive and load mechanisms and slippage between the belts and pulleys, the pinion speed fluctuates and this makes gearbox fault diagnosis under fluctuating speed conditions a challenging task. Fig. 5.1 shows the experimental set-up employed in the present work for acquiring the gearbox vibration signatures.

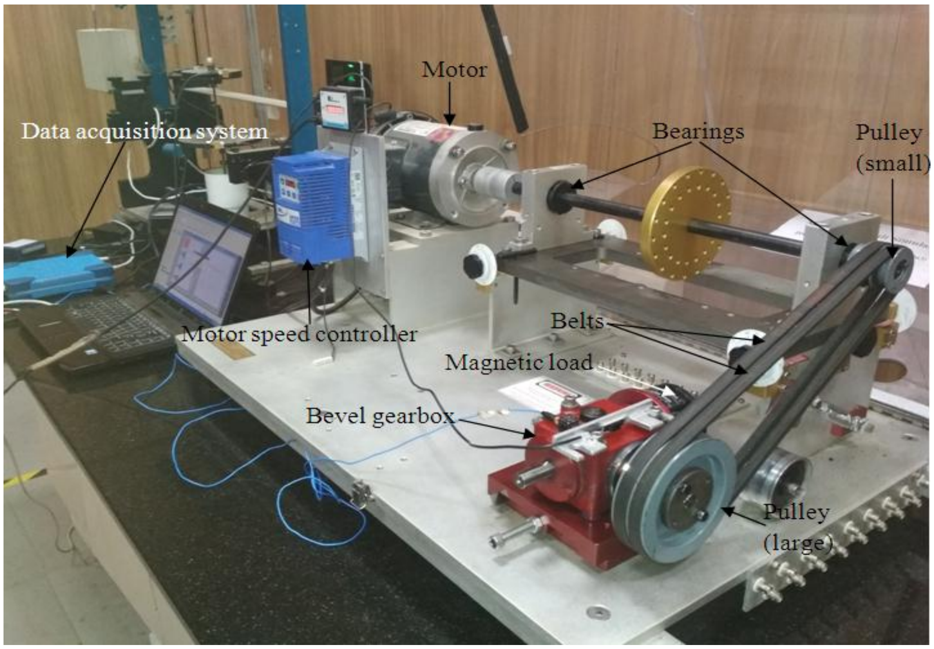

Fig. 5.1. *Bevel gearbox experimental set-up (machinery fault simulator)*

An accelerometer mounted on the gearbox casing measures vibration signals in the z-axis as shown in Fig. 5.2. The larger of the two pulleys is mounted with two reflective strips spaced 146˚ apart on the inner surface. Such a multiple pulse tachometer arrangement ensures that the time instants at three different shaft angular positions during each revolution are known. This is a pre-requisite of the IAR technique which is employed in the present work for converting non-stationary signals in the time domain into quasi-stationary signals in the angular domain. The accelerometer and tachometer are interfaced to a PC via a data acquisition system.

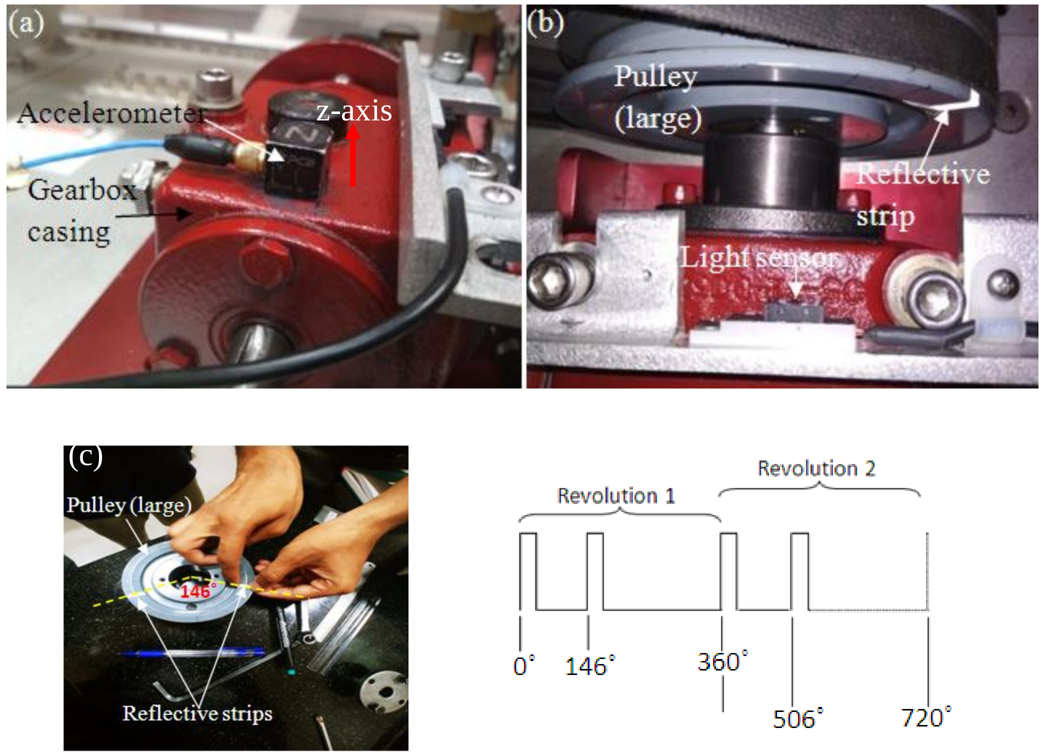

Fig. 5.2. *(a) Accelerometer and (b), (c) multiple pulse tachometer arrangement*

Gearbox vibration signatures are acquired under three different pinion health conditions, viz., healthy pinion (HP), chipped tooth (CHT) pinion and missing tooth (MT) pinion. The gear wheel remains the same in each of the experiments. Fig. 5.3 shows the healthy pinion, chipped tooth pinion and missing tooth pinion employed for the experiments.

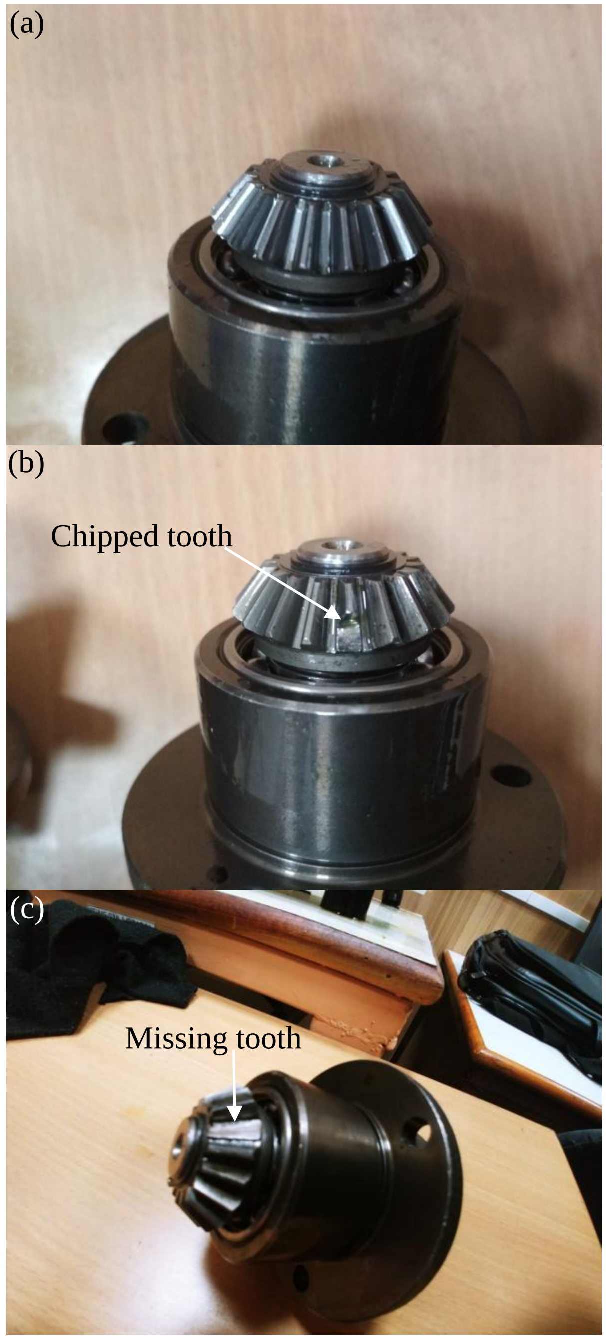

Fig. 5.3. *(a) Healthy pinion, (b) chipped tooth pinion and (c) missing tooth pinion*

The motor rotational speed is set to 30 Hz while aquiring the gearbox vibration signatures and the sampling frequency is selected as 12,800 Hz. Fig. 5.4 shows the time domain vibration signals acquired over 30 complete revolutions of the pinion at 0% load. Two readings were acquired under each identical load-speed condition of which only reading 1 (R1) is being analyzed in the present work.

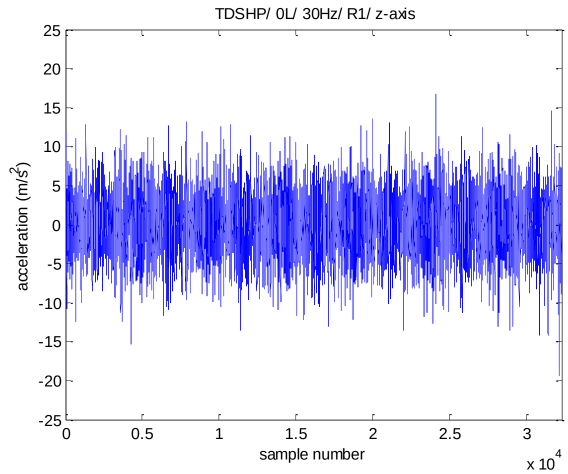

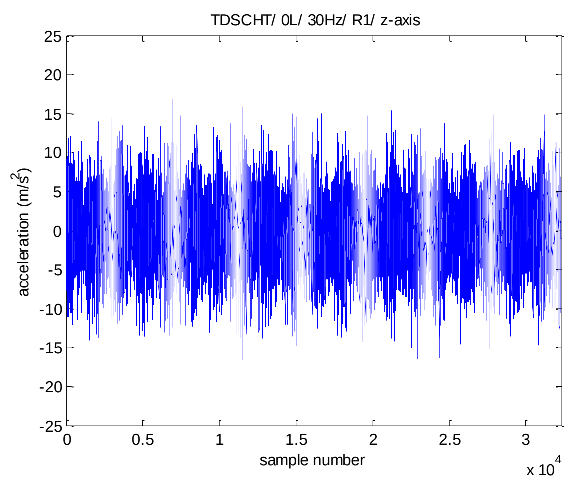

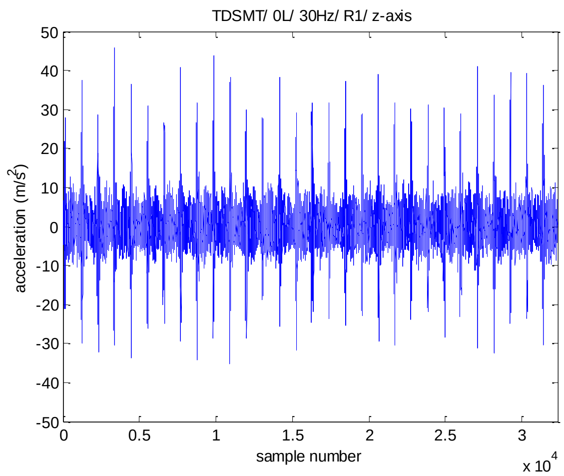

Fig. 5.4. *Time domain vibration signals acquired from the gearbox installed with healthy pinion, chipped tooth pinion and missing tooth pinion*

Though it is difficult to distinguish between the healthy and chipped tooth pinions from only a visual inspection of the vibration signals, the missing tooth pinion signal clearly exhibits impulses of large amplitude which is characterstic of a broken tooth. The independent angular re-sampling technique is employed in the present work for converting the gearbox vibration signatures from the time domain into the angular domain. In the initial part of this Chapter, we deal with the analysis of the gearbox vibration signals acquired from the bevel gearbox. A similar analysis of gearbox vibration signatures collected from a single stage spur gearbox is the subject of Section 5.6.

5.3. The IAR technique as applied to the present problem

The independent angular re-sampling (IAR) technique helps convert the time domain signal into the angular domain. More precisely, the technique converts the original time domain signal into a number of angular domain signals, each representing one revolution of the pinion. These independent angular domain signals can then be merged to generate the angular domain signal corresponding to the original time domain signal. This combined angular domain signal can be decomposed using

CWT and the resulting wavelet amplitude map (WAM) utilized to compute the energy-entropy ratio of CWCs with the objective of identifying the optimal scales. Alternatively, the independent angular domain signals generated from the IAR technique can be averaged in order to improve the signal to noise ratio (SNR). Fig. 5.5 shows the combined angular domain signals corresponding to the three pinion health conditions.

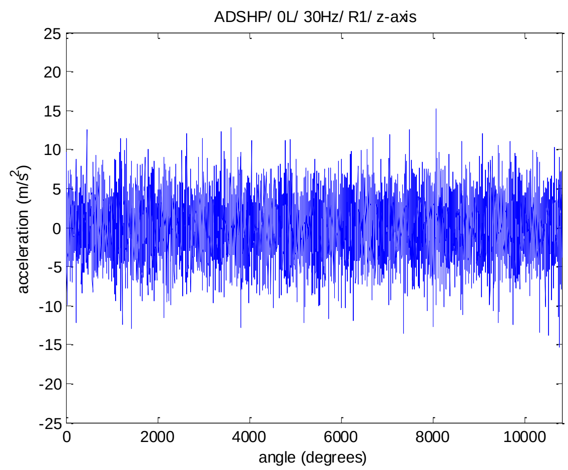

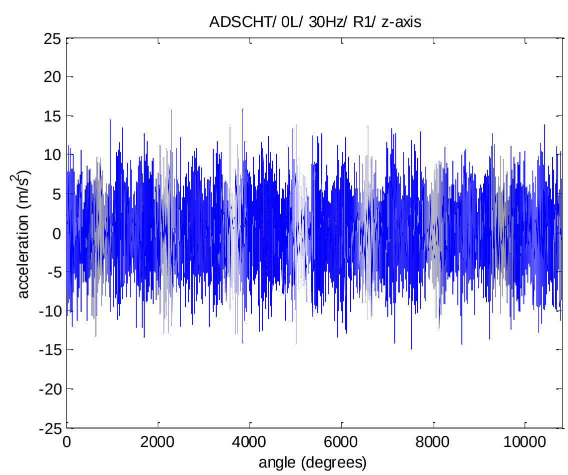

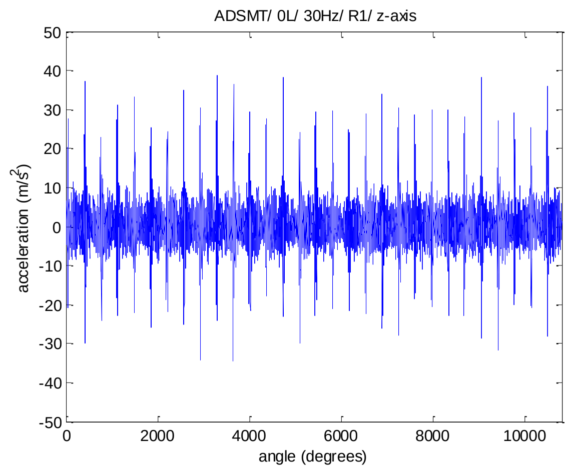

Fig. 5.5. *IAR technique-generated angular domain vibration signals for the gearbox with healthy pinion, chipped tooth pinion and missing tooth pinion*

There is striking similarity between the time domain signals acquired using the accelerometer and the angular domain signals generated using the IAR technique. The change in axes from sample number in Fig. 5.4 to angle (in degrees) in Fig. 5.5 is to be noted. While the number of samples in the three cases in Fig. 5.4 is unequal (owing to fluctuations in pinion speed), the number of samples in Fig. 5.5 is equal representing 30 complete revolutions of the pinion.

Under fluctuating speed conditions (such as in the case under study), techniques such as conventional time synchronous averaging (TSA) cannot be directly applied to improve the SNR. Another effective method of improving the SNR is to carry out averaging of signals in the angular domain. The IAR technique helps generate a number of angular domain signals, each representing one revolution of the pinion. These signals can be averaged to improve the SNR resuting in angular domain averaged (ADA) signals for each pinion health condition. Some of the phenomena which may not be evident in the time domain signal may reveal itself in the ADA signals. Fig. 5.6 shows the ADA signals for the three pinion health conditions.

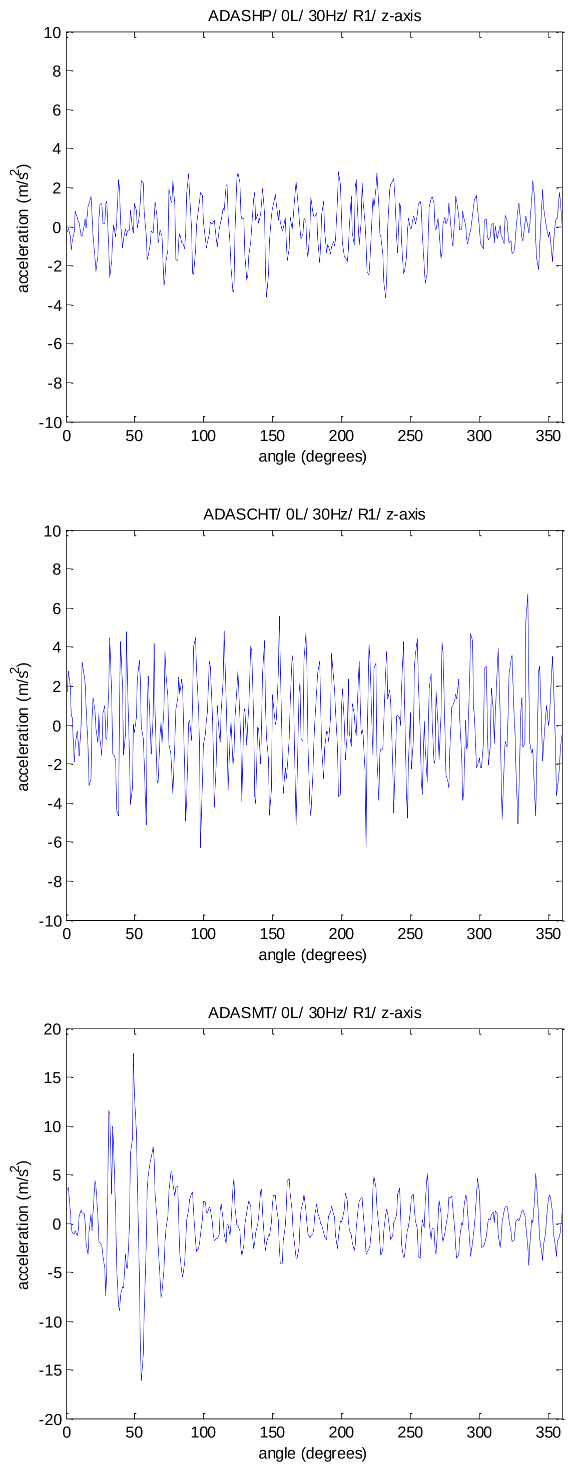

Fig. 5.6. *ADA signals for the healthy pinion, chipped tooth pinion and missing tooth pinion*

It can be observed from Fig. 5.6 that the amplitude of the ADA signal for the chipped tooth pinion is higher than the amplitude of the

ADA signal for the healthy pinion. Moreover, the ADA signal for the missing tooth pinion exhibits high amplitude impulses at around 50 degrees of rotation. This indicates the missing tooth pinion location which was not evident in the time domain or the angular domain vibration signals.

The above methods of gear fault diagnosis, however, are to a great extent dependent on the judgement of the operator and are, therefore, susceptible to error. It is desirable to have an automated method of gearbox fault diagnosis wherein the condition of the gearbox can be ascertained automatically by feeding in parameters derived from the gearbox signatures. This is accomplished in the present work by employing an ANFIS classifier which is fed in with CWCs derived from gearbox vibration signals.

5.4. Continuous wavelet transform (CWT)

The continuous wavelet transform of a signal $x(t)$ is defined as a convolution integral of $x(t)$ with scaled and dilated versions of a mother wavelet function $\Psi_{s,\tau}(t)$ and is given by Eq. (2.12).

Jedlinski and Jonak [131] proposed that the method of feeding CWCs directly to an intelligent classifier such as an ANN or support vector machine (SVM) results in superior gear fault diagnostic accuracy rather than when statistical parameters derived from raw vibration signals are employed for fault diagnosis. In the present work, the independent angular domain signals (obtained from the IAR technique) are segmented into 6 parts, each representing 60 degrees of pinion rotation. These signals with 6 data samples each are averaged to arrive at angular domain averaged (ADA) signals for each pinion health condition. The ADA signals are then decomposed with CWT and CWCs from the various scales fed directly as inputs to an ANFIS classifier.

Bafroui and Ohadi [51] reported an improvement in the test accuracy of an ANN when parameters derived from CWCs at an optimal range of scales were fed to the ANN. They proposed a method of identifying the optimal scales based on energy-Shannon's entropy ratio of CWCs. Fig. 5.7 shows the WAM corresponding to combined angular domain signal of Fig. 5.5 (a). In the present work, the Morlet wavelet is employed as the mother wavelet owing to its similarity to an impulse component that is characteristic of a fault in a geared system.

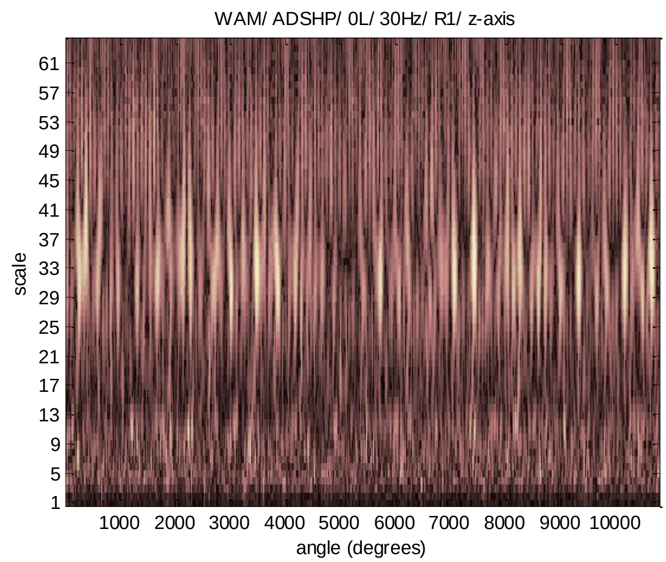

Fig. 5.7. *WAM corresponding to the angular domain signal of Fig.5.5(a)*

The energy-entropy ratio of CWCs at the 64 scales of the WAM pertaining to the healthy pinion is represented graphically in Fig. 5.8. The range of scales from 25 to 49 has higher energy-entropy ratio compared to the other scales and is referred to as the optimal range of scales.

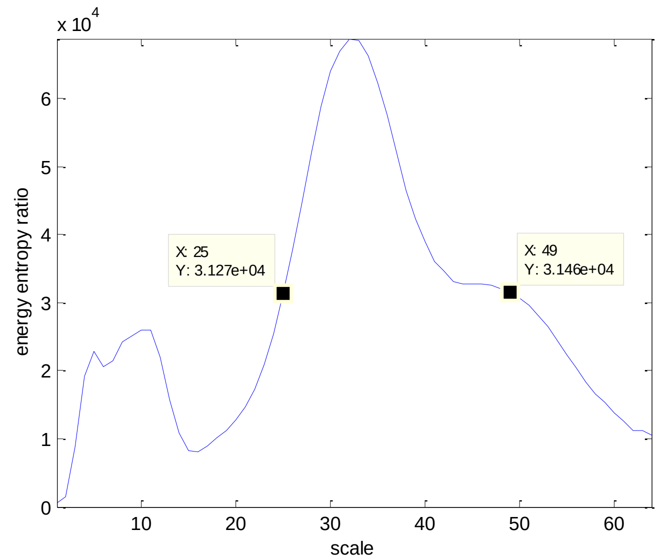

Fig. 5.8. *Energy-Shannon's entropy ratio plot corresponding to the WAM of Fig.5.7*

5.5. Results and discussions

The WAMs corresponding to the angular domain averaged signals consist of 6 segments representing 60º, 120º, 180º, 240º, 300º and 360º rotation of the pinion. Fig. 5.9 shows the angular domain averaged WAMs corresponding to the three pinion health conditions.

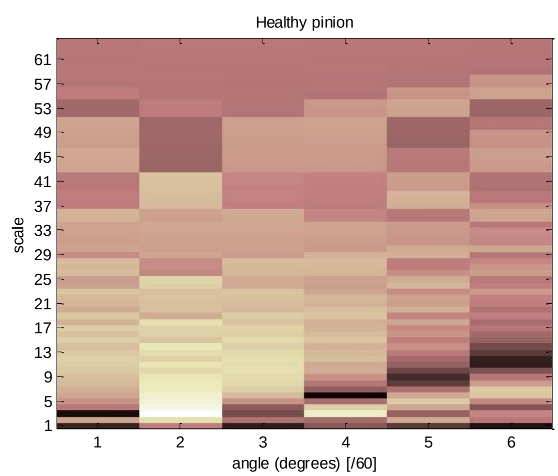

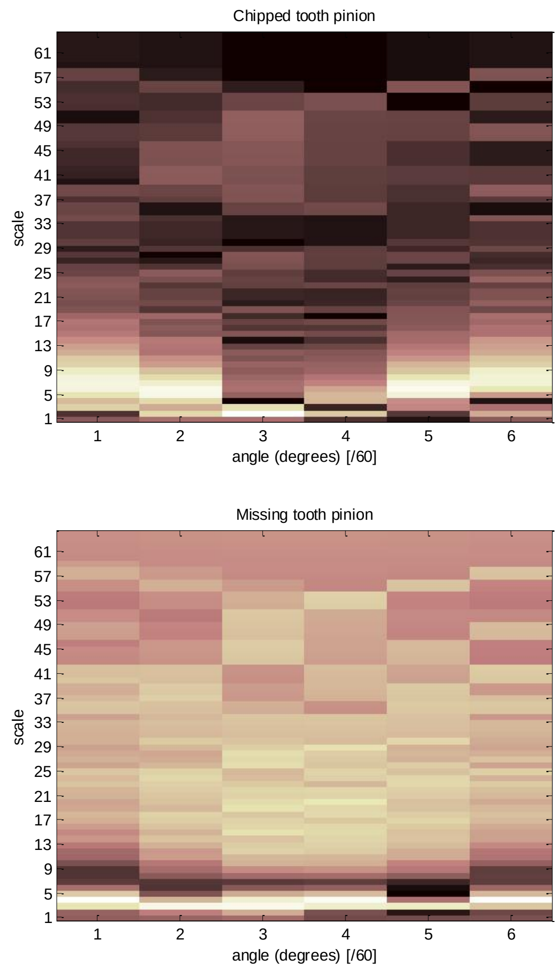

Fig. 5.9. *Segmented WAMs for the three pinion health conditions*

The three WAMs in Fig. 5.9 appear different from each other and can be utilized to ascertain the condition of the gearbox by feeding in CWCs directly to an ANFIS classifier. CWCs from all scales as well as from only the optimal scales are employed in the form of input columns to the ANFIS. The Gaussian membership functions are chosen for the inputs to the ANFIS and each such input is divided into two regions: small and large. The number of data samples from each class is 64 when data is fed in from all scales and 25 when data is fed in from only the optimal scales. In each case, 50% of the randomly selected data samples from each class are utilized for training the ANFIS while the remaining 50% are reserved for testing. Thus, two cases, as enumerated in Table 5.1, are considered in the present work.

Table 5.1

Breakdown of training and test data samples from each class.

Signal type	Case	No. of data samples from each class	No. of training data samples from each class	No. of test data samples from each class
Vibration (z-axis)	1	64	32	32
	2	25	13	12

Case 1: Data is fed in from all 64 scales, i.e., there are 6 columns consisting of CWCs from all 64 scales pertaining to the three classes.

When the ANFIS is trained with 32 randomly selected data samples from each class, the final error convergence value is 0.00020132 over 400 training epochs as shown in Fig. 5.10.

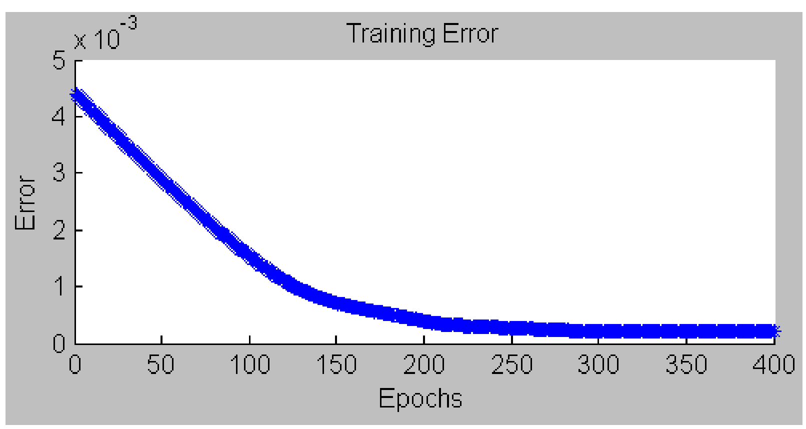

Fig. 5.10. *Network error convergence curve (Case 1)*

Fig. 5.11 shows the classification accuracy of the trained ANFIS with training data samples. It can be observed that all the 32 training data samples from each class are correctly classified.

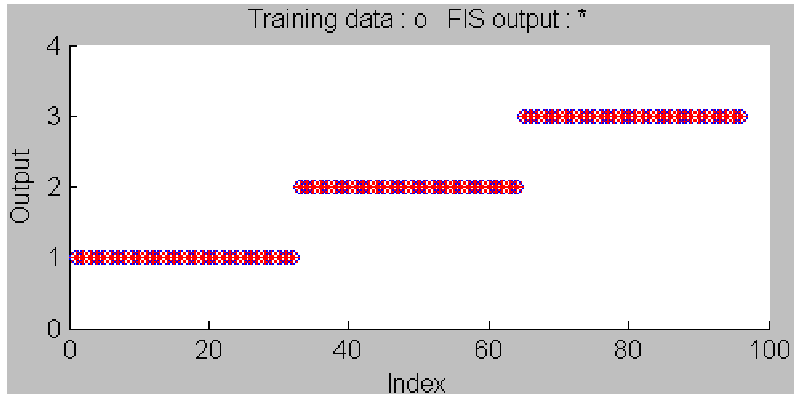

Fig. 5.11. *Classification accuracy of the trained ANFIS with the training data samples*

After the ANFIS has been trained with the training data set (in this case, with 32 randomly data samples from each class), its classification accuracy with the test data set is tested. Fig. 5.12 shows the classification accuracy of the trained ANFIS with the test data samples. It can be observed that some of the test data samples are incorrectly classified.

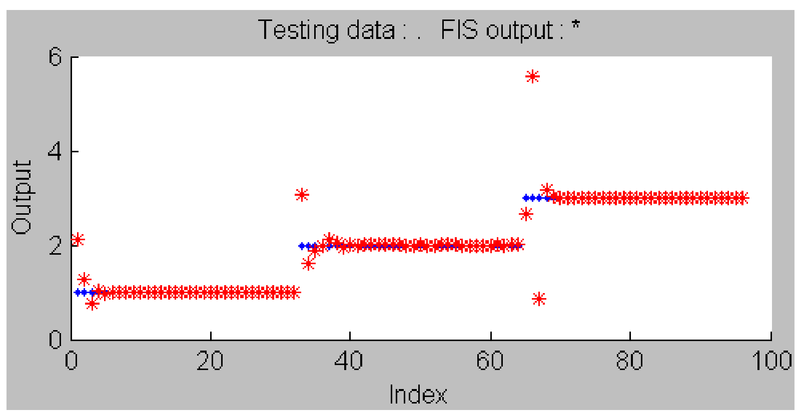

Fig. 5.12. *Classification accuracy of the trained ANFIS with test data samples*

Case 2: The ANFIS is trained and tested with data samples belonging to the optimal scales (25 to 49). There are still 6 columns consisting of CWCs. Here, only the number of data samples has been reduced from 64 to 25 from each class. Amongst the 25 data samples from each class, 13 data samples are used to train the ANFIS while the remaining 12 data samples are reserved for testing. Fig. 5.13 shows the network error convergence curve wherein the final training error over 200 training epochs is 0.00026494.

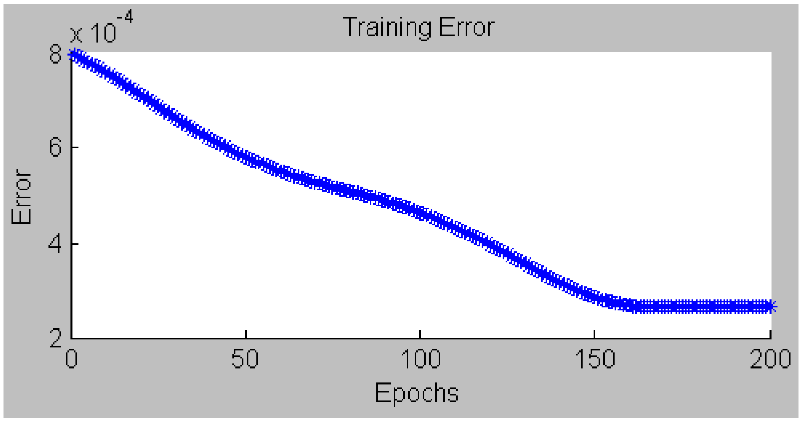

Fig. 5.13. *Network error convergence curve (Case 2)*

Fig. 5.14 shows the classification accuracy of the trained ANFIS with the training data set. All the 13 data samples from each class are correctly classified.

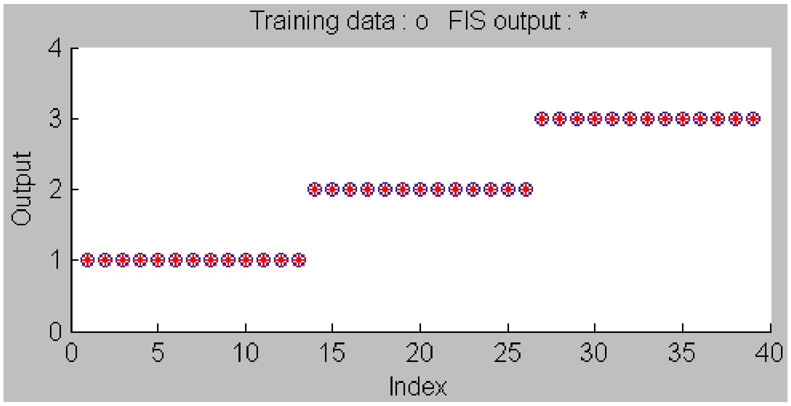

Fig. 5.14. *Classification accuracy of the trained ANFIS with the training data set*

Fig. 5.15 shows the test accuracy of the trained ANFIS with the test data set. All the 12 data samples from each class are correctly classified. The test results are unlike Case 1 where some of the test instances were incorrectly classified.

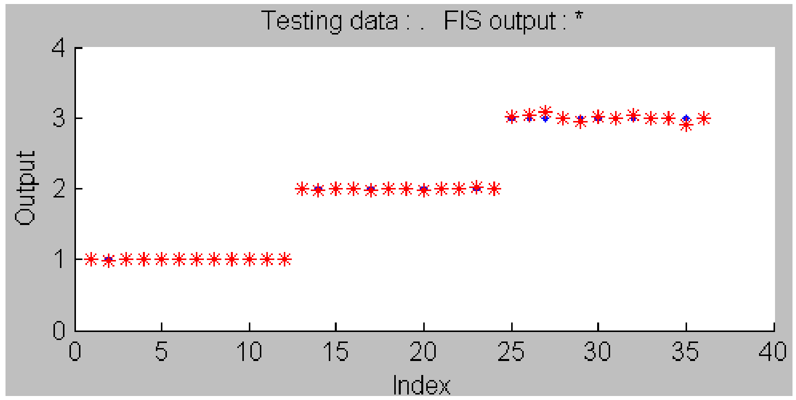

Fig. 5.15. *Classification accuracy of the trained ANFIS with the test data set*

The results demonstrate that data samples from the optimal scales of the vibration signals' WAMs have superior fault discrimination potential. In order to test the proposed method for its generalization to other types of gearboxes, the procedure is repeated for fault diagnosis of a single stage spur gearbox. However, this time the procedure is applied to a four-class problem instead of the three-class problem as in the case of the bevel gearbox.

5.6. Fault diagnosis of a single stage spur gearbox

The experimental set-up consists of a single stage spur gearbox that forms an integral part of the drive train diagnostic simulator (DDS) shown in Fig. 5.16.

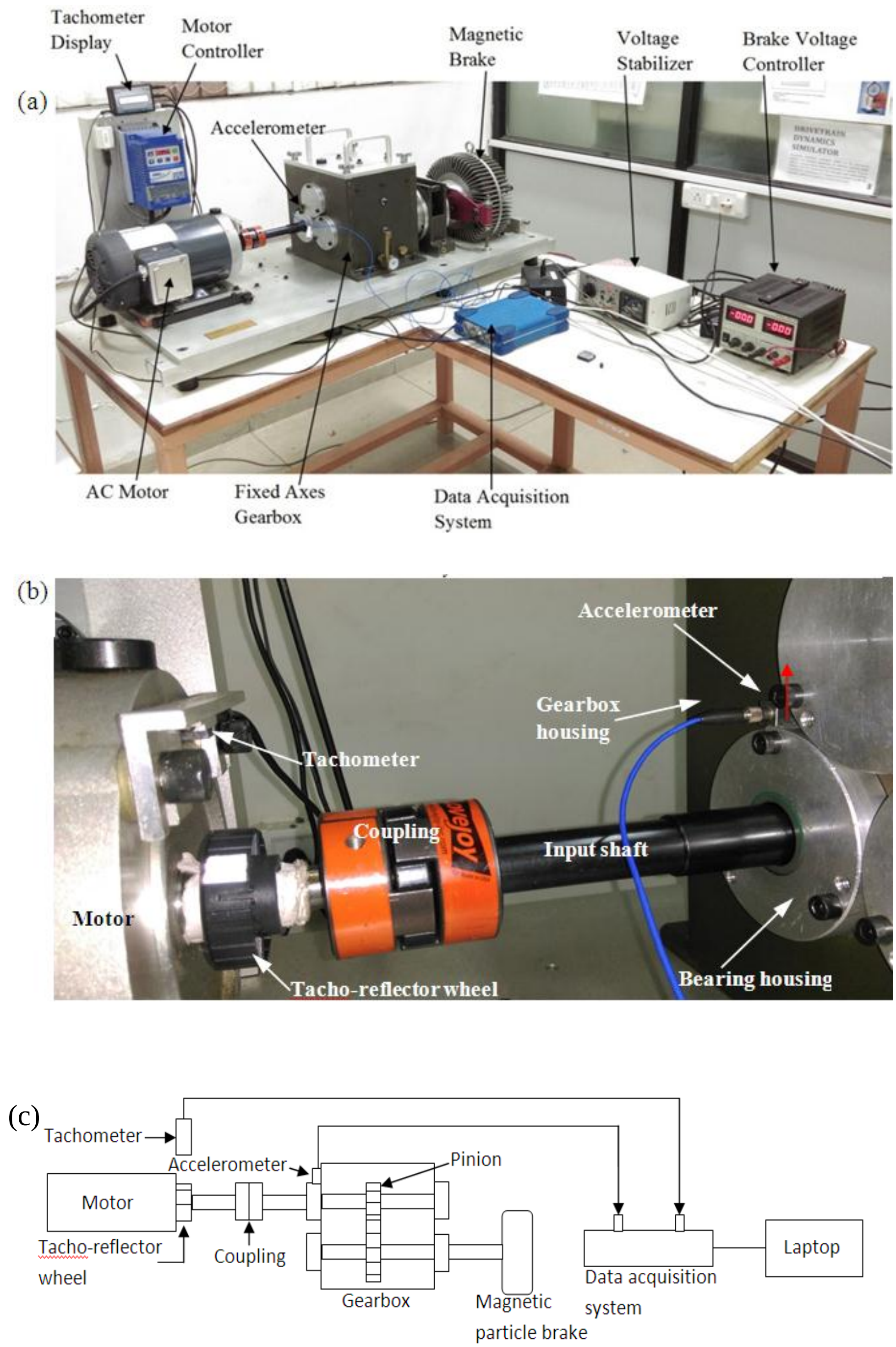

Fig. 5.16. *(a) Drive train diagnostic simulator (DDS), (b) sensor arrangement and (c) schematic diagram of the DDS*

The accelerometer for acquiring the vibration signal is mounted on the bearing housing of the gearbox input shaft. Vibration signals are measured along the z-axis as indicated by a red arrow in Fig. 5.16 (b). The multiple pulse tachometer arrangement is facilitated by mounting a multiple strip tacho-reflector wheel on the motor output shaft. The accelerometer and tachometer are interfaced to a PC via a data acquisition system.

Vibration signals are acquired under four different pinion health conditions (healthy, cracked tooth, chipped tooth and missing tooth) at a constant speed of 20 Hz at 0% load. Some of the pinion wheels employed for the experiments are shown in Fig. 5.17.

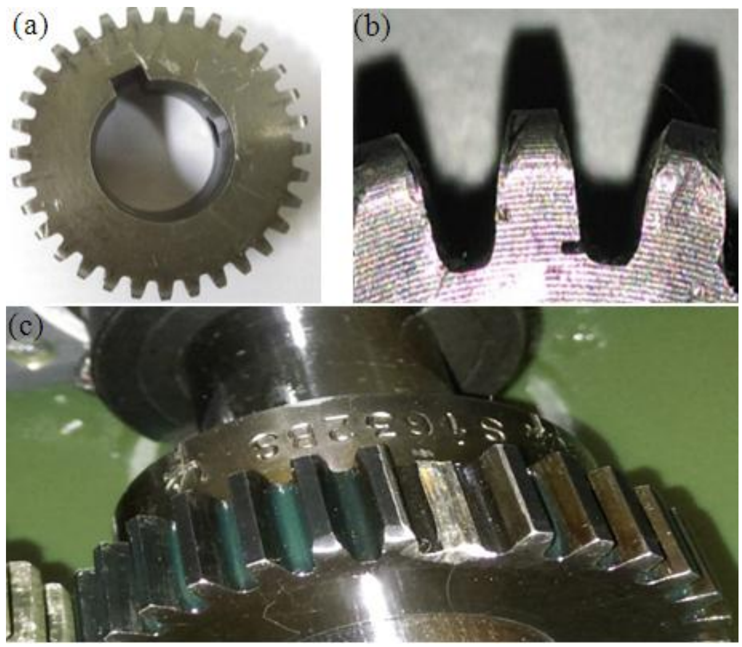

Fig. 5.17. *(a) Healthy pinion (b) cracked tooth pinion and (c) missing tooth pinion*

The sampling frequency is selected as 8192 Hz and the gear wheel remains the same in each of the experiments. Segments of vibration signals during which the gearbox drive shaft undergoes 50 complete revolutions have been considered for analysis. Fig. 5.18 shows the vibration signals acquired from the gearbox under various pinion health conditions. The number of samples corresponding to 50 revolutions is not the same in each of the four cases owing to fluctuations in speed of the gearbox drive shaft.

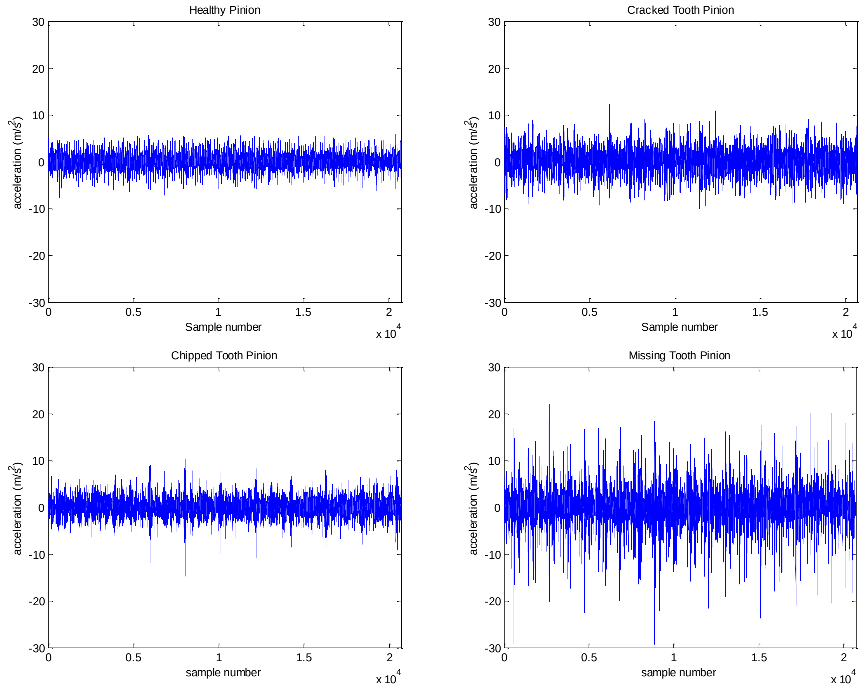

Fig. 5.18. *Vibration signals over 50 complete revolutions of the gearbox drive shaft with healthy pinion, cracked tooth pinion, chipped tooth pinion and missing tooth pinion*

It can be observed from Fig. 5.18 that the amplitude of the vibration signal acquired with the healthy pinion is lower than the other cases. However, it is difficult to distinguish between the healthy pinion and the cracked tooth pinion from only a visual inspection of the time domain vibration signals. Further, impulses at regular intervals are observed in case of the chipped tooth pinion while impacts of large amplitude are observed in case of the missing tooth pinion. Though a visual inspection of the acquired time domain vibration signals may help an operator diagnose the condition of the gearbox, an automated method of gearbox fault diagnosis is desirable in order to minimize human error.

As in the case of the bevel gearbox, the IAR technique is employed to convert the non-stationary time domain vibration signals into quasi-stationary signals in the angular domain. Fig. 5.19 shows the combined angular domain signal for the healthy pinion and the corresponding WAM.

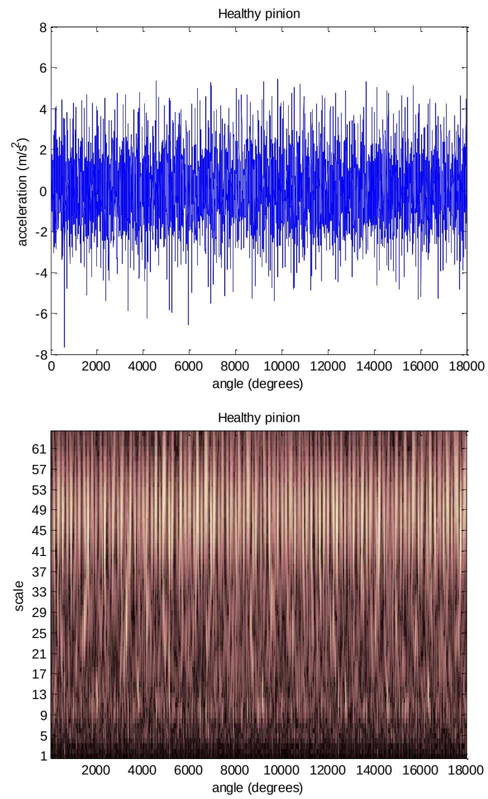

Fig. 5.19. *Angular domain signal for the healthy pinion and the corresponding WAM*

Fig. 5.20 shows the energy-Shannon's entropy ratio of CWCs at the 64 scales of the WAM in case of the healthy pinion. The scales ranging from 32 to 61 (30 scales) have higher energy-Shannon's entropy ratio compared to the other scales and are referred to as the optimal scales.

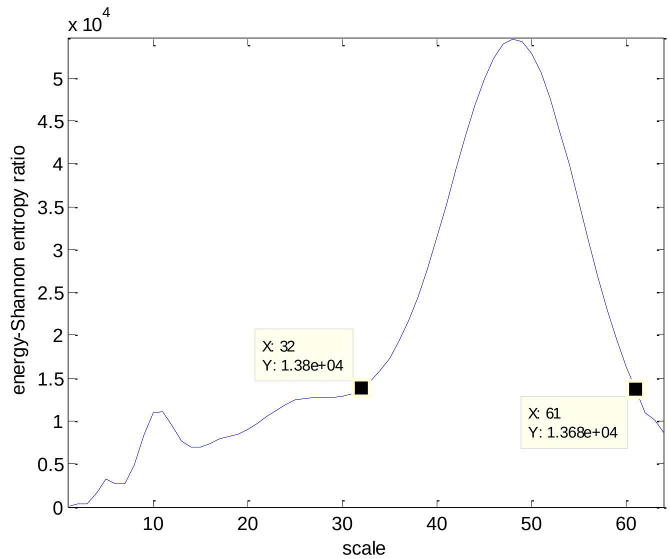

Fig. 5.20. *Energy-Shannon's entropy ratio at the 64 scales of the WAM in case of the healthy pinion*

The 360° of rotation associated with each independent revolution is divided into 6 segments, each representing 60° of rotation. Fig. 5.21 shows the angular domain averaged WAMs for the four pinion health conditions segmented into 6 regions. CWCs from segments 1 to 6 are employed directly as six inputs to the ANFIS.

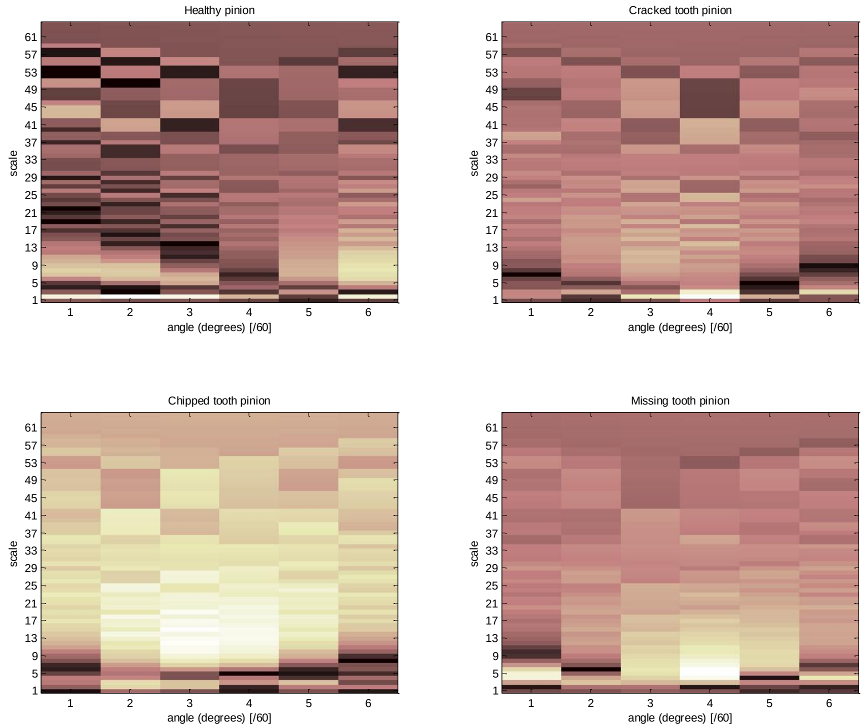

Fig. 5.21. *Angular domain averaged WAMs representing 360° of rotation in segments of 60°*

First, CWCs from all scales are utilized to train and test the ANFIS. There are 6 columns of CWCs and 64 data samples from each class of which 32 randomly selected data samples are used to train the ANFIS while the remaining 32 data samples are used for testing. Fig. 5.22 shows that over 200 training epochs, the final error convergence value is 0.021458.

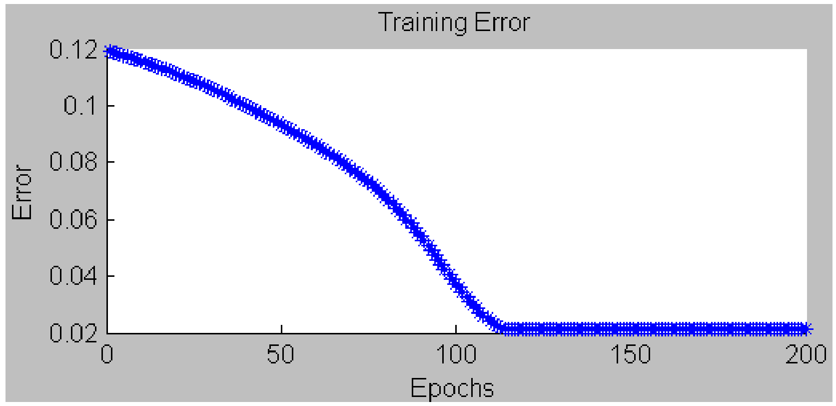

Fig. 5.22. *ANFIS error convergence curve*

Fig. 5.23 and Fig. 5.24 show the training and test accuracy of the trained ANFIS when fed with CWCs from all scales. The training accuracy when CWCs from all scales are directly fed to the trained ANFIS is 100%. However, it can be observed from Fig. 5.24 that a number of test instances are misclassified.

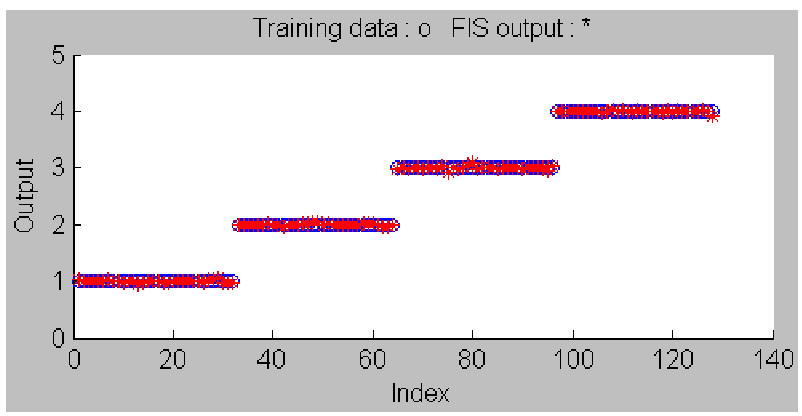

Fig. 5.23. *Classification accuracy of the trained ANFIS when fed with training data samples*

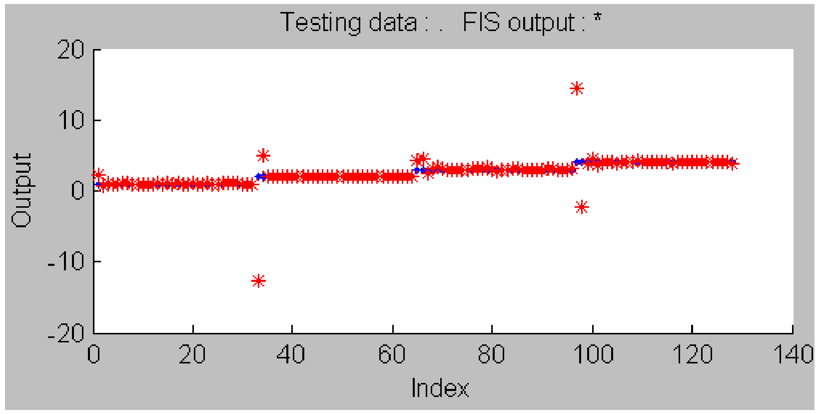

Fig. 5.24. *Classification accuracy of the trained ANFIS when fed with test data samples*

When CWCs from only the optimal scales are utilized to train and test the ANFIS, the final error convergence value over 150 training epochs is 0.00083938 as shown in Fig 5.25.

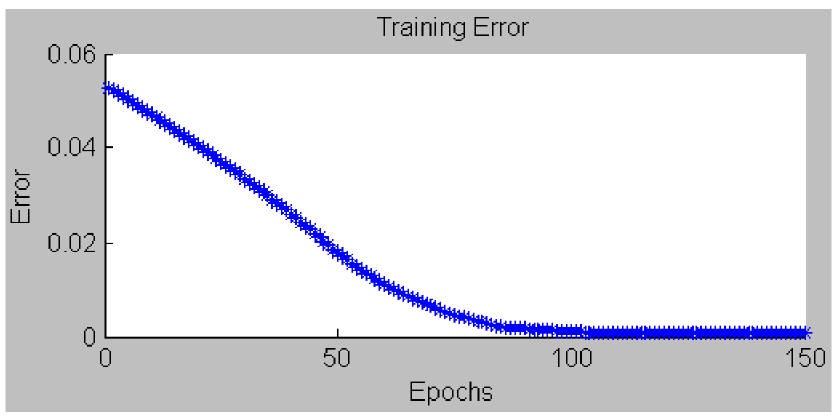

Fig. 5.25. *Error convergence curve when CWCs from optimal scales are fed to the ANFIS*

Fig. 5.26 and Fig. 5.27 show the training and test accuracy of the trained ANFIS when fed with CWCs from the optimal scales. 15 randomly selected data samples from the optimal range of scales are used to train the ANFIS while the remaining 15 data samples from each class are reserved for testing the classification accuracy of the trained ANFIS.

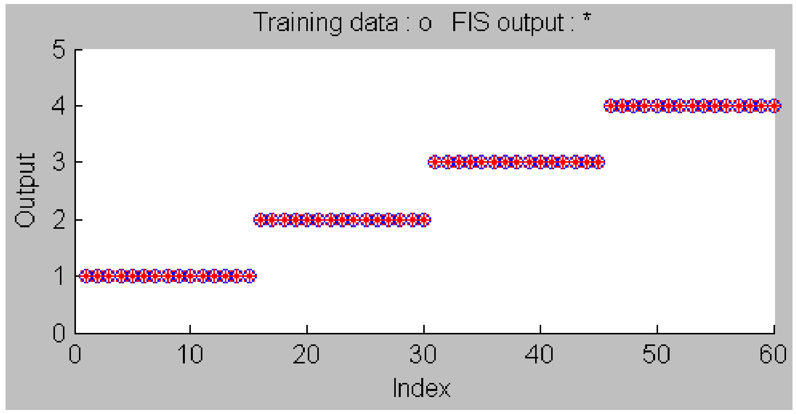

Fig. 5.26. *Classification accuracy of the trained ANFIS when fed with training data samples*

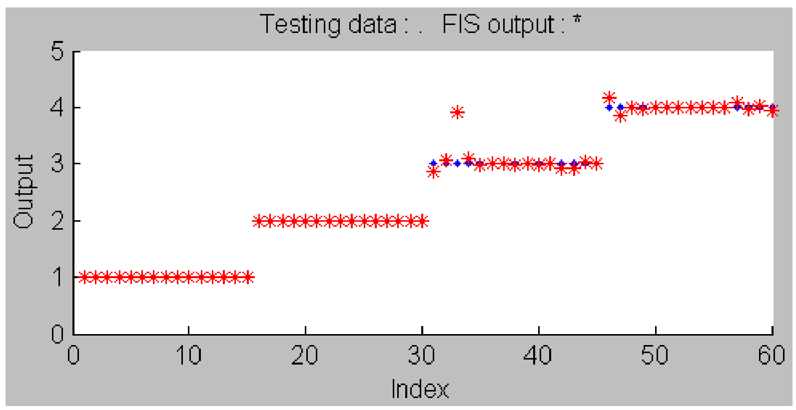

Fig. 5.27. *Classification accuracy of the trained ANFIS when fed with test data samples*

CWCs from the optimal range of scales when employed directly as inputs to the ANFIS, result in reasonably good training and test accuracy. As seen in Fig. 5.27, only one of the test samples belonging to Class 3 (chipped tooth pinion) is misclassified as Class 4 (missing tooth pinion). The other test samples are nearly correctly classified.

5.7. Conclusion

This Chapter attempts to diagnose faults in a bevel gearbox under non-stationary conditions feeding CWCs directly as inputs to an ANFIS classifier. First, the non-stationary vibration signals acquired from the gearbox are converted into quasi-stationary signals in the angular domain employing the IAR technique. Implementation of the IAR technique demands only minor changes in hardware such as the introduction of an additional tachometer reflective strip. The combined angular domain signals obtained from the IAR technique are decomposed using CWT and a range of optimal continuous wavelet scales identified based on the energy-Shannon's entropy ratio of CWCs. The independent angular domain signals are segmented into six parts, each representing 60° rotation of the pinion. A number of such angular domain signals from each class are averaged to arrive at angular domain averaged signals which are decomposed using CWT. Thus, each angular domain averaged WAM consists of 6 data samples, each representing 60° of pinion rotation. CWCs from each segment are then employed directly as inputs to an ANFIS classifier. Reasonably good training and test accuracy is attained when CWCs from only the optimal range of scales are employed directly as inputs to the ANFIS. The procedure is repeated for vibration signatures acquired over approximately 2.5 s duration in case of a single stage spur gearbox. Reasonably good training and test accuracy is obtained when CWCs from only the optimal range of scales are employed to train and test the ANFIS. The results obtained in the present work demonstrate the simplicity and effectiveness of the IAR technique, continuous wavelet transform and ANFIS in diagnosing faults under non-stationary conditions in both the bevel as well as the spur gearbox.

Chapter 6

Conclusion and scope for further research

Considering the widespread application of gearboxes and their significance in power transmission, considerable amount of research efforts have been devoted in the recent past to devise new and effective methods of GFD. However, an automated method of GFD is desirable such that the occurrence of a defect can be identified automatically with minimal intervention of the operator. Further, the designed system must be able to diagnose faults under the realistic non-stationary conditions to which the gearbox is subjected. This study involves the application of AI to GFD under non-stationary conditions. In particular, the BPNN and ANFIS are employed as two intelligent classifiers for diagnosing faults such as a cracked tooth, chipped tooth and missing tooth in a single stage gearbox.

It has been shown in this study that gearbox vibration and acoustic signatures have a natural propensity to be non-stationary. The methods proposed in this thesis have been applied successfully in diagnosing gearbox faults under non-stationary conditions. As a novel approach, a simple yet powerful technique called the IAR technique, is proposed to convert non-stationary signals in the time domain into quasi-stationary signals in the angular domain. The IAR technique demands only minor changes in hardware such as the introduction of an additional tachometer reflective strip.

Chapter 2 of this study is based on the application of ANN in diagnosing gearbox faults under fluctuating load conditions. Sinusoidal load fluctuations at the output invariably produce speed fluctuations resulting in non-stationary conditions. The angular domain signals generated from the IAR technique are merged to produce the combined angular domain signal corresponding to the complete rotational period.

This combined angular domain signal is decomposed using CWT and a range of optimal continuous wavelet scales identified based on the energy-Shannon’s entropy ratio of the CWCs. The classification accuracy of an ANN is compared when CWCs from all scales and when CWCs from only the optimal scales are employed as input feature vectors. When CWCs from only the optimal scales are employed as input feature vectors, not only is the training time of the ANN reduced but also the test accuracy is enhanced. Reasonably good gear fault diagnostic accuracy is obtained when the proposed method is employed to diagnose faults such as a cracked tooth and missing tooth under fluctuating load conditions.

Unlike in Chapter 2 where gearbox vibration signatures acquired under fluctuating load conditions are analyzed, in Chapter 3 gearbox vibration and sound emission signatures acquired at a constant programmed speed of rotation are analyzed. Vibration signatures are acquired in two mutually perpendicular directions in order to study whether there is any advantage in the gear fault diagnostic accuracy by acquiring signatures in a particular direction. It is revealed that gearbox vibration and sound emission signatures have a natural tendency to be non-stationary. This is evident from an unequal number of samples between tachometer pulses. Under such non-stationary conditions, techniques such as TSA cannot be directly employed to improve the signal to noise ratio. Since the acquired gearbox signatures are non-stationary, the IAR technique is combined with PCHI to generate a number of angular domain signals, each representing one revolution of the gearbox drive shaft. The resulting angular domain signals are averaged in order to improve the signal to noise ratio. The ADA signals thus obtained are decomposed using CWT and CWCs from the 64 scales employed directly as inputs to a BPNN. The dimensionality of the input feature vectors is 360 and the number of output neurons is 4 since the problem is a four class gear fault identification problem. The number of neurons in the hidden layer is determined by trial and error. Reasonably good gear fault diagnostic accuracy is attained when the proposed method is applied to diagnose faults such as a cracked tooth, chipped tooth and missing tooth in a single stage spur gearbox. Marginally superior results are obtained when the sound emission signatures are analyzed to ascertain the condition of the gearbox. Moreover, no clear advantage in terms of the gear fault diagnostic accuracy is obtained when vibration signatures acquired in two mutually perpendicular directions are analyzed for fault diagnosis.

Unlike Chapters 2 and 3 which are based on the application of vibration signals and BPNN to GFD, Chapter 4 employs the ANFIS to diagnose faults such as a cracked tooth and chipped tooth in a single stage spur gearbox. Acoustic signatures are acquired under three different gearbox health conditions at a constant programmed speed of 10 Hz. The acoustic signals are synchronized from the revolution point of view and the resulting ADA signals decomposed using CWT choosing the number of scales to be 128. A range of optimal scales is identified based on the energy-entropy ratio of CWCs from the WAM pertaining to the healthy pinion. Wavelet amplitude maps for the three pinion health conditions are segmented and CWCs from optimal scales fed directly in the form of data samples to an ANFIS with the objective of identifying the condition of the gearbox. The Gaussian membership function is chosen for the inputs to the classifier. Each of the 6 inputs to the ANFIS is divided into two Gaussian membership functions, viz., small and large. Through a combination of the IAR technique, continuous wavelet transform and ANFIS, acoustic signals are effectively utilized for diagnosing the condition of a gearbox.

Chapter 5 attempts to diagnose faults in a bevel gearbox under non-stationary conditions feeding CWCs directly as inputs to an ANFIS classifier. First, the non-stationary vibration signals acquired from the gearbox are converted into quasi-stationary signals in the angular domain employing the IAR technique. The combined angular domain signals obtained from the IAR technique are decomposed using CWT and a range of optimal continuous wavelet scales identified based on the energy-Shannon's entropy ratio of CWCs. The independent angular domain signals are segmented into six parts, each representing 60° rotation of the pinion. A number of such angular domain signals from each class are averaged to arrive at angular domain averaged signals which are decomposed using CWT. Thus, each angular domain averaged WAM consists of 6 data samples, each representing 60° of pinion rotation. CWCs from each segment are then employed directly as inputs to an ANFIS classifier. Reasonably good training and test accuracy is attained when CWCs from only the optimal range of scales are employed directly as inputs to the ANFIS. The procedure is repeated for vibration signatures acquired over approximately 2.5 s duration in case of a single stage spur gearbox. Reasonably good training and test accuracy is obtained when CWCs from only the optimal range of scales are employed to train and test the ANFIS. The results obtained in the present work demonstrate the simplicity and effectiveness of the IAR technique, continuous wavelet transform and ANFIS in diagnosing faults under non-stationary conditions in both the bevel as well as the spur gearbox.

It is evident from the present study that an analysis of acoustic signatures may serve as a promising alternative to diagnose the condition of the gearbox. However, at the time of writing this thesis, the number of research papers based on an analysis of acoustic signatures to diagnose gearbox faults using AI is limited. To the best of the author's knowledge, the application of ANFIS to diagnose gearbox faults based on acoustic signatures has not been attempted as a novel work in this research and may be a subject of further research. The methods proposed in this thesis have been successfully applied to GFD by acquiring signatures from an experimental set-up. The proposed methods can be extended to real life applications where the acquired signals are non–stationary.

REFERENCES

[1] P. Association, North Sea Helicopter Crash Report Says Gearbox Failed After Maintenance Error, The Guardian, 2011.

[2] Lei Y.G., Zuo M.J., He Z.J. *et al* (2010) A multidimensional hybrid intelligent method for gear fault diagnosis, Expert Systems with Applications, 37, 1419–1430.

[3] Lebold M., McClintic K., Campbell R. *et al* (2000) Review of vibration analysis methods for gearbox diagnostics and prognostics, In: Proceedings of the 54th Meeting of the Society for Machinery Failure Prevention Technology, Virginia Beach, VA, pp. 623–634.

[4] Bajric´ R., Sprecˇic´ D. & Zuber N. (2011) Review of vibration signal processing techniques towards gear pairs damage identification, International Journal of Engineering & Technology, 11, 124–128.

[5] Lei Y., Lin J., Zuo M.J. *et al* (2014) Condition monitoring and fault diagnosis of planetary gearboxes: A review, Measurement, 48, 292–305.

[6] Feng Z., Zuo M.J. & Chu F. (2010) Application of regularization dimension to gear damage assessment, Mech. Syst. Signal Process., 24, 1081–1098.

[7] Feng Z. & Zuo M.J. (2013) Fault diagnosis of planetary gearboxes via torsional vibration signal analysis, Mech. Syst. Signal Process., 36, 401–421.

[8] Lei Y. & Zuo M.J. (2009) Gear crack level identification based on weighted k nearest neighbor classification algorithm, Mech. Syst. Signal Process., 23, 1535–1547.

[9] Bartelmus W. (2013) New focus on gearbox condition monitoring for failure prevention technology, Key Eng. Mater., 588, 184–191.

[10] Bartelmus W. (2014) Object and operation supported maintenance for mining equipment, Min. Sci., 21, 7–21.

[11] Bartelmus W. & Zimroz R. (2009) A new feature for monitoring the condition of gearboxes in non-stationary operating conditions, Mech. Syst. Signal Process., 23, 1528–1534.

[12] Zimroz R. & Bartelmus W. (2009) Gearbox condition estimation using cyclo-stationary properties of vibration signal, Key Eng. Mater., 413, 471–478.

[13] Bartelmus W. & Zimroz R. (2008) Problems and solutions in condition monitoring and diagnostic of open cast monster machinery driving systems, Diagnostyka, 3, 55–60.

[14] Bartelmus W. (2008) Root cause and vibration signal analysis for gearbox condition monitoring, Insight – Non-Destr. Test. Cond. Monit., 50, 195–201.

[15] Bartelmus W. & Zimroz R. (2009) Vibration condition monitoring of planetary gearbox under varying external load, Mech. Syst. Signal Process., 23, 246–257.

[16] Bartelmus W. & Zimroz R. (2011) Vibration spectra characteristic frequencies for condition monitoring of mining machinery compound and complex gearboxes, Pr. Nauk. Inst. Gór. Politech. Wroc. Stud. Mater., 133, 17–34.

[17] Randall R.B. (1982), A new method of modeling gear faults, J. Mech. Des., 104, 259–267.

[18] McFadden P.D. & Smith J.D. (1985) An explanation for the asymmetry of the modulation sidebands about the tooth meshing frequency in epicyclic gear vibration, Proc. Inst. Mech. Eng. Part C J. Mech. Eng. Sci., 199, 65–70.

[19] McFadden P.D. (1986) Detecting fatigue cracks in gears by amplitude and phase demodulation of the meshing vibration, J. Vib. Acoust., 108, 165–170.

[20] Inalpolat M. & Kahraman A. (2009) A theoretical and experimental investigation of modulation sidebands of planetary gear sets, J. Sound Vib. 323, 677–696.

[21] Feng Z. & Zuo M.J. (2012) Vibration signal models for fault diagnosis of planetary gearboxes, J. Sound Vib., 331, 4919–4939.

[22] Patrick R., Ferri A. & Vachtsevanos G. (2012) Effect of planetary gear carrier-plate cracks on vibration spectrum, J. Vib. Acoust., 134, 61001-61007.

[23] Liang X., Zuo M.J. & Chen W. (2017) Dynamics based vibration signal modeling for tooth fault diagnosis of planetary gearboxes, In: M. Demetgul, M. Ünal (Eds.), Fault Diagnosis and Detection, In Tech.

[24] De Silva C.W. (2009), Modeling and Control of Engineering Systems, CRC Press, Boca Raton, FL, pp 11-20 (ISBN 13: 978-1-4200-7687-5)

[25] Leonard J.W. & Nath J.H. (1981) Comparison of finite element and lumped parameter methods for oceanic cables, Eng. Struct., 3, 153–167.

[26] Liang X., Zhang H., Liu L. *et al* (2016) The influence of tooth pitting on the mesh stiffness of a pair of external spur gears, Mech. Mach. Theory, 106, 1–15.

[27] Liang X., Zuo M.J. & Pandey M. (2014) Analytically evaluating the influence of crack on the mesh stiffness of a planetary gear set, Mech. Mach. Theory 76, 20–38.

[28] Liang X., Zuo M.J. & Feng Z. (2018) Dynamic modeling of gearbox faults: A review, Mechanical Systems an
d Signal Processing, 98, 852–876**.**

[29] Ma H., Zeng J., Feng R. *et al* (2015) Review on dynamics of cracked gear systems, Eng. Fail. Anal., 55, 224–245.

[30] Blau P.J. (1992) ASM handbook, Volume 18 – Friction, Lubrication, and Wear Technology, 2017 edition, ASM International (ISBN: 978-1-62708-141-2)

[31] Rexnord Industries, LLC, Technical Report (1978) Failure-Analysis: Gears-Shafts-Bearings-Seals. https://rexnord.com. Accessed Jan 2017

[32] Cooley C.G. & Parker R.G. (2014) A review of planetary and epicyclic gear dynamics and vibrations research, Appl. Mech. Rev., 66, 1–15.

[33] Hammami A., Rincon A.F.D., Chaari F. *et al* (2015) Dynamic behaviour of back to back planetary gear in run up and run down transient regimes, J. Mech., 31, 481–491.

[34] Chaari F., Bartelmus W., Zimroz R. *et al* (2012) Effect of load shape in cyclic load variation on dynamic behavior of spur gear system, Key Eng. Mater., 518, 119–126.

[35] Hammami A., Rincon A.F.D., Chaari F. *et al* (2016), Effects of variable loading conditions on the dynamic behaviour of planetary gear with power recirculation, Measurement, 94, 306–315.

[36] Bartelmus W. (2001) Gearbox dynamic modelling, J. Theor. Appl. Mech., 39, 989–999.

[37] Bartelmus W. (2014) Gearbox dynamic multi-body modelling for condition monitoring under the case of varying operating condition, J. Coupled Syst. Multiscale Dyn., 2, 224–237.

[38] Chaari F., Bartelmus W., Zimroz R. *et. al* (2012) Gearbox vibration signal amplitude and frequency modulation, Shock Vib., 19, 635–652.

[39] Bartelmus W., Chaari F. & Zimroz R. (2012) Modeling of transmission used in wind turbines, In: British Institute of Non-Destructive Testing, London, UK, pp. 1–9.

[40] Hammami A., Rincon A.F.D., F. Chaari *et. al* (2017) Planet load sharing behavior during run up, In: Adv. Acoust. Vib., Springer, Cham, pp. 165–173.

[41] Khabou M.T., Bouchaala N., Chaari F. *et al* (2011) Study of a spur gear dynamic behavior in transient regime, Mech. Syst. Signal Process., 25, 3089–3101.

[42] Chaari R., Khabou M.T., Barkallah M. *et al* (2016) Dynamic analysis of gearbox behaviour in milling process: non-stationary operations, Proc. Inst. Mech. Eng. Part C J. Mech. Eng. Sci., 230, 3372–3388.

[43] Bartelmus W., Chaari F., Zimroz R. *et al* (2010) Modelling of gearbox dynamics under time-varying non-stationary load for distributed fault detection and diagnosis, Eur. J. Mech. – A Solids, 29, 637–646.

[44] Chaari F., Zimroz R., Bartelmus W. *et al* (2012) Model based investigation on a two stages gearbox dynamics under non-stationary operations, In: Cond. Monit. Mach. Non-Station. Oper., Springer, Berlin, Heidelberg, pp. 133–142.

[45] Chaari F., Zimroz R., Bartelmus W. *et al* (2011) Modeling of local damages in spur gears and effects on dynamics response in presence of varying load conditions, Proc. Surveill., 6, 1–19.

[46] Bartelmus W., Grabski J. (2016) Modelling and simulation of gear systems dynamics for supporting condition monitoring using mathematica, In: Chaari F., Zimroz R., Bartelmus E. *et al* (Eds.), Adv. Cond. Monit. Mach. Non-Station. Oper., Springer International Publishing, Cham, pp. 375–384.

[47] Li H. & Zhang Y (2008) Angle domain average and CWT for fault detection of gear crack, In: Proceedings of the IEEE Transaction, Fifth International Conference on Fuzzy Systems and Knowledge Discovery 3, Jinan, Shandong, China, pp. 137-141.

[48] Meltzer G. & Ivanov Y (2003) Fault detection in gear drives with non-stationary rotational speed - part I: the time-frequency approach, Mech. Syst. Signal Process., 17, 1033-1047.

[49] Meltzer G. & Ivanov Y. (2003) Fault detection in gear drives with non-stationary rotational speed - part II: the time-quefrency approach, Mech. Syst. Signal Process., 17, 273-283.

[50] Li H. & Zhang Y. (2009) Gear fault detection and diagnosis under speed-up condition based on order cepstrum and radial basis function neural network, J. Mech. Sci. Technol., 23, 2780-2789.

[51] Bafroui H.H. & Ohadi A. (2014) Application of wavelet energy and Shannon entropy for feature extraction in gearbox fault detection under varying speed conditions, Neurocomputing, 133, 437-445.

[52] Jafarizadeh M.A, Hasannejad R., Ettefagh M.M. *et al* (2008) Asynchronous input gear damage diagnosis using time averaging and wavelet filtering, Mech. Syst. Signal Process, 22, 172–201.

[53] Ahamed N., Pandya Y. & Parey A. (2014) Spur gear tooth root crack detection using time synchronous averaging under fluctuating speed, Measurement, 52,1-11.

[54] Sharma V. & Parey A. (2016), Gear crack detection using modified TSA and proposed fault indicators for fluctuating speed conditions, Measurement, 90, 560–575.

[55] Sharma V. & Parey A. (2016) A review of gear fault diagnosis using various condition indicators, 12th International Conference on Vibration Problems, ICOVP 2015, Procedia Engineering, 144, 253 – 263.

[56] Decker H. J. (2002) Crack detection for aerospace quality spur gears, NASA TM-2002-211492, ARL-TR-2682, NASA and the US Army Research Laboratory.

[57] Eltabach M., Vervaeke T., Sieg-Zieba S. *et al* (2013) Features extraction using vibration signals for condition monitoring of lifting cranes. https://www.cetim.fr. Accessed 26 Jul 17.

[58] Decker H. J. (2003) Effects on diagnostic parameters after removing additional synchronous gear meshes, Technical Report NASA TM-2003-212312, ARL-TR-2933, NASA and the US Army Research Laboratory.

[59] Decker H. J., & Lewicki D.G. (2003) Spiral bevel pinion crack detection in a helicopter gearbox. In Proceedings of the American helicopter society, 59th annual forum, Phoenix, AZ, pp. 1222–1232.

[60] Samuel P. D. & Pines D. J. (2005) A review of vibration-based techniques for helicopter transmission diagnostics, Journal of Sound and Vibration, 282, 475–508.

[61] Zuo M. J., Li W. & Fan X. F. (2005) Statistical methods for low speed planetary gearbox monitoring, Technical Report, Department of Mechanical Engineering, University of Alberta, Edmonton, pp 12.

[62] Zakrajsek J. J., Townsend D. P., Decker H. J. (1993) An analysis of gear fault detection methods as applied to pitting fatigue failure data, NASA TM-105950, AVSCOM TR-92-C-035, NASA and the US Army Aviation Systems Command, January 1993.

[63] Zakrajsek, J. J., Handschuh, R. F. & Decker, H. J. (1994) Application of Fault Detection Techniques to Spiral Bevel Gear Fatigue Data, In: Proceedings of 48th Meeting of the Society for Mechanical Failure Prevention Technology, Wakefield, ME.

[64] Ma J. (1995) Energy operator and other demodulation approaches to gear defect detection, In: Proceedings of the 49th Meeting of the Society for Machinery Failure Prevention Technology (MFPT), Virginia Beach, VA, pp. 127–140.

[65] McDonald G. L., Zhao Q. & Zuo M. J. (2012) Maximum correlated kurtosis de-convolution and application on gear tooth chip fault detection", Mechanical Systems and Signal Processing, 33, 237–255.

[66] Szczepanik A. (1989) Time Synchronous Averaging of Ball Mill Vibration, Mechanical Systems and Signal Processing, 3, 99–107.

[67] Lei Y. G., He Z. J., Zi Y. Y., *et al* (2007) Fault diagnosis of rotating machinery based on multiple ANFIS combination with Gas, Mechanical Systems and Signal Processing, 21, 2280–2294.

[68] Večeř P., Kreidl M. & Šmíd R. (2005) Condition Indicators for Gearbox Condition Monitoring Systems, Acta Polytechnica, 45(6), 35-43.

[69] Rafiee J, Arvani F., Harifi A. *et al* (2007) Intelligent condition monitoring of a gearbox using artificial neural network, Mechanical Systems and Signal Processing, 21 (4), 1746–1754.

[70] Saravanan, N. & Ramachandran, K.I. (2010) Incipient gear box fault diagnosis using discrete wavelet transform (DWT) for feature extraction and classification using artificial neural network (ANN), Expert Systems with Applications, 37 (6), 4168–4181.

[71] Paya B.A., Esat I.I. & Badi M.N.M. (1997) Artificial neural network based fault diagnostics of rotating machinery using wavelet transforms as a preprocessor, Mechanical Systems and Signal Processing, 11 (5), 751–765.

[72] Sanz J., Perera R. & Huerta C. (2012) Gear dynamics monitoring using discrete wavelet transformation and multi-layer perceptron neural networks, Applied Soft Computing, 12 (9), 2867–2878.

[73] Wu J. & Fang L. (2013) A fault diagnosis system for a mechanical reducer gear-set using Wigner-Ville distribution and an artificial neural network, Paper presented at the 13th International Conference on Computational Science and Its Applications (ICCSA), Ho Chi Minh City.

[74] Tang J., Liu Y. & Wu, F. (2010) Levenberg-Marquardt neural network for gear fault diagnosis, Paper presented at the 2nd International Conference on Networking and Digital Society, Wenzhou.

[75] Yang Z., Wang B., Dong X. *et al* (2012) Expert System of Fault Diagnosis for Gear Box in Wind Turbine, Systems Engineering Procedia, 4, 189–195.

[76] Sanchez R., Arpi A. & Minchala, L. (2012) Fault identification and classification of spur gearbox with feed forward back propagation artificial neural network, Paper presented at the VI Andean Region International Conference, Cuenca.

[77] Xiang X., Ruiping Z. & Zhixiong L. (2010) Virtual simulation analysis and experimental study on gear fault diagnosis based on wavelet neural network, Paper presented at the International Conference on Machine Vision and Human-Machine Interface, Kaifeng, China.

[78] Shang W., Zhou X. & Yuan J. (2014) An intelligent fault diagnosis system for newly assembled transmission, Expert Systems with Applications, 41 (9), 4060–4072.

[79] Cover T.M. (1965) Geometrical and statistical properties of systems of linear inequalities with applications in pattern recognition, IEEE Transactions on Electronic Computers, 14 (3), 326 – 334.

[80] Wuxing L., Tse P.W., Guicai Z. *et al* (2004) Classification of gear faults using cumulants and the radial basis function network, Mechanical Systems and Signal Processing, 18, 381–389.

[81] Li H., Zhang Y. & Zheng H. (2009) Gear fault detection and diagnosis under speed-up condition based on order cepstrum and radial basis function neural network, Journal of Mechanical Science and Technology, 23, 2780-2789.

[82] Li Z., Yan X., Yuan C. *et al* (2011) Fault detection and diagnosis of a gearbox in marine propulsion systems using bispectrum analysis and artificial neural networks, Journal of Marine Science and Application, 10 (1), 17-24.

[83] Kohonen, T. (1989) Self Organization and Associative Memory, second edition, Springer-Verlag, New York, pp. 130-132 (ISBN 978-3-540-18314-3).

[84] Cheng G., Cheng Y., Shen L. *et al* (2013) Gear fault identification based on Hilbert–Huang transform and SOM neural network, Measurement, 46 (3), 1137–1146.

[85] Yu J., Zhixiong L. & Yuancheng G. (2010) Research on AR modeling method with SOFM-based classifier applied to gear multi-faults diagnosis, Paper presented at the 2nd International Asia Conference on Informatics in Control, Automation and Robotics, Wuhan.

[86] Yu S., Fengxia, W. & Lu, Y. (2012) The fault diagnosis research based on SOM-BP composite neural network learning algorithm, Paper presented at the International Conference on Control Engineering and Communication Technology, Liaoning.

[87] Vapnik V.N. (1999) An overview of statistical learning theory, IEEE Transactions on Neural Networks, 10, 988–1000.

[88] Bansal S., Sahoo S., Tiwari R. *et al.* (2013) Multiclass fault diagnosis in gears using support vector machine algorithms based on frequency domain data, Measurement, 46 (9), 3469–3481.

[89] Bordoloi D.J. & Tiwari R. (2014) Support vector machine based optimization of multi-fault classification of gears with evolutionary algorithms from time–frequency vibration data, Measurement, 55, 1–14.

[90] Bordoloi D.J. & Tiwari R. (2014) Optimum multi-fault classification of gears with integration of evolutionary and SVM algorithms, Mechanism and Machine Theory, 73, 49–60.

[91] Wu T.Y., Chen J.C. & Wang C.C. (2012) Characterization of gear faults in variable rotating speed using Hilbert-Huang Transform and instantaneous dimensionless frequency normalization, Mechanical Systems and Signal Processing, 30,103–122.

[92] Shen Z., Chen X., Zhang X. *et al* (2012) A novel intelligent gear fault diagnosis model based on EMD and multi-class TSVM, Measurement, 45 (1), 30–40.

[93] Zamanian A.H., Ohadi A. (2011) Gear fault diagnosis based on Gaussian correlation of vibrations signals and wavelet coefficients, Applied Soft Computing, 11 (8) 4807–4819.

[94] Saravanan N., Siddabattuni V.N.S.K. & Ramachandran K.I. (2010) Fault diagnosis of spur bevel gear box using artificial neural network (ANN) and proximal support vector machine (PSVM), Applied Soft Computing, 10 (1), 344–360.

[95] Saravanan N., Siddabattuni V.N.S.K. & Ramachandran, K.I. (2008) A comparative study on classification of features by SVM and PSVM extracted using Morlet wavelet for fault diagnosis of spur bevel gear box, Expert Systems with Applications, 35 (3), 1351–1366.

[96] Saravanan N. & Ramachandran K.I. (2009) A case study on classification of features by fast single-shot multiclass PSVM using Morlet wavelet for fault diagnosis of spur bevel gear box, Expert Systems with Applications, 36 (8), 10854–10862.

[97] Tang B., Song T., Li F. *et al* (2014) Fault diagnosis for a wind turbine transmission system based on manifold learning and Shannon wavelet support vector machine, Renewable Energy, 62, 1–9.

[98] Wenyi L., Zhenfeng W., Jiguang H. *et al* (2013) Wind turbine fault diagnosis method based on diagonal spectrum and clustering binary tree SVM, Renewable Energy, 50, 1–6.

[99] Jiang Z., Feng X. *et al* (2010) Investigation of the mechanical faults classification using support vector machine approach, Paper presented at the 2nd International Conference on Intelligent Human-Machine Systems and Cybernetics, Nanjing, Jiangsu.

[100] Yang Z., Zhong J. & Wong S.F. (2011) Machine learning method with compensation distance technique for gear fault detection, Paper presented at the 9th World Congress on Intelligent Control and Automation, Taipei.

[101] Gao, Yu Z. & Guanghuang D. (2006) Intelligent fault identification based on wavelet packet energy analysis and SVM, Paper presented at the 9th International Conference on Control, Automation, Robotics and Vision, Singapore.

[102] Ma S., Liu G. & Xu Y. (2010) Gear fault diagnosis based on SVM, Paper presented at the International Conference on Wavelet Analysis and Pattern Recognition, Qingdao.

[103] Li B., Zhang P., Liang S. *et al* (2008) Feature extraction and selection for fault diagnosis of gear using wavelet entropy and mutual information, Paper presented at the 9th International Conference on Signal Processing, Beijing, China.

[104] Zhang C., Yang L. & Chen J. (2011) Fault diagnosis of gear cases based on entropy of singular values and support vector machine, Paper presented at the International Conference on Electric Information and Control Engineering, Wuhan.

[105] Kang J, Zhang X. & Zhao J. (2012) Gearbox fault diagnosis method based on wavelet packet analysis and support vector machine, IEEE Conference on Prognostics and System Health Management, Beijing, China.

[106] Samanta B. (2004) Gear fault detection using artificial neural networks and support vector machines with genetic algorithms, Mechanical Systems and Signal Processing, 18 (3), 625–644.

[107] Chen F., Tang B. & Chen R. (2013) A novel fault diagnosis model for gearbox based on wavelet support vector machine with immune genetic algorithm, Measurement, 46 (1), 220–232.

[108] Wu J. & Hsu C. (2009) Fault gear identification using vibration signal with discrete wavelet transform technique and fuzzy–logic inference, Expert Systems with Applications, 36 (2), 3785–3794.

[109] Saravanan N., Cholairajan S. & Ramachandran K.I. (2009) Vibration-based fault diagnosis of spur bevel gear box using fuzzy technique, Expert Systems with Applications, 36 (2), 3119–3135.

[110] Mitchell, T.M. (1997) Machine Learning, McGraw-Hill Science, pp. 250-255 (ISBN 0071154671).

[111] Yang Z., Hoi W.I. & Zhong J. (2011) Gearbox fault diagnosis based on artificial neural network and genetic algorithms, Paper presented at the International Conference on System Science and Engineering, Macao, China.

[112] Tang J., Cai Q. & Liu Y. (2010) Gear fault diagnosis with neural network based on Niche genetic algorithm, International Conference on Machine Vision and Human-Machine Interface, Kaifeng, China.

[113] Hajnayeb A., Ghasemloonia A., Khadem, S.E. *et al* (2011) Application and comparison of an ANN-based feature selection method and the genetic algorithm in gearbox fault diagnosis, Expert Systems with Applications, 38 (8), 10205–10209.

[114] Jang J.S.R. (1992) Self-learning fuzzy controllers based on temporal back propagation, IEEE Transactions on Neural Networks, 3 (5), 714–23.

[115] Jang J.S.R. (1993) ANFIS: Adaptive-network-based fuzzy inference system, IEEE Transactions on Systems, Man and Cybernetics, 23 (3), 665–685.

[116] Jian-Da W., Chuang-Chin H. & Guo-Zhen W. (2009) Fault gear identification and classification using discrete wavelet transform and adaptive neuro-fuzzy inference, Expert Systems with Applications 36 6244 – 6255.

[117] Attoui I., Boudiaf A., Fergani N. *et al* (2015) Vibration-based gearbox fault diagnosis by DWPT and PCA approaches and an adaptive neuro-fuzzy inference system, 16th International Conference on Sciences and Techniques of Automatic Control and Computer Engineering (STA), Tunisia.

[118] Zhang L., Xiong G., Liu L. *et al* (2018) Gearbox health identification by neuro-fuzzy ensemble, Journal of Mechanical Science and Technology, 3, 603-608.

[119] Soleimani A. (2012) Gear fault identification using artificial neural network and adaptive neuro-fuzzy inference system, Applied Mechanics, 110-116, 2562 – 2569.

[120] Guler I. & Ubeyli E.D. (2004) Application of adaptive neuro-fuzzy inference system for detection of electrocardiographic changes in patients with partial epilepsy using feature extraction, Expert Systems with Applications 27 (3) 323 – 330.

[121] Guler I. & Ubeyli E.D. (2005) Adaptive neuro-fuzzy inference system for classification of EEG signals using wavelet coefficients, Journal of Neuroscience Methods, 148(2), 113-121.

[122] Elbaset A.A. & Hiyama T. (2009) Fault detection and classification in transmission lines using ANFIS, IEEJ Transactions on Industry Applications, 129 (7), 705 – 713.

[123] Wu J.D. & Kuo J.M. (2010) Fault conditions classification of automotive generator using an adaptive neuro-fuzzy inference system, Expert Systems with Applications, 37, 7901 – 7907.

[124] Zhang L., Xiong G., Liu H. *et al* (2010) Bearing fault diagnosis using multi-scale entropy and adaptive neuro-fuzzy inference, Expert Systems with Applications, 37, 6077 – 6085.

[125] Moosavian A., Khazaee M., Ahmadi H. *et al* (2015) Fault diagnosis and classification of water pump using adaptive neuro-fuzzy inference system based on vibration signals, Structural Health Monitoring, 14(5), 402 – 410.

[126] Bahrami M., Javadikia H., E. Ebrahimi *et al* (2015) Application of a continuous wavelet transforms and ANFIS to fault diagnosis of a gearbox of tractor, Agricultural Engineering International: The CIGR e-journal, 17 (1), 94 – 100.

[127] Ebrahimi E. & Mollazade K. (2010) Intelligent fault classification of a tractor starter motor using vibration monitoring and adaptive neuro-fuzzy inference system, Insight, 52 (10), 561 – 566.

[128] Baydar N. & Ball A. (2001) A comparative study of acoustic and vibration signals in detection of gear failures using Wigner-Ville distribution, Mech. Syst. Signal Process, 15, 1091-1107.

[129] Baydar N. & A. Ball (2003) Detection of gear failures via vibration and acoustic signals using wavelet transform, Mechanical Systems and Signal Processing, 4, 787-804.

[130] Wu J., & Chan J. (2009) Faulted gear identification of a rotating machinery based on wavelet transform and artificial neural network, Expert Systems with Applications, 36, 8862-8875.

[131] Jedlinski L. & Jonak J. (2015) Early fault detection in gearboxes based on support vector machines and multilayer perceptron with a continuous wavelet transform, Applied Soft Computing, 30, 636-641.

[132] Fritsch F.N. & Carlson R.E. (1980) Monotone piecewise cubic interpolation, SIAM Journal of Numerical Analysis, 14, 238-246.

[133] McClelland J.L. & Rumelhart D.E. (1986) Parallel distributed processing, Explorations in the microstructure of cognition, 1, 547.

[134] Haykin S. (1998) Neural Networks: A Comprehensive Foundation, second ed., Pearson Education, Delhi, pp. 183-195 (81-7808-300-00).

[135] Colvin F.H. & Stanley F.A. (1914) American Machinists’ Handbook and Dictionary of Shop Terms: A Reference Book of Machine Shop and Drawing Room Data, Methods and Definitions, McGraw-Hill book Company, pp. 121.

[136] Saravanan N. & Ramachandran K.I. (2009) Fault diagnosis of spur bevel gearbox using discrete wavelet features and decision tree classification, Expert Systems with Applications, 36 (5), 9564-9573.

[137] Polikar R. (2006) The Wavelet Tutorial, second ed., Part 1, Fundamental concepts and an overview of the wavelet theory. https://cseweb.ucsd.edu. Accessed Jun 2017.

LIST OF PUBLICATIONS

Journal Papers:

1. Singh A. & Parey A. (2017) Gearbox fault diagnosis under fluctuating load conditions with independent angular re-sampling technique, continuous wavelet transform and multilayer perceptron neural network, I. E. T. Science, Measurement and Technology, 11 (2), 220 - 225.

2. Singh A. & Parey A. (2019) Gearbox fault diagnosis under non-stationary conditions with independent angular re-sampling technique applied to vibration and sound emission signals, Applied Acoustics, 144, 11 - 22.

3. Parey A. & Singh A. (2019) Gearbox fault diagnosis using acoustic signals, continuous wavelet transform and adaptive neuro-fuzzy inference system, Applied Acoustics, 147, 133-140.

Book Chapter:

1. Parey A. & Ahuja A.S. (2016) Application of Artificial Intelligence to Gearbox Fault Diagnosis: A Review. In: Sunil Jacob John (ed.), Handbook of Research on Generalized and Hybrid Set Structures and Applications for Soft Computing, IGI Global, pp. 536-562.